BENDING AND VIBRATION IN PLATES OF VARIABLE THICKNESS

Thesis for the Degree of Ph. D.

MICHIGAN STATE UNIVERSITY

B. Basava Raju

1961

THESIS

This is to certify that the

thesis entitled

Bending and Vibration in Plates of
Variable Thickness

presented by

B. Basava Raju

has been accepted towards fulfillment
of the requirements for

Ph.D. degree in Applied Mechanics

William A. Bradley
Major professor

Date FEBRUARY 21, 1962

O-169

LIBRARY
Michigan State
University

ABSTRACT

In this investigation a comparative study is made of variable thickness square plates with clamped and simply supported boundary conditions. The thickness variation in the plates is linear. The objects of this investigation are: (a) To experimentally determine the deflections and moments in uniformly loaded, clamped and simply supported square plates of variable thickness, (b) To compare the values obtained by experiment with those obtained by finite difference analysis, (c) To experimentally determine the natural frequencies and nodal patterns in the case of clamped and simply supported square plates of variable thickness, and (d) To compare the experimental and finite difference results.

The theory used is subject to the following restrictions: (1) the plate material obeys Hooke's Law; (2) the plate material is isotropic; (3) the deflections of the plate are small in comparison with the thickness; (4) the thickness of the plate is small in relation to the other dimensions.

The Moirē method is used to find the moments and deflections. Moirē fringe patterns for different plate models are shown and they are analysed to find the deflections and moments in the plates. The differential equation of variable thickness plate is approximated by a difference equation and the plate problem is solved for different boundary conditions and for different grid spacings by the use of the Digital Computer. The natural frequencies and the node patterns have been found experimentally using a Pulsed-air Vibrator. Finite difference approximation is used to solve the vibrating plate problem and

the resulting eigen value problem is solved by the use of digital computer.

The Moiré method seems to be better suited for finding deflections than for moments. The principal reasons for inaccuracies in the determination of moments are: (a) the actual models different from the ideal models used for mathematical analysis; (b) support conditions other than assumed, (c) the errors in calibration of the material and the reduction of data. With the setup and the models used and the general procedure followed in reducing data, the inaccuracies in moments varied from a very small value to about 10 per cent, although for some regions such as valleys and ridges the inaccuracies were quite high. The experimental and theoretical deflections agreed within 3 per cent. With improved models (both material and workmanship) and the improved support conditions (especially simple support) the inaccuracies in moments could be kept well below 10 per cent. The effect on moments and deflections of increasing or decreasing the edge thickness compared to the center thickness in clamped as well as simply supported plates is shown in the discussion of results.

The finite difference approximation used in this study gives sufficient accuracy for variable thickness plate problems. This method is applicable to plates with any boundary conditions, acted upon by any type of loading, and with arbitrary thickness variation.

The convergence of the difference method is very good both for deflections and moments. In the case of plate vibrations, for lower modes, grid sizes of a/6 and a/8 give good convergence,

but for higher modes, still finer grids should be used in order to give reasonable convergence. For still higher modes (beyond sixth mode) the rotatory inertia and shear should be included in the difference equation of the variable thickness plate to give good accuracy.

The experimental values of the vibration frequencies are in fair agreement with the finite difference results. The inaccuracies are due to the actual model deviating from the ideal model and support conditions being other than assumed. In this work, the inaccuracies range from very small amounts to about 6 per cent, although in a few cases, the inaccuracy was as great as 13 per cent. With better models, and improved support conditions, an accuracy of one per cent can be achieved with the Pulsed-air Vibrator. The experimentally observed nodal lines are in fair agreement with the calculated positions of node lines. Ultraharmonic resonance was observed for nearly all modes studied.

The results indicate that the finite difference approximation used for solving variable thickness plate problems gives results with reasonable convergence. The values obtained by the difference method agree quite well with those determined by experiment.

BENDING AND VIBRATION IN PLATES OF VARIABLE THICKNESS

By

B. Basava Raju

A THESIS

Submitted to
Michigan State University
in partial fulfillment of the requirements
for the degree of

DOCTOR OF PHILOSOPHY

Department of Applied Mechanics

1961

G 22223
2178 K2

ACKNOWLEDGEMENTS

The author wishes to express his sincere gratitude to Dr. William A. Bradley for the suggestion of this problem and for his guidance throughout this project. Sincere appreciation is expressed to Dr. Clement A. Tatro for his valuable help in instrumentation. Sincere thanks are due to the members of the guidance committee, Dr. George E. Mase, Dr. Charles P. Wells, and Dr. Robert K. L. Wen.

The author is grateful to Mr. J. Hoffman and the Division of Engineering Research for the support of this work.

Thanks are also due to Mr. Donald Childs and Mr. R. Jenkins for their cooperation and assistance in building and setting up the apparatus.

TABLE OF CONTENTS

	Page
LIST OF TABLES	v
LIST OF FIGURES	vi
NOTATIONS	ix
CHAPTER I INTRODUCTION; Historical Background	1
CHAPTER II FINITE DIFFERENCE ANALYSIS	6
CHAPTER III EXPERIMENTAL METHOD	18
Pulsed-Air Vibrator	19
(a) Variable Speed D. C. Motor	19
(b) Photo-Tube Speed Indicator	21
(c) Air Supply	21
(d) Pipe Assembly with Rotating and Stationary Wheels	21
(e) Plate Model	25
(f) Support	27
(g) SR-4 Gauge Station	28
(h) Camera to Record Node Lines	28
Experimental Procedure	28
CHAPTER IV RESULTS	31
Bending Results for Plate Models A, B	31
Bending Results for Plate Models D, E	49
Discussion of Bending Results	49
Vibration Results for Plate Models A, B, C, D, E, and F	55
Discussion of the Results	76
(a) Determination of Exact Resonance	77
(b) Errors in the Reading Instruments	77
(c) The Actual Plate Model Different from the Ideal Finite Difference Model	77

Page

(d) Inaccuracies in the Determination of Physical Constants 78

(e) Support Conditions Other than Assumed 78

(f) Vibration of Support 78

(g) Large Amplitudes 78

(h) Effect of Rotatory Inertia and Shear 80

(i) Damping in the Material 80

(j) The Effect of Air Mass 80

CHAPTER IV SUMMARY AND CONCLUSIONS 83

BIBLIOGRAPHY 87

APPENDIX A 89

APPENDIX B 97

LIST OF TABLES

		Page
TABLE 1.	Designation of Models	15
TABLE 2.	Deflections in Plate Model A	34
TABLE 3.	Deflections in Plate Model B	37
TABLE 4.	Deflections in Plate Model D	41
TABLE 5.	Deflections in Plate Model E	44
TABLE 6.	Extrapolated and Moiré Moments and Deflections	47
TABLE 7.	Natural Frequencies in Clamped Variable Thickness Plates	56
TABLE 8.	Natural Frequencies in Simply Supported Variable Thickness Plates	57
TABLE 9.	Physical Constants of the Plate Material	58

LIST OF FIGURES

		Page
FIGURE 1.	Notation of Points in the Difference Method	8
FIGURE 2.	Finite Difference Pattern of Plate Equation	9
FIGURE 3.	Plate Equation Pattern for a Point on the Free Edge	10
FIGURE 4.	Plate Equation Pattern for a First Interior Point from Free Edge	10
FIGURE 5.	Plate Equation Pattern for a Point Once Removed from Free Corner	11
FIGURE 6.	Plate Equation Pattern for a First Interior Point from Free Corner	11
FIGURE 7.	Plate Equation Pattern for a Free Corner	12
FIGURE 8.	Reactions in the Case of Simply Supported and Clamped Plates	12
FIGURE 9.	Thickness Variation in Plate Models	14
FIGURE 10.	Finite Difference Grid ($\lambda = a/6$) for Vibration in Plates	17
FIGURE 11.	General View of Test Setup	20
FIGURE 12.	Schematic of Pulsed-Air Vibrator	23
FIGURE 13.	Pipe Assembly with Different Size Nozzles	24
FIGURE 14.	Steel Support with Clamped and Simple Plate Supports	26
FIGURE 15.	Models for Simple and Clamped Supports	26
FIGURE 16.	Fringe Patterns for Uniformly Loaded Clamped Plate	32
FIGURE 17.	Finite Difference Grid used in Plate Modes A, B, D, E	33
FIGURE 18.	Moments for Plate Model A	35
FIGURE 19.	Moments and Deflections for Plate Model A	36

Page

FIGURE 20. Moments for Plate Model B 38

FIGURE 21. Moments and Deflections for Plate Model B 39

FIGURE 22. Fringe Patterns for Uniformly Loaded Simply Supported Plate 40

FIGURE 23. Moments for Plate Model D 42

FIGURE 24. Moments and Deflections for Plate Model D 43

FIGURE 25. Fringe Patterns for Uniformly Loaded Simply Supported Plate 44

FIGURE 26. Moments for Plate Model E 46

FIGURE 27. Moments and Deflections for Plate Model E 47

FIGURE 28. Comparison of Moments and Deflections along Centerline of Plate Model A and B with a Uniformly Loaded Clamped Plate of Constant Thickness 52

FIGURE 29. Comparison of Moments and Deflections along Centerline of Plate Model D and E with a Uniformly Loaded Simply Supported Plate of Constant Thickness 53

FIGURE 30. Node Pattern on Plate Model A 59

FIGURE 31. Node Pattern on Plate Model B 60

FIGURE 32. Node Patterns on Plate Model C 61

FIGURE 33. Node Patterns on Plate Model D 62

FIGURE 34. Node Patterns on Plate Model F 62

FIGURE 35. Node Patterns on Plate Model E 63

FIGURE 36. Relative Amplitudes in Plate Model A 64

FIGURE 37. Relative Amplitudes in Plate Model A 65

FIGURE 38. Relative Amplitudes in Plate Model A 66

FIGURE 39. Relative Amplitudes in Plate Model B 67

FIGURE 40. Relative Amplitude in Plate Model B 68

FIGURE 41. Relative Amplitude in Plate Model B 69

FIGURE 42. Relative Amplitude in Plate Model D 70

Page

FIGURE 43. Relative Amplitudes in Plate Model D 71

FIGURE 44. Relative Amplitudes in Plate Model D 72

FIGURE 45. Relative Amplitudes in Plate Model E 73

FIGURE 46. Relative Amplitudes in Plate Model E 74

FIGURE 47. Relative Amplitudes in Plate Model E 75

FIGURE 48. Effect of Large Amplitudes in Plate Model B 79

FIGURE 49. Forces Acting on Elements of Analogous Plate Structure at a General Point of a Variable Thickness Plate 90

FIGURE 50. Forces Acting on Elements of Analogous Plate Structure at a Point on the Simply Supported Edge of a Variable Thickness Plate 93

FIGURE 51. Forces Acting on Elements of Analogous Plate Structure at the Corner of a Simply Supported Plate of Variable Thickness 94

FIGURE 52. Moments and Forces Acting on a Plate Element of Variable Thickness 98

FIGURE 53. Finite Difference Approximation for Plate Equation of Variable Thickness 101

NOTATION

a	Side dimension of square plate
D_i	$\frac{E t^3_i}{12(1 - \nu^2)}$ plate rigidity at a point 'i'
D_r	Plate rigidity at a reference point
E	Modulus of Elasticity
ν	Poisson's ratio
t	plate thickness
q	Distributed load per unit area, with positive load downward.
M_x, M_y	Bending moments per unit of width acting on sections perpendicular to the x and y axes, respectively.
M_{xy}	Twisting moment per unit width in the x and y directions.
x, y	Horizontal and vertical coordinate axes. In all fringe photos, origin is taken at upper left corner with x positive to the right and y positive downward.
λ	a/n, the spacing of grid used in the difference method.
ρ	Mass density of plate material
τ	time variable
ω	angular frequency
ω_r	a parameter in terms of which frequency is expressed $\left(\sqrt{\frac{Dr}{\rho t_r a^4}} \right)$
α	ω/ω_r , a dimensionless number
δ_i,	Di/Dr variable thickness plate rigidity ratio

CHAPTER I

INTRODUCTION

In continuum mechanics, the term 'plate' may be applied to bodies bounded by two surfaces, the distance between the surfaces being small compared to the other dimensions. The middle surface is defined by the locus of points which lie at equal distances from these two surfaces. At any arbitrary point of the middle surface, the thickness is defined as the length of a line perpendicular to the middle surface and intercepted between the bounded surfaces. In general the thickness may vary in magnitude from point to point in the middle surface and hence may depend on the coordinates of the arbitrary point in the middle surface.

To study the plate problem in the light of the classical theory of Elasticity, it is usual to assume that the material of the plate is isotropic and obeys Hooke's Law and that the displacements at a point are small in comparison with the thickness of the plate. Further assumptions analogues to those used in the theory of beams were introduced by Lagrange. Lagrange's assumptions may be stated as follows: a) The straight fibres of a plate which are perpendicular to the middle surface before deformation remain so after deformation and do not change their length. b) The normal stresses acting on planes parallel to the middle surface may be neglected in comparison with the other stresses.

If the thickness of the plate is considered as a constant, the solution of the plate problem is further simplified. Solutions in the form of series, numerical solutions, and experimental solutions are available to this plate problem. A simple approach to the problem of variable

thickness platesis impossible, if one has in mind a general solution which is to apply to all problems in variable thickness plates. Thus, it leads to the study of less general problems in variable thickness plate, wherein the thickness variation is assumed to follow a predetermined law.

In this study, clamped and simply supported square plates are considered. The variation of thickness is linear and symmetric about the diagonals as well as the lines joining the midpoints of the sides of the square. The symmetry is used to simplify the numerical analysis. The purposes of this study then are to:

(1) Experimentally determine the deflection and moments in uniformly loaded, clamped, and simply supported square plates of variable thickness.

(2) Compare the values obtained by experiment with the values obtained by finite difference analysis.

(3) Experimentally determine the natural frequencies and nodal patterns in the case of clamped and simply supported square plates of variable thickness.

(4) Compare the values obtained by experiment with the values obtained by finite differences.

Besides the above applications, finite difference method with the use of digital computer can be applied to plates with various other boundary conditions, subjected to any conceivable type of loading and the thickness variation being quite arbitrary. The loading and thickness functions could be continuous or discontinuous functions of x and y.

Historical Background

A few series solutions of the differential equation of variable thickness plate have been obtained. Among them, the bending of rectangular plates with the flexural rigidity being a linear function of one of the independent variables of the problem has been considered by R. Gran Olsson [1].* He assumes a Levy type of series and obtains the solution in terms of exponential integrals. For a plate whose thickness is an exponential function of one of the independent variables, R. Gran Olsson [2] obtains a Levy type of solution for the bending case.

Henry Favre and Bernhard Gilg [3] have considered plates whose thickness is a linear function of one of the independent variables (x or y). A perturbation method is used to get a better approximation. Solutions have been worked out for a simply supported rectangular plate whose thickness varies linearly in a direction parallel to one of the sides, and plate being loaded hydrostatically. The Navier type as well as Levy type series have been used and the simplicity and advantage of Levy type series over Navier type series is shown.

The fundamental differential equation of variable thickness plates admits of a relatively simple treatment when $\nu = 1/3$ and this special case is discussed by Contri, L. [5, 6] who obtains a rigorous solution using the Levy-Estanave simple series solution. He considers linear variation of the plate along a direction parallel to one of the edges, the plate being restricted to be simply supported along two opposite edges, the other two edges being quite general. An iterative method of successive approximation is suggested when Poisson's ratio is not 1/3.

*Numbers in square brackets refer to the Bibliography.

Electrical analogy offers a powerful general method for problems involving deflections under constant load, transient vibrations, or normal modes in plates of constant as well as variable thickness. In the electrical-anology method, the problem is formulated in finite-difference terms, and the solution of the difference equations is carried out on an electrical-analog computer. No restrictions are made on the elastic properties of the plate as regards homogeneity and isotropy. The free edges cause no particular difficulty, and the irregular edges can also be handled by the electrical analogy. R. H. McNeal [7] gives a detailed description of the representation of the boundary conditions for a rectangular variable thickness plate. The principal difficult requirement of the plate analogy is the existence of a large number of essentially perfect transformers.

Y. C. Fung [8] treats the free edge boundary conditions in a way different from the Kirchhoff-Love formulation of free edge boundary conditions. He uses two "stress functions" of such form that the boundary conditions can be expressed in terms of two functions and their first derivatives. This theory is applied to a square plate with linear thickness variation (double-wedge section) simply supported at two diagonal corners and loaded by concentrated forces at the other two corners. Southwell's relaxation procedure is used to obtain the stresses and deflections. This is checked experimentally also. This procedure is also applied to obtain stresses in a 45^{o} swept wing of variable thickness.

Exact solutions are not available for the frequency of vibration of rectangular plates of variable thickness. Kogaev, V. P. [10] uses the Ritz method to find the frequencies in the blades of hydraulic turbines. Polynomials are used as co-ordinating functions as they

insure rapid convergence and give considerable simplification in calculating integrals from co-ordinating functions. Gumenyuk, V. S. [9] uses a finite difference approximation to find frequencies in plates in the form of a rectangle and an isosceles triangle, the thickness being regarded as dependent only on one co-ordinate and varying by a linear law, while the edges of the plate are free.

CHAPTER II

FINITE DIFFERENCE ANALYSIS

With the assumptions made in Chapter I, the differential equation for the bending of plates of variable thickness can be represented by

$$D\Delta\Delta w + 2\frac{\partial D}{\partial x}\frac{\partial}{\partial x}\Delta w + 2\frac{\partial D}{\partial y}\frac{\partial}{\partial y}\Delta w + \Delta D\,\Delta w - (1-\nu)\left(\frac{\partial^2 D}{\partial x^2}\frac{\partial^2 w}{\partial y^2} - 2\frac{\partial^2 D}{\partial x \partial y}\frac{\partial^2 w}{\partial x \partial y} + \frac{\partial^2 D}{\partial y^2}\frac{\partial^2 w}{\partial x^2}\right) = q(x, y) \qquad (1)$$

where

$$\Delta = \frac{\partial^2}{\partial x^2} + \frac{\partial^2}{\partial y^2}$$

$$D = \frac{Et^3}{12(1-\nu^2)}$$

q = Lateral load on the plate

w = Lateral deflection, a function of x and y,

ν = Poisson's ratio.

If w is now considered as a function of x, y and time τ, the static lateral loads on the plate could be replaced by equivalent inertia forces, namely, $-\rho t \frac{\partial^2 w}{\partial \tau^2}$, to obtain the governing differential equation of a freely vibrating plate of variable thickness,

where

ρ = Mass density of plate material

t = Plate thickness,

τ = time.

For a variable thickness plate vibrating harmonically with an amplitude $\phi(x, y)$

$$w(x, y, \tau) = \phi(x, y) \cos \omega \tau , \qquad (2)$$

where ω is the angular frequency. For the sake of convenience in writing, $\phi(x, y)$ is replaced by $w(x, y)$, then the right hand side of equation (1) would be $\rho t \omega^2 w(x, y)$.

In Appendix A the difference equation (shown in Fig. 2) is derived for variable thickness plate by plate analogy. Some of the boundary conditions and reactions shown in Figures 3 - 8 are also derived by plate analogy in Appendix A. In Appendix B, the differential equation of variable thickness is approximated by replacing the partial derivatives by the equivalent finite differences. Both the approximations lead to a system of linear algebraic equations for the bending case which could be solved by a digital computer to give the deflection at the nodal points. Knowing the deflections, moments are calculated by the various differential relations.

In the case of vibration, the resulting simultaneous linear algebraic equations may be written in matrix form as

$$[A - \chi B] w = 0 \qquad (3)$$

where A = Matrix of coefficients of terms on the left hand side of the equation shown in Figure 2,

B = Diagonal matrix resulting from right hand side of equation shown in Figure 2.

w = Column matrix of deflections

$$\chi = \frac{\rho \omega_n^2 \lambda^4}{D_o} ,$$

$\lambda = a/n$ = grid spacing.

Equation (3) is in standard eigen value form and the eigen values

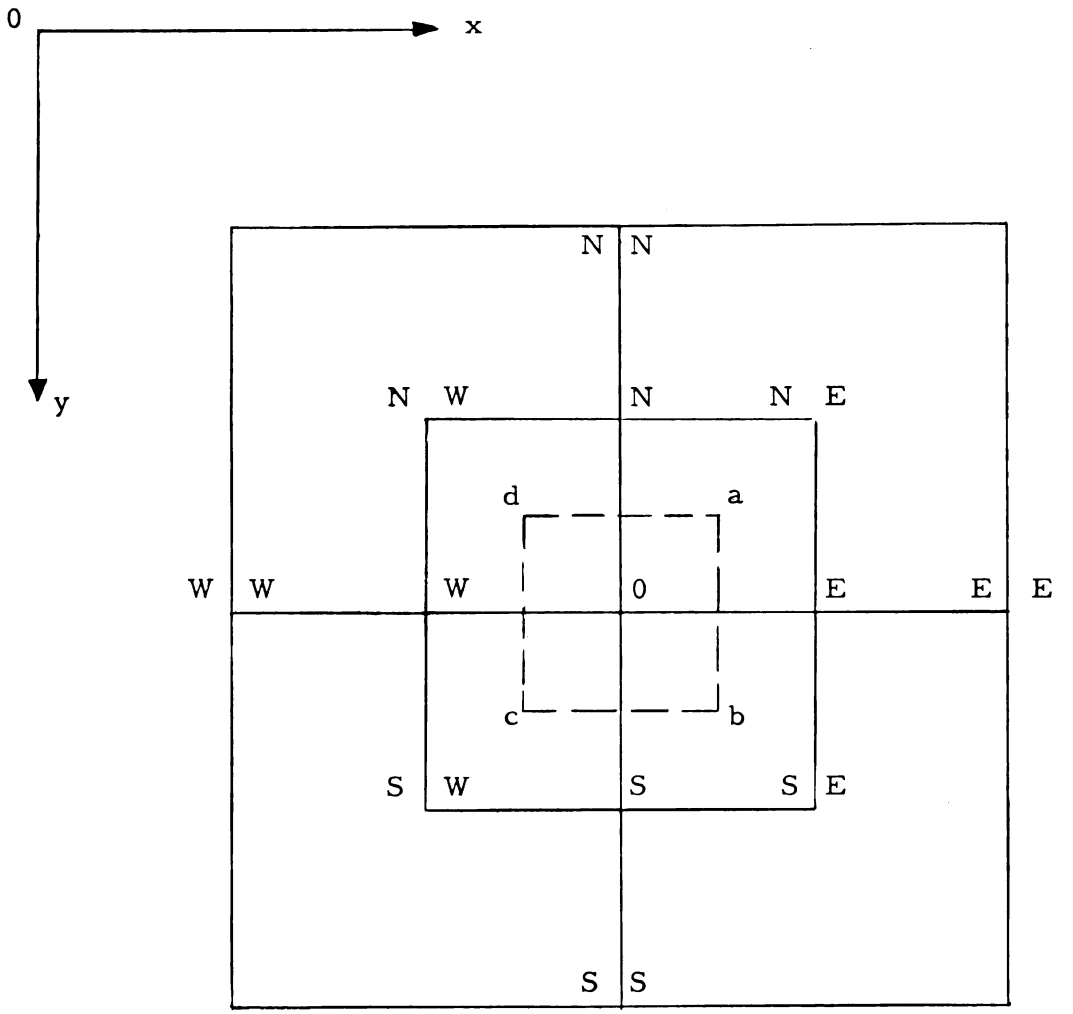

FIGURE 1. Notation of Points in the Difference Method

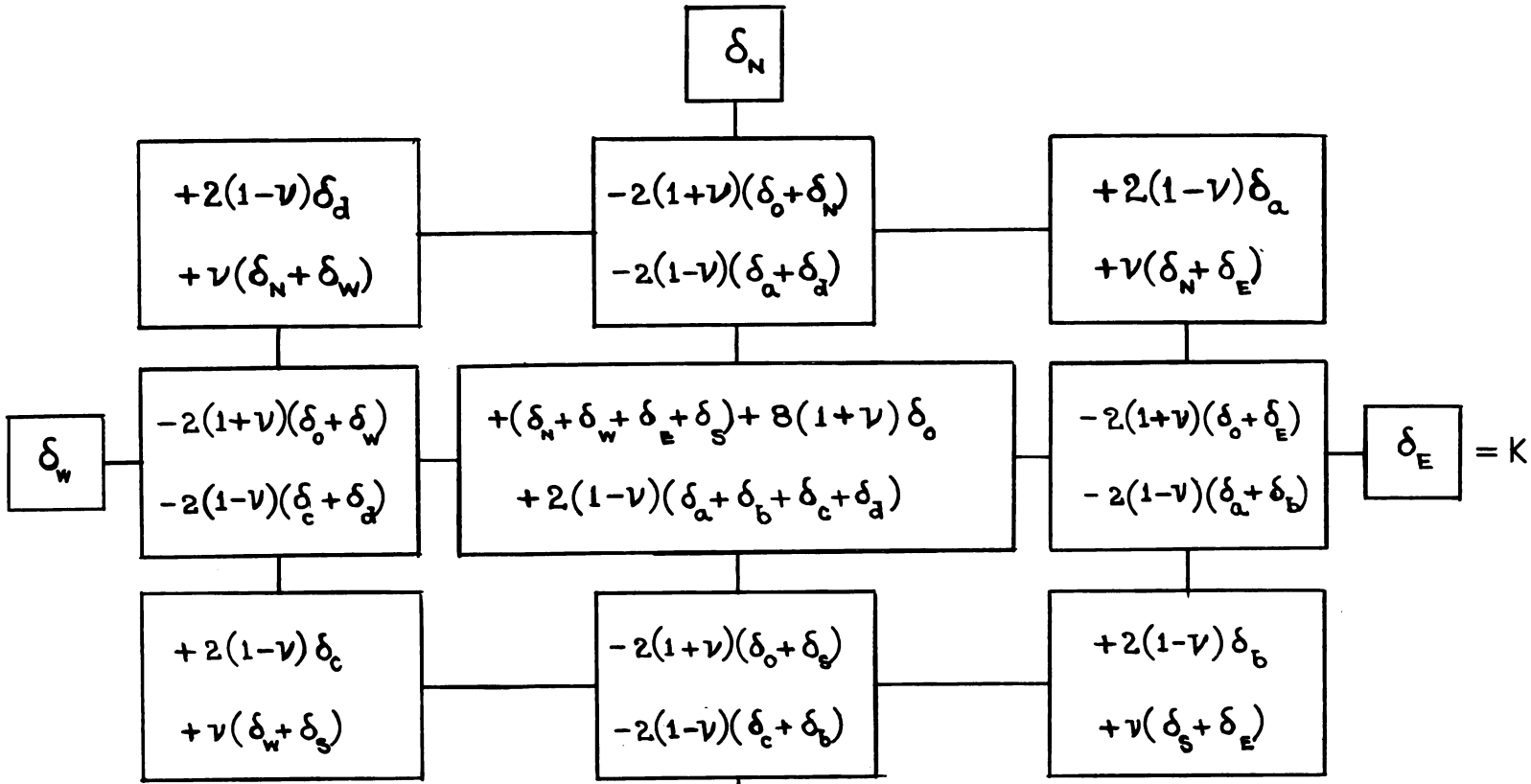

" r " is particular point in plate used as reference.

FIGURE 2. Finite Difference Pattern for Plate Equation

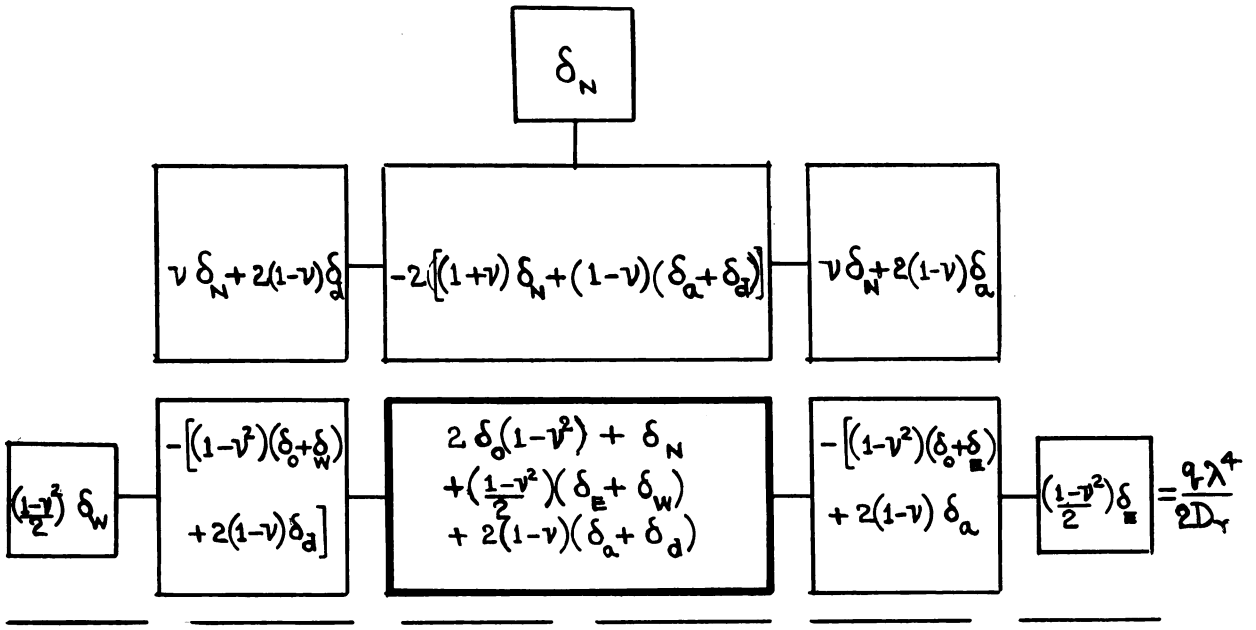

FIGURE 3. Plate Equation Pattern for a Point on the Free Edge

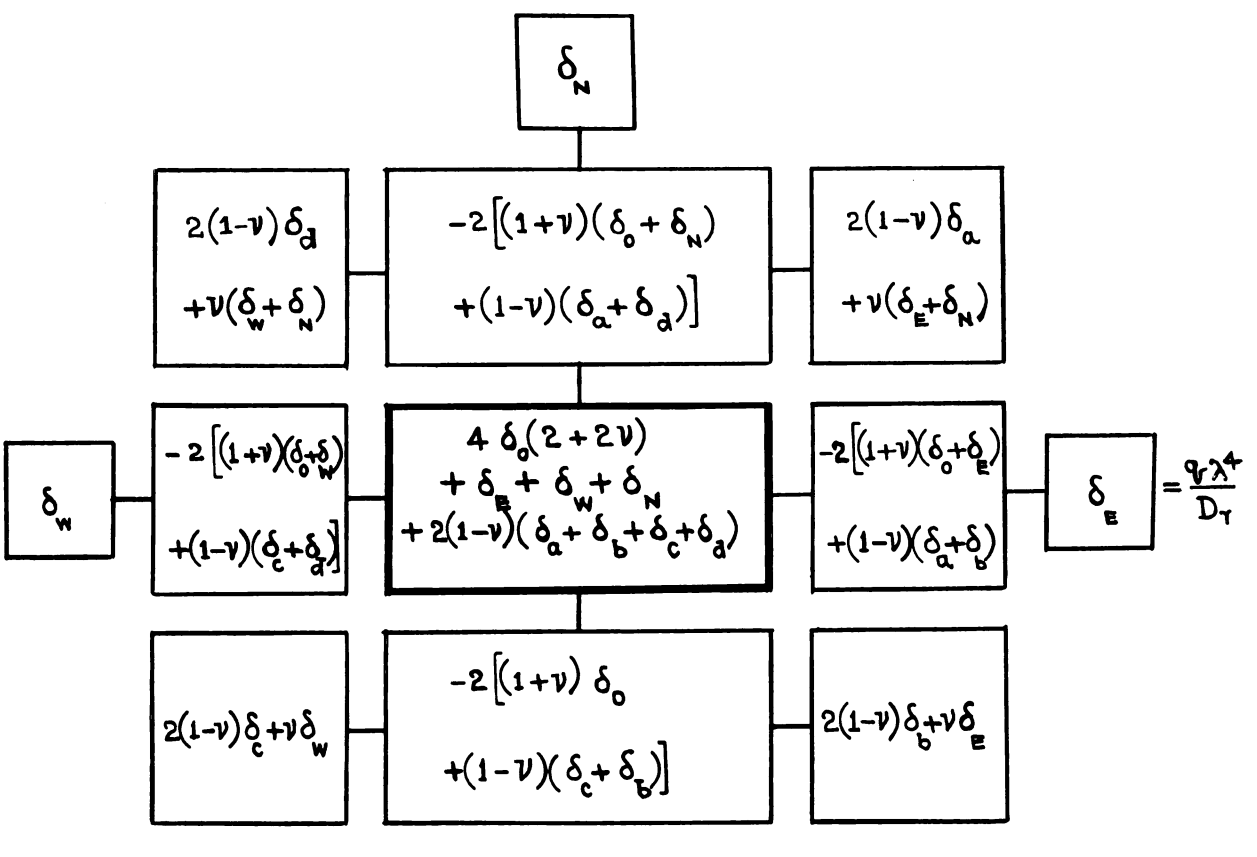

FIGURE 4. Plate Equation Pattern for a First Interior Point from Free Edge

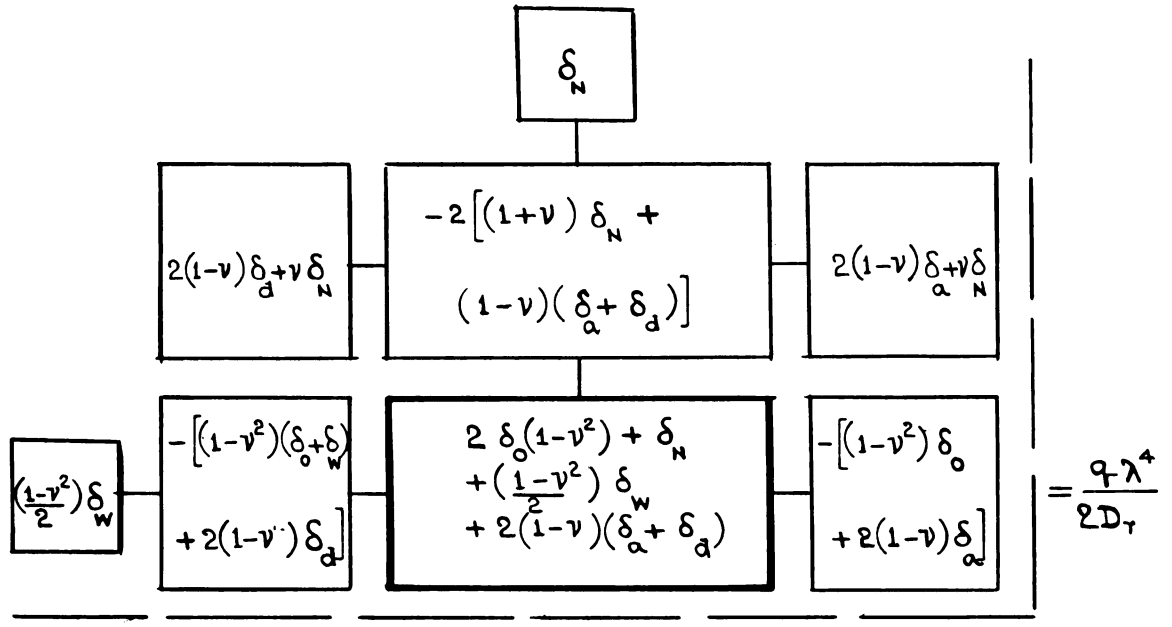

FIGURE 5. Plate Equation Pattern for a Point Once Removed from Free Corner

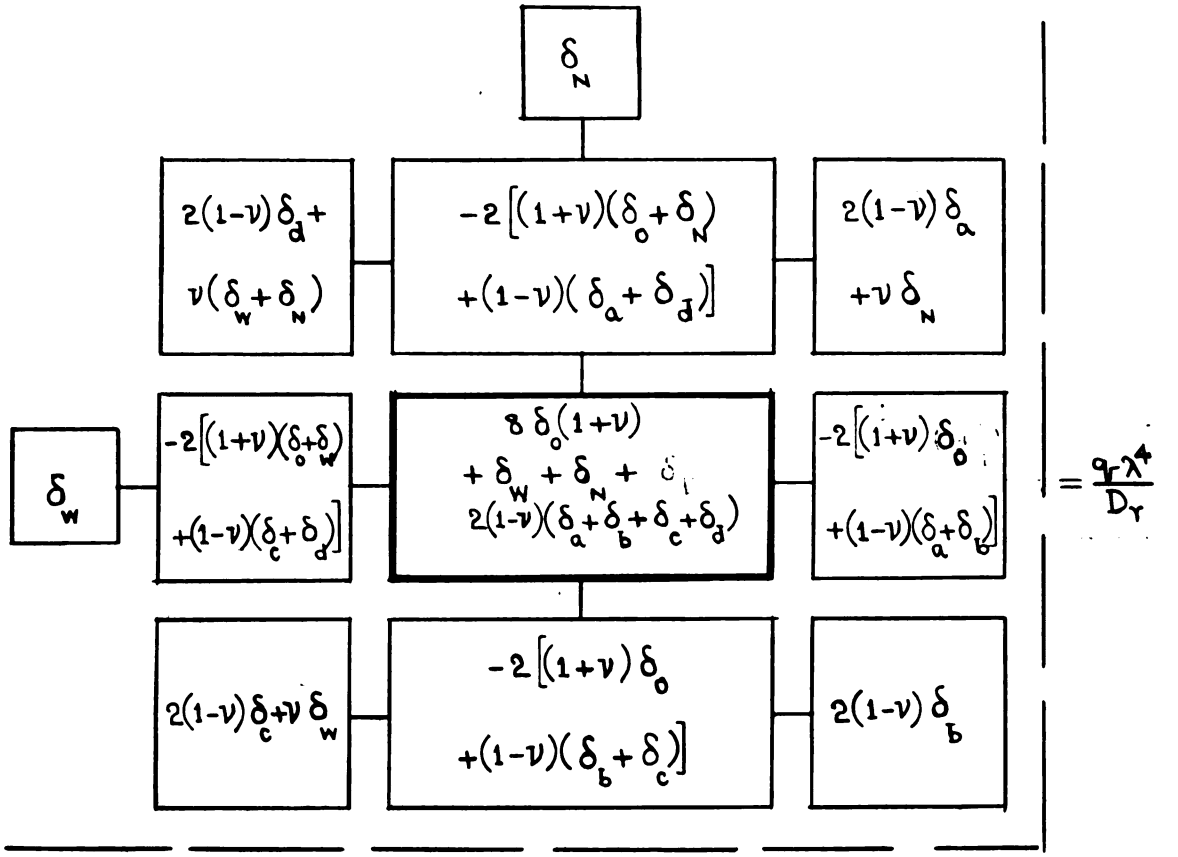

FIGURE 6. Plate Equation Pattern for a First Interior Point from Free Corner

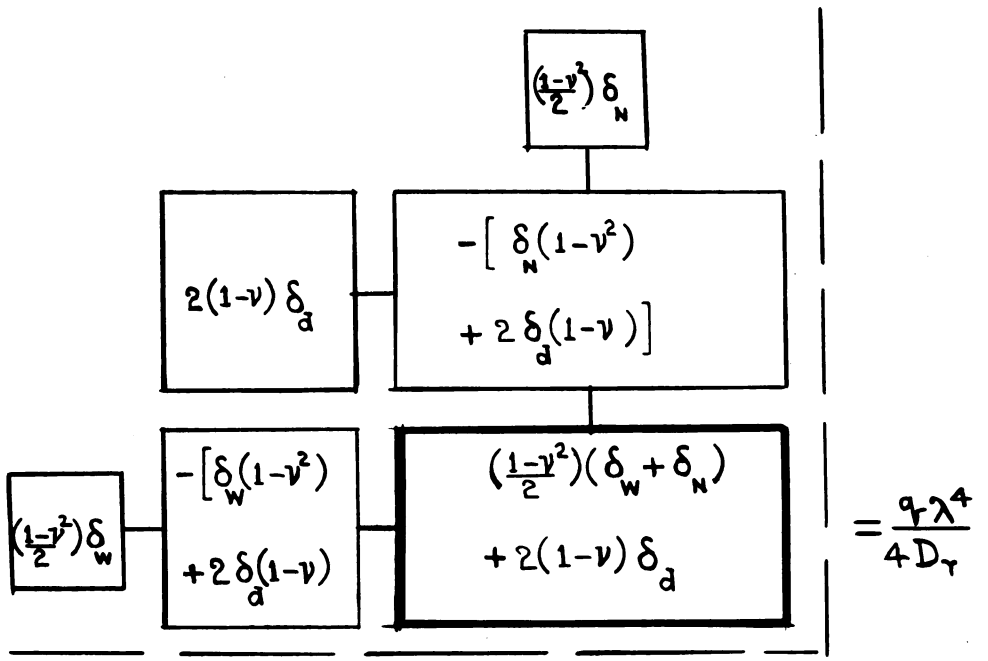

FIGURE 7. Plate Equation Pattern for a Free Corner

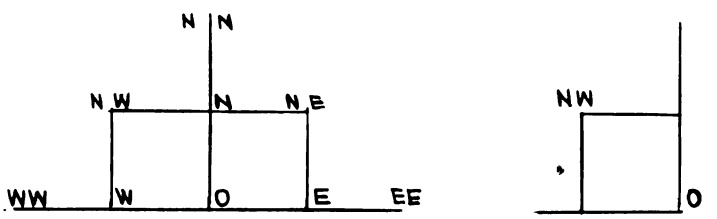

Simply Supported Edge Reaction

$$V_o = \frac{D_r}{\lambda^3}\left[w_{NN}\delta_N + w_{NW}\left[\nu\delta_N + 2(1-\nu)\delta_d\right] + w_{NE}\left[\nu\delta_N + 2(1-\nu)\delta_d\right] - 2w_N\left[(1+\nu)\delta_N + (1-\nu)(\delta_d+\delta_d)\right]\right] - \frac{q\lambda}{2}$$

Fixed Edge Reaction

$$V_o = \frac{D_r}{\lambda^3}\left[w_{NNN}\delta_{NNN} + w_{NW}\left[2(1-\nu)\delta_d + \nu(\delta_N+\delta_W)\right] + w_{NE}\left[2(1-\nu)\delta_d + \nu(\delta_N+\delta_E)\right] - 2w_N\left[(1+\nu)(\delta_O+\delta_N) + (1-\nu)(\delta_d+\delta_d)\right]\right] - \frac{q\lambda}{2}$$

Simply Supported Corner Reaction

$$R = \frac{D_r}{\lambda^2}\cdot 2(1-\nu)\delta_d w_{NW} - \frac{q\lambda}{4}$$

Fixed Corner Reaction

$$R = \frac{D_r}{\lambda^2}\left[2(1-\nu)\delta_d + \nu(\delta_N+\delta_W)\right] - \frac{q\lambda}{4}$$

FIGURE 8. Reactions in the Case of Simply Supported and Clamped Plates

and the eigen vectors could be obtained by the use of a digital computer.* The eigen values give the frequencies of freely vibrating plate of variable thickness and for each eigen value the corresponding eigen vector gives the relative amplitudes of vibration.

The difference approximation developed in Appendix A, besides facilitating writing the equations, yields a symmetric positive definite matrix A. This leads to the easy accessibility to complete programs like M5 which calculates both the eigen values and eigen vectors. Hence, in this study the difference approximation of Appendix A is used.

The square plates with the thickness variations considered in this study are shown in Figure 9. For the bending case, the clamped as well as simply supported plates have their edge thickness twice or half as much as the center thickness of the plate. The load is uniformly distributed over the surface of the plate. Further, the single taper on one side of the plate is assumed to be equivalent to a double taper plate symmetrical about the middle surface of the plate. For example, the plate (b) in Figure 9 is equivalent to a double-wedge section. This assumption holds true if the slope of the tapered face is small [11] . Three grid spacings, namely $\lambda = \frac{a}{6}, \frac{a}{8}, \frac{a}{10}$ are used, and extrapolations are used wherever possible.

For the vibration case, the thickness ratios of $\frac{t}{t_o} = 1/2, 2$ 5.3 were considered for both clamped and simply supported plates (Table I). The grid spacings are $\lambda = a/6$ and $\lambda = a/8$. The bending mode was obtained by numbering the nodal points only over the 1/8 of the plate surface (see Fig. 10 (a) for $\lambda = a/6$), thus making use of the

*In this work, the MISTIC was used with standard M5 program.

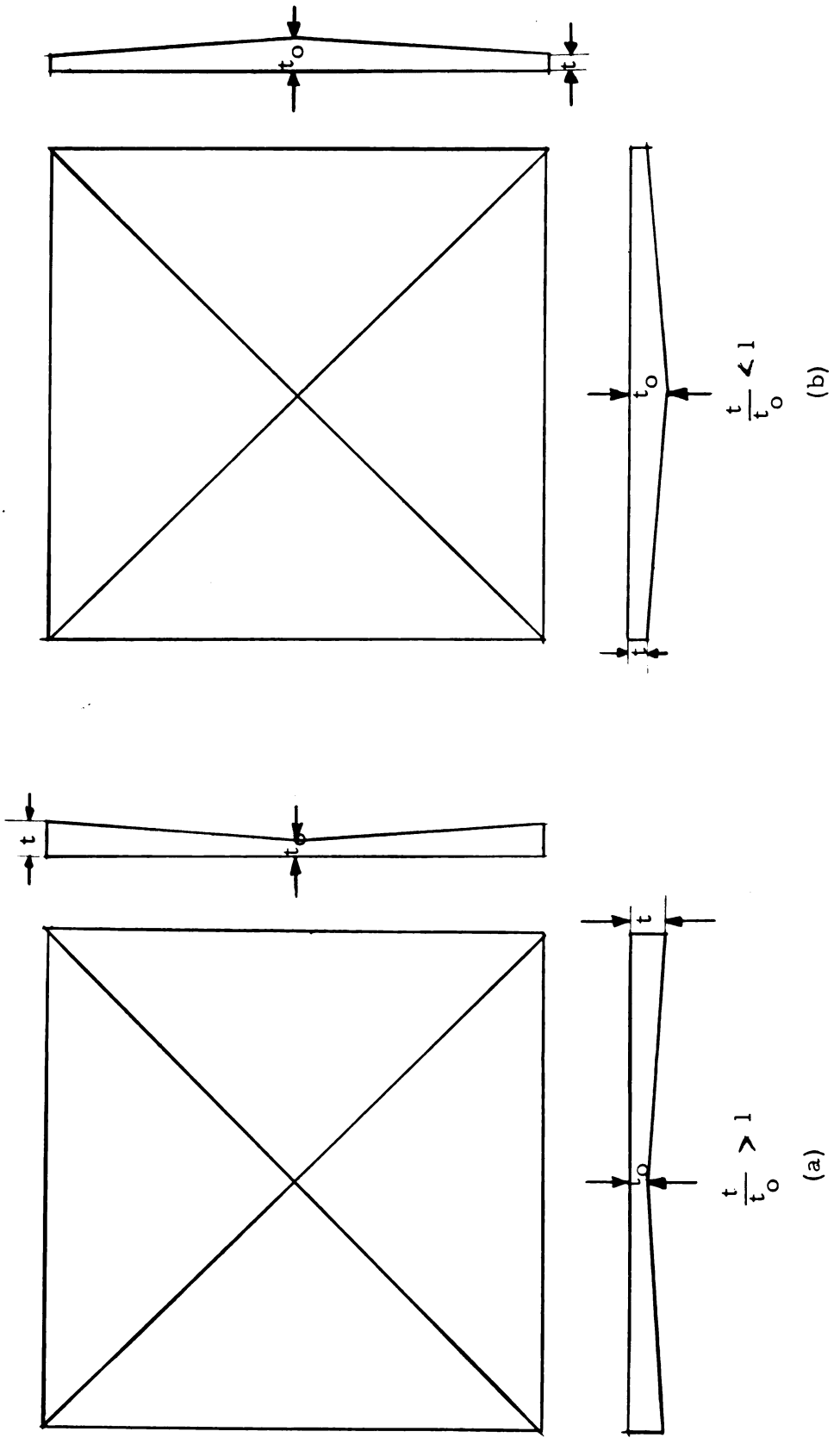

FIGURE 9. Thickness Variation in Plate Models

TABLE 1. Designation of Models

Edge Condition of Plate	t/t_o	Name of Plate Model
Clamped	2	A
Clamped	1/2	B
Clamped	5·3	C
Simply Supported	2	D
Simply Supported	1/2	E
Simply Supported	5·3	F

Model Materials:

Static Loading - Perspex

Vibration Studies - Aluminium

Poisson's ratio $= \frac{1}{3}$ for all finite difference and experimental calculations.

symmetry. This yields the fifth mode also. For the torsional mode or second mode, node lines are considered as shown in Fig. 10 (b). For the third and fourth mode the node lines are shown in Fig. 10 (c) and (d).

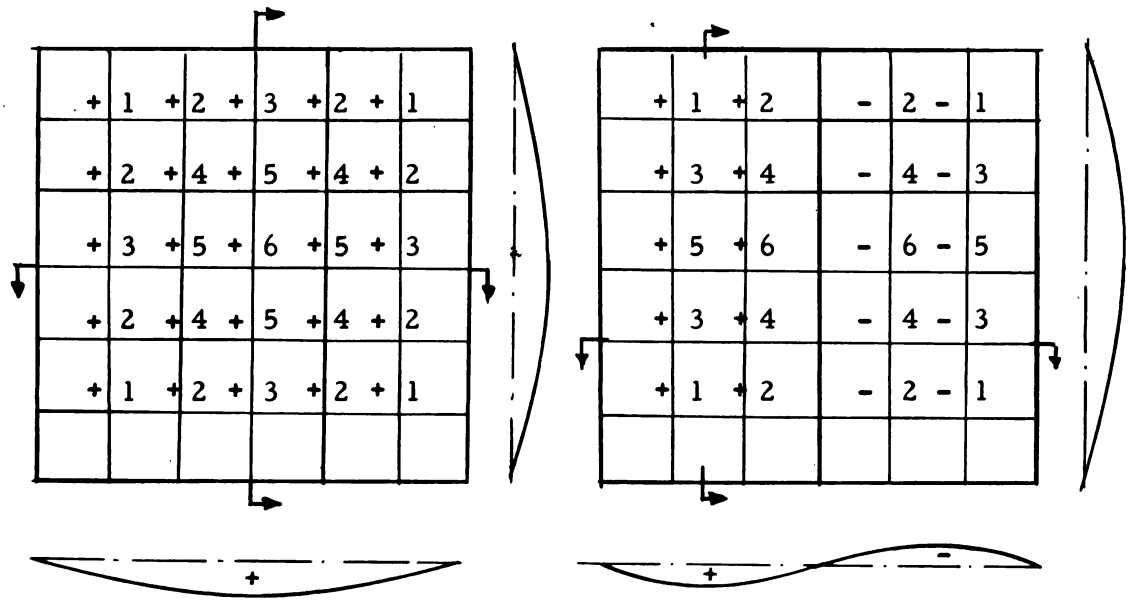

(a) FIRST MODE

(b) SECOND MODE

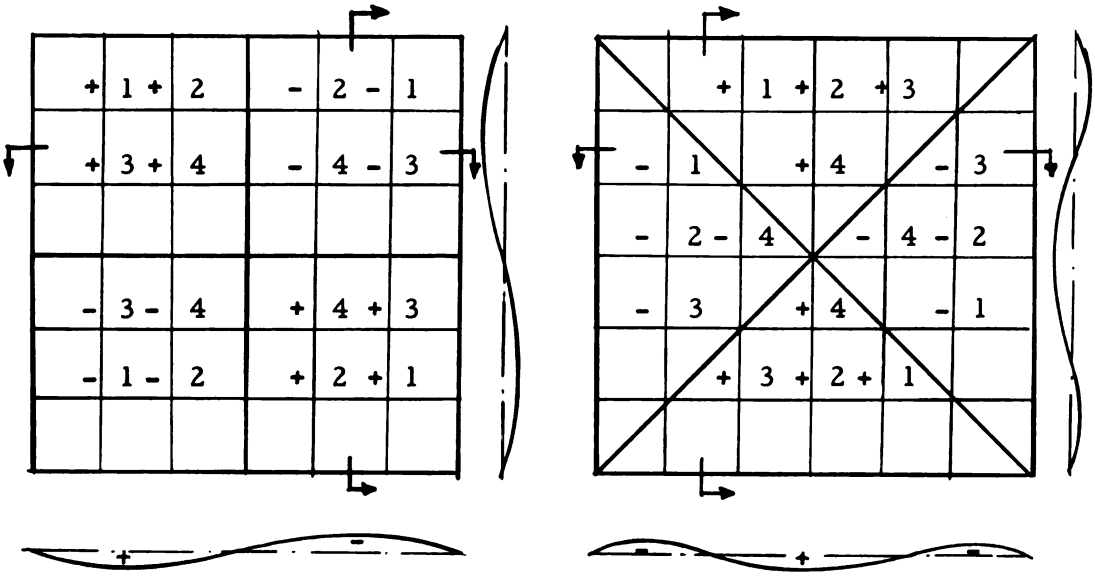

(c) THIRD MODE

(d) FOURTH MODE

FIGURE 10. Finite Difference Grid ($\lambda = a/6$) for Vibration in Plates

CHAPTER III

EXPERIMENTAL METHOD

The experimental verification of the results obtained by the finite difference analysis can be separated into two parts:

a) The use of the Moiré method for deflections and moments.

b) Use of a pulsed-air vibrator for exciting the plate model in vibration studies.

The Moiré technique has been described in references [12] and [13] and is not repeated here. The equipment used and procedures followed in the vibration studies are described in detail, however, since they were newly developed.

The requirements governing the design of the pulsed-air vibrator are as follows:

(1) Excitation frequency should be variable continuously from 10 cps to 1,000 cps.

(2) The excitation frequency for a particular setting should remain fixed, thus permitting continued running at the particular resonant frequency chosen.

(3) The amplitudes of vibrating plate should be easily variable.

(4) There should be no restrictions on the material of plate (e.g. - magnetic).

(5) The source of excitation should be sufficiently independent of the plate response to permit any mode of vibration within the frequency range to be excited.

(6) The response of the support should be sufficiently far away from

the plate response to permit any mode of vibration within the frequency range to be excited.

Pulsed-Air Vibrator

The pulsed-air vibrator consists of:

(a) Variable speed D.C. motor.

(b) Photo-tube speed indicator.

(c) Air supply.

(d) Pipe assembly with rotating and stationary wheels.

(e) Plate model.

(f) Support.

(g) SR-4 gauge station

(h) Camera to record nodal lines.

(a) Variable speed D.C. motor. (See Fig. 11)

The complete Reliance V * S Jr. Drive consists of three parts: the adjustable-speed d-c drive motor, the control unit, and the operator's control station. The control unit is mounted in a vertical position on a wheeled cart so that the ventilation through the louvered portions at the front, bottom and top-side portions of the cabinet is not restricted. The control unit is located so as to receive a minimum amount of vibration, and is supplied with a 440-volt, 50 cycle input. The adjustable speed drive motor can develop a maximum of 2 h.p. at 2500 r.p.m. and it is wired to the control unit. The operator's control station includes a start-stop pushbotton, a speed adjustor, and a jog-run toggle switch. The operator's control station is wired to the control unit.

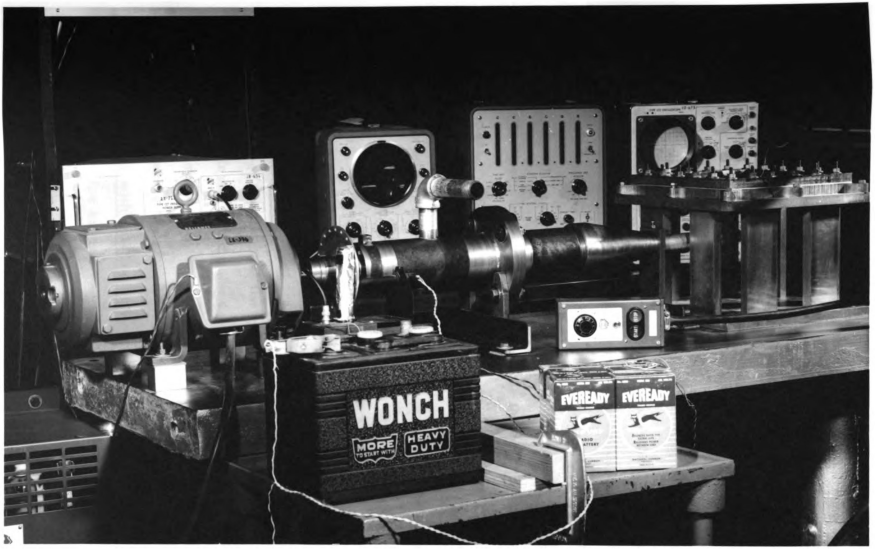

FIGURE 11. General View of Test Setup

(b) Photo-tube speed indicator. (see Fig. 11, 12)

A Photo-tube circuit is introduced as a device to measure the excitation frequency. The light from a 6 volt bulb is interrupted by a rotating slotted wheel mounted on the motor shaft. Since the photo-cell represents a variable resistance depending upon the quantity of light falling on it, this interrupted light produces an alternating output voltage. A capacitor introduced in the circuit permits only the alternating signal to the Tektronix preamplifier. The output from this preamplifier is fed to Hewlett-Packard Electronic Counter as well as to a Hewlett-Packard Oscilloscope. The oscilloscope trace detects any stray signals in the circuit. The photo-tube is shielded with aluminum foil which is grounded. This, as well as the use of shielded cables for interconnection, eliminates the erratic signals to a great extent.

(c) Air supply.

The air supply to the pulsed-air vibrator is provided by Joy Air Compressor, Class WG9, 8 in. bore and 7 in. stroke run by a 60 h.p. motor. It develops a maximum pressure of 100 p.s.i., the capacity at delivery being 162 cft/min. The inlet to the vibration tester is connected to the outlet from the air reservoir through a pressure rubber hose, in order that the vibrations from the compressor may not be transfered to the pulsed-air vibrator. The air inlet is controlled by a mechanically operated valve which can regulate the amount of air entering the vibrator.

(d) Pipe assembly with rotating and stationary wheels.

The whole pipe assembly of the pulsed-air vibrator is built

in four segments: two standard weight steel pipes of nominal size 3 joined together by a flanged joint, a reducer, and a nozzle (see Fig. 13). The segment of the steel pipe towards the motor end houses a rotating perforated wheel connected to the motor shaft by means of a 7/8" diameter shaft, the two shafts being connected by a Spartan flexible coupling. The shaft is supported inside the pipe on a thrust bearing at the entrance of the pipe and a Torrington needle bearing on a spider nearer to the rotating perforated wheel. A Victoprene oil seal located at the end of the pipe prevents any air leakage around the shaft. A circular annular disc threaded towards the motor end of the pipe, besides blocking the air in the pipe, helps in the adjustment of the gap between the rotating wheel and the stationary plate. Any further air leaks between the rim of the circular disc and the pipe are prevented by the use of an oil ring and another annular circular disc which is bolted on the first disc. The rotating wheel is of thickness 1/4 inch and it is smoothly machined so that it can freely rotate inside the pipe with a clearance of about 10 mils. 20 holes of 1/4 inch diameter are equally spaced on a circle of 2-5/8 inches diameter on the rotating plate. The stationary plate is located in the second segment of the standard weight steel pipe. The perforations in this plate are made to match exactly the perforations in the rotating wheel, the distance between the two plates being from 3 to 4 mils. The two pipes are joined by a standard flanged joint with four bolts. The rotating and the stationary plates are located at this joint. The air inlet is located on the first section of the pipe. The holding fixtures of the pipes to the table are provided with rubber sheet to provide effective damping.

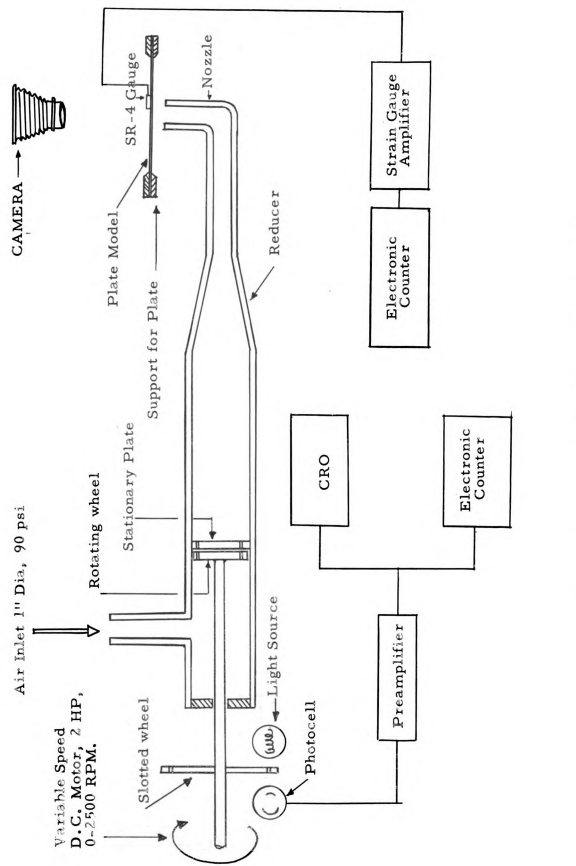

FIGURE 12. Schematic of Pulsed-Air Vibrator

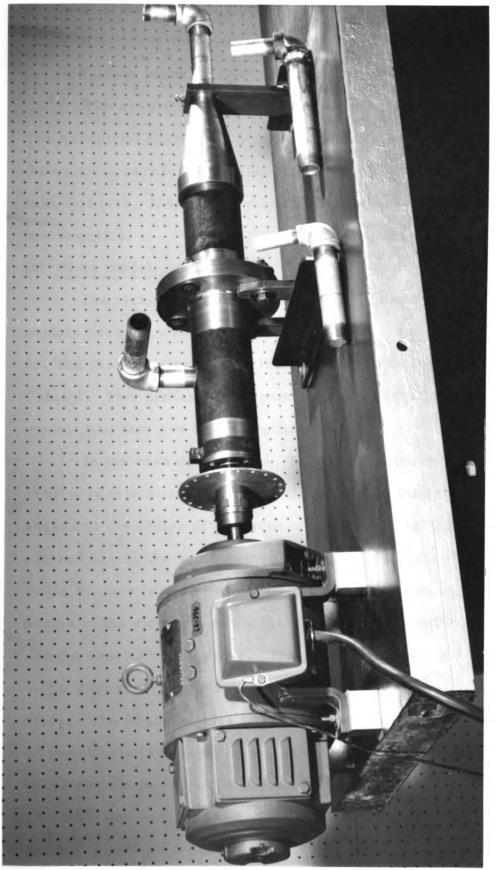

FIGURE 13. Pipe Assembly with Different Size Nozzles

The reducer is bored and machined from a cylindrical block of steel. It tapers from 3 inch diameter to 1 inch diameter over a length of 6 inches thus providing a gradual transition. The reducer is fitted to the pipes by standard pipe threads.

The nozzle consists of two short pipes joined by a 90^{o} elbow. The horizontal portion of the nozzle is threaded into the reducer; the vertical part is of variable diameter. Three different sizes- namely, 1 inch, 3/4 inch and 1/2 inch-have been tried in this investigation.

(e) Plate model.

Six aluminium models have been studied for vibration. The models have been designated A, B, C, D, E, and F as shown in Table 1. The thickness ratios and the support conditions are shown in Table 1. Two methods have been followed in the preparation of the models, and they are briefly outlined below.

In the case of models A, B, and C an end mill is used. First of all a 12 inch square plate is cut out from a uniform thickness large sheet and the center of this square is marked. A 9 inch square is marked having the same center as the large square. A Universal Angle Fixture is truly levelled and one of its sides is set at right angles to the direction of the table of a vertical milling machine by using a sensitive dial gauge. The 12 inch square plate is gripped firmly on the Universal Angle Fixture by means of a Vacuum Chuck, and some studs. The Angle Fixture is tilted so that the desired taper is obtained on the plate. (The taper is adjusted by the use of a dial gauge mounted to the spindle temporarily). A Half inch end mill is used with 1400 R.P.M. The table and saddle feed are 3 to 4-1/2 inches per minute. The milling is started from the edge of a 9 inch square and worked inwards.

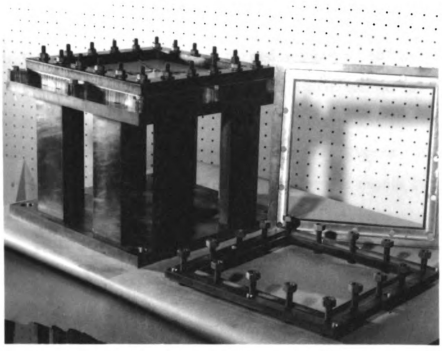

FIGURE 14. Steel Support with Clamped and Simple Plate Supports

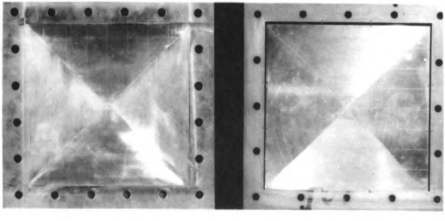

FIGURE 15. Models for Simple and Clamped Supports

The first operation in milling is usually of a deeper cut, which is followed by finer ones. If the table feed and the saddle feed are started together, the table moves along the diagonal of the square, thus giving the required taper along the valleys of the model. After final milling is done, the plate is removed and turned around by 90^{o} and the same procedure is repeated. This is repeated in turn till all the four parts of the square are completed. A fine finish is given to the surface by a fine emery paper fixed on a wooden block (see Figure 15).

In the second method, which is used for the model E, a Fly Cutter is used at 1400 R.P.M. The procedure is the same as before except we start with a 9-1/4 inch square plate. The ridges in this case need no special treatment as they are swept out by the fly cutter as each side is finished.

(f) Support.

In order to obtain nodal lines the plate should be supported horizontally. The response of the support should be sufficiently far away from the plate response to permit any mode of vibration within the frequency range to be excited. These two requirements dictated the construction of a sturdy steel support on which the plate supports are tightly fastened by means of bolts (see Figure 14). The steel support is made of 2 cold rolled steel plates of 14 inch square and 3/4 inch thick. On the top plate a 9 inch square is cut out of the 14 inch square plate so that both the plates have the same center. These two plates are held by means of 8 vertical posts of 8 inch height and having a section 3/4 inch x 3 inches (see Figure 14). Countersunk bolts are used to connect the plates to the vertical post. On the top plate 8 holes are drilled and tapped (3/8 inch size) on the corners and the centers of the sides of a 13 inch square so that the clamped plate support may

be fastened to the steel support by 3/8 inch bolts. Similar holes are drilled and tapped on a 11 inch square to accommodate the simple plate support. A description of the clamped plate support and simple support is given in references [12] and [13].

(g) SR-4 gauge station.

In order to determine the actual plate response, an A-8 type SR-4 gauge was mounted on the vibrating plate at a point very close to the center of the plate. It has a gauge factor of 1.83 ± 2% and resistance of 120 ± 0.3 ohms. The strain gauge is connected to type Q plug-in unit used along with a Tektronix Oscilloscope. The output from Tektronix amplifier is fed to Hewlett-Packard Electronic counter which reads directly the frequencies of the vibrating plate.

(h) Camera to record node lines.

A Burke and James View Camera (f = 21 cm) is mounted at 3 feet directly over the plate by means of a bent steel bar 2 inches x 1/2 inch fixed to the table. Two photo flood lights are focussed on the plate while photographing the nodal lines.

Experimental Procedure

In order to achieve the full potential of the pulsed-air vibrator, the experimenter should control carefully such factors as air flow, relative location of the nozzle with respect to the nodal lines of the vibrating plate, nozzle size, elimination of stray signals in the electrical circuit, rotor speed, damping in the holding fixtures, vibration of the support and the high noise levels. The following is an outline of the steps followed and the factors controlled in a typical vibration test.

Of the 3 sizes of nozzles used, 1 inch and 3/4 inch diameter nozzles seem to work better than 1/2 inch diameter nozzle. In order

to obtain the maximum amplitude of vibration, the nozzle should be near the region of antinode. It is preferred to let a small amount of air pass through the 'chopper' sufficient to notice the amplitudes. The presence of amplitudes is rendered more significant by first sprinkling a small quantity of adsorption alumina (a white powder of 80-200 mesh) on the surface of the plate. The rotor speed is gradually varied until the resonance occurs. At resonance, the alumina powder bounces rapidly near the regions of antinodes, thus showing high amplitudes, and forms a heap along nodal lines and the edge of the plate where amplitudes are zero. The range of frequency variations for a particular mode can be narrowed by reducing the air supply low enough to just notice the movement of alumina powder near the antinode region. Any further refined adjustment of the rotor speed should be made at this stage in order to improve the above observation. The excitation frequency as shown on the Hewlett-Packard Electronic counter is recorded. The Hewlett– Packard Oscilloscope trace is checked so that no stray signals are picked up by the photocell. The nodal lines exhibited by each mode are photographed. A check on the simple support is achieved by noting that the alumina powder at the support is at rest, while those very close to the support tend to bounce up and down.

The type Q plug-in unit is a self contained bridge circuit which is balanced for each test. If the strain gauge is unstressed and the bridge is balanced,no signal should appear on the oscilloscope trace. When the plate is vibrating, the oscilloscope trace shows the strains, which in turn are functions of amplitudes of vibration. At resonance, the oscilloscope trace would show the maximum signal. The finer

adjustments of air supply and rotor speed are made, and resonant frequency recorded.

CHAPTER IV

RESULTS

In this chapter, the bending and vibration test results are compared with the finite difference results. The merits and demerits of the experimental and finite difference results are discussed.

Plate Models A, B

The Moiré fringe patterns for slopes in plate model A are shown in Figure 16 for different loads and different grid positions. Moments and deflections have been found from the enlargements of photos (Fig. 16 b and d) at intervals of 0.1a where 'a' is the side dimension of the plate. Moments and deflections have also been calculated by finite differences for grid spacings of $\lambda = a/6$, $\lambda = a/8$ and $\lambda = a/10$ (Table 2). Moments and deflections found by the Moiré method and those found by finite differences ($\lambda = a/10$) are compared in Figures 18 and 19. Dashed lines show values determined by finite differences ($\lambda = a/10$), while solid lines show those determined by the Moiré method. The top numbers represent the finite difference values while the numbers below them refer to Moiré values. The numbers in the last row represent the Moiré values for corresponding symmetric points in the lower left quadrant of the plate. Extrapolations of the values obtained with three different grid spacings have been worked out wherever permissible and these values are tabulated in Table 6. The extrapolated values are compared with the values obtained by the Moiré method.

In the case of model B, only the finite difference moments and deflections are shown in Figures 20 and 21. The extrapolations of

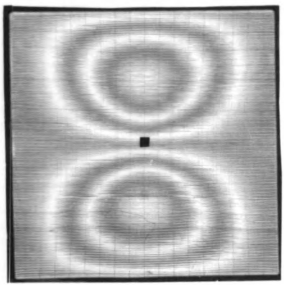

a) $\frac{\partial w}{\partial y}$ Slopes: Load 0.18 psi

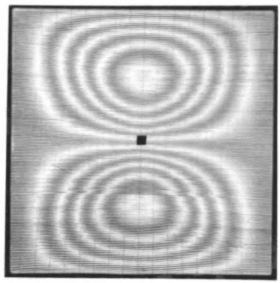

b) $\frac{\partial w}{\partial y}$ Slopes: Load 0.36 psi

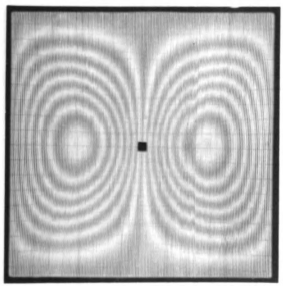

c) $\frac{\partial w}{\partial x}$ Slopes: Load 0.54 psi

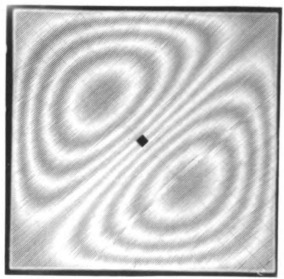

d) $\frac{\partial w}{\partial n}$ ($\theta = 45^{\circ}$) Slopes: Load 0.36 psi

FIGURE 16. Fringe Patterns for Uniformly Loaded Clamped Plate $t_{edge} = 2\, t_{center}$ (Plate Model A)

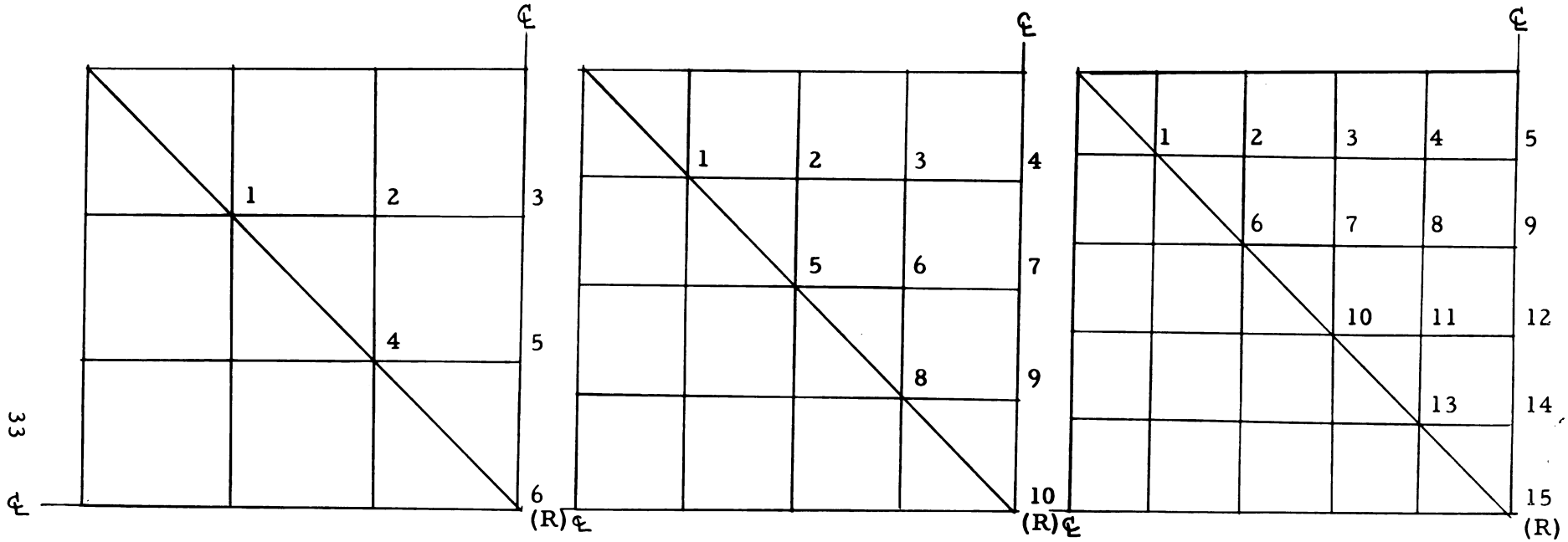

(a) Grid Spacing a/6 (b) Grid Spacing a/8 (c) Grid Spacing a/10

FIGURE 17. Finite Difference Grid used in Plate Models A, B, D, E

TABLE 2. Deflections in Plate Model A

Point	Deflections $\frac{qa^4}{Dr} \cdot 10^{-4}$		
	Grid Spacing a/6	Grid Spacing a/8	Grid Spacing a/10
1	0.356,938,9	0.132,547,1	0.058,628,3
2	0.805,880,1	0.344,480,2	0.167,376,9
3	0.992,517,2	0.511,469,3	0.272,953,3
4	2.116,952,3	0.573,371,7	0.346,074,7
5	2.712,930,2	0.985,146,1	0.371,986,3
6 (R)	3.860,582,7	1.524,806,3	0.506,025,3
7		1.731,159,7	0.852,298,9
8		2.543,140,6	1.099,844,5
9		2.951,975,4	1.188,955,7
10 (R)		3.612,161,0	1.512,951,4
11			2.003,302,5
12			2.183,066,6
13			2.775,661,5
14			3.067,726,7
15 (R)			3.494,591,4

Extrapolations for common point R

6, 8 : 3.292,761,7

6, 10 : 3.285,578,7

6, 8, 10 : 3.281,538,2

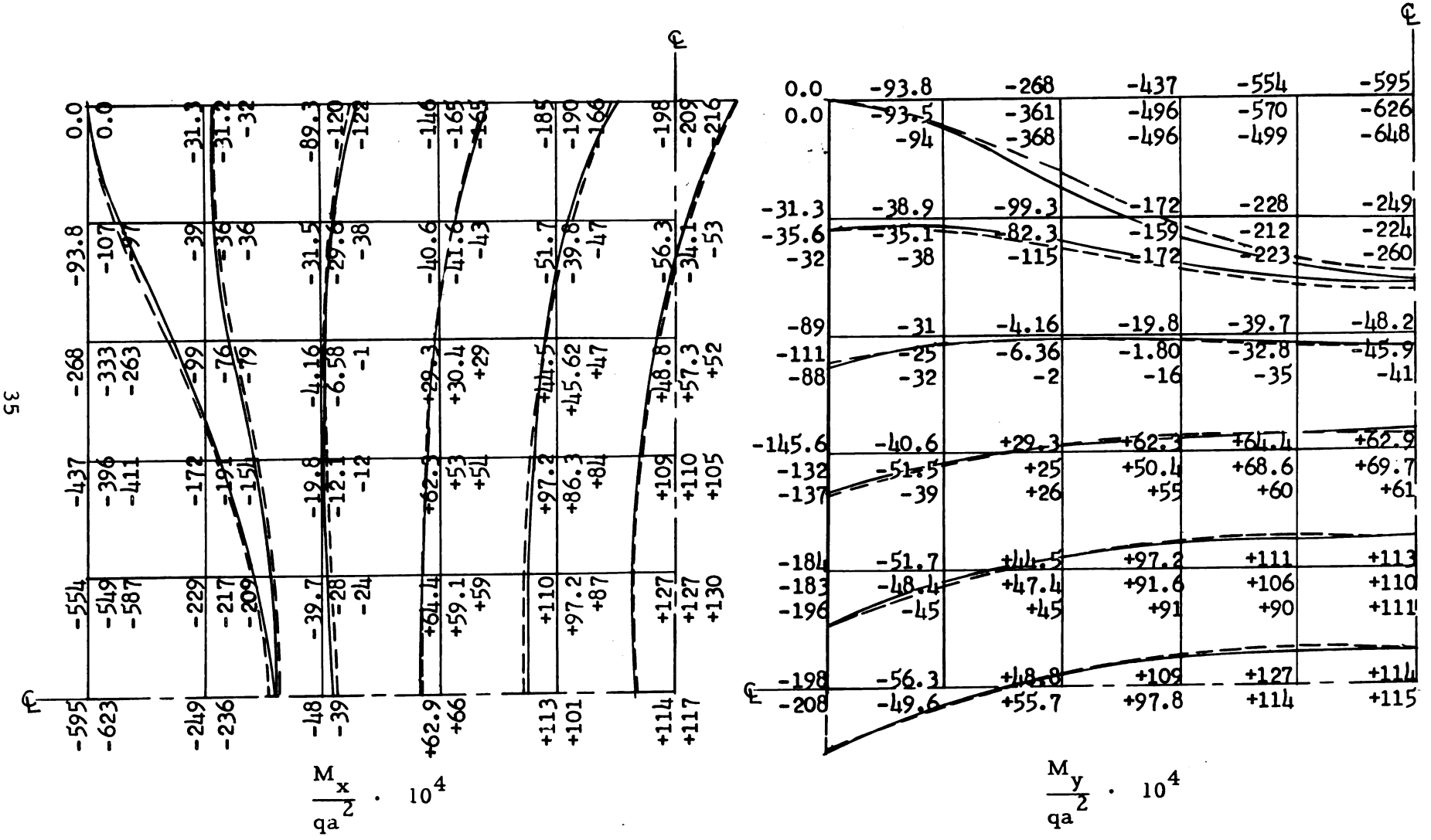

FIGURE 18. Moments for Plate Model A

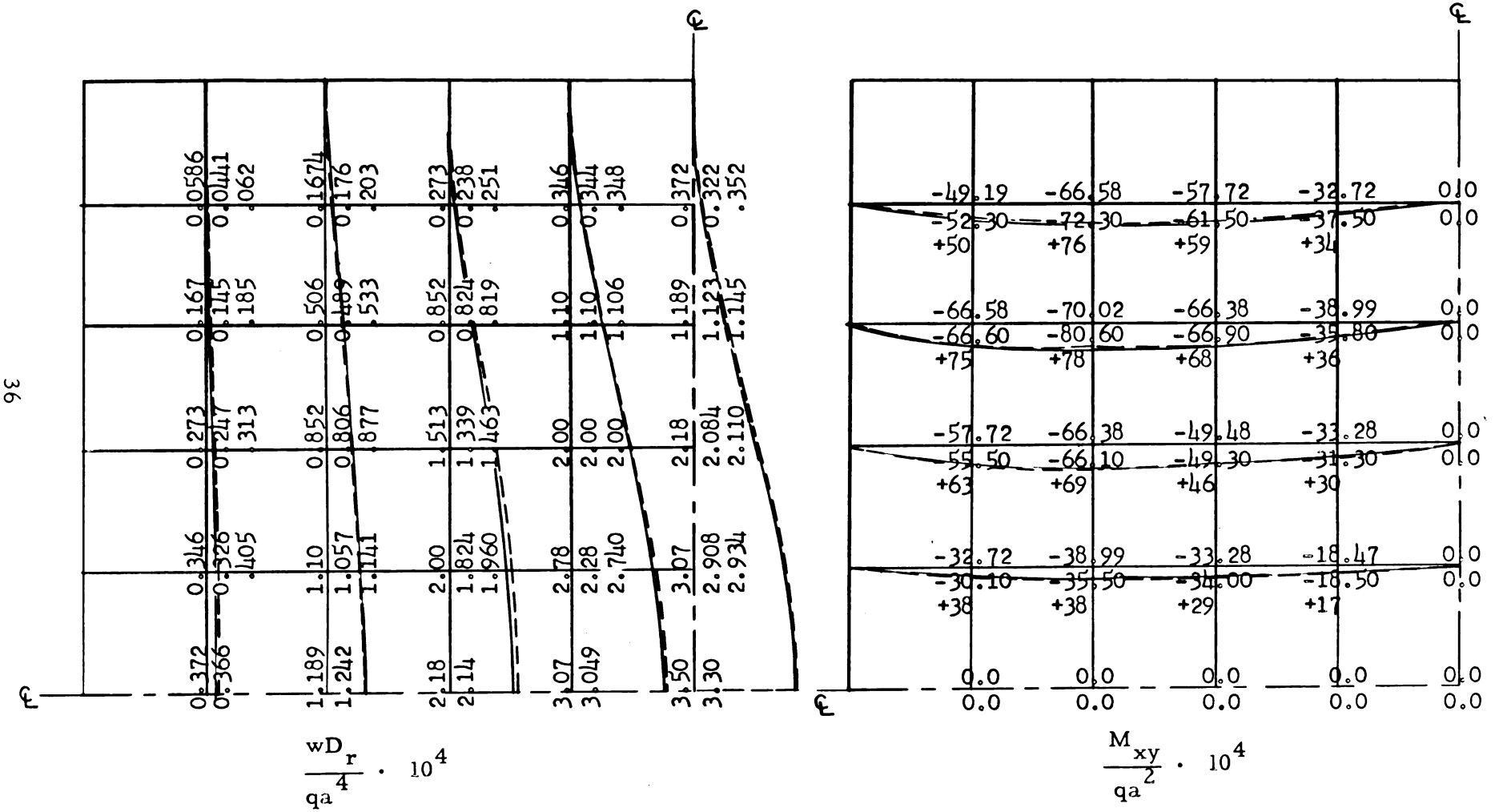

FIGURE 19. Moments and Deflections for Plate Model A

TABLE 3. Deflections in Plate Model B

Point	Deflections $\frac{qa^4}{Dr} \cdot 10^{-4}$		
	Grid Spacing a/6	Grid Spacing a/8	Grid Spacing a/10
1	15.380,521	6.900,719	3.402,714
2	27.011,120	13.948,333	7.606,581
3	30.985,906	18.460,574	10.954,079
4	43.589,674	19.969,298	12.994,944
5	49.248,634	26.449.952	13.672,161
6 (R)	54.045,204	34.478.553	16.106,684
7		37.186,091	22.902,049
8		43.427,288	27.100,369
9		46.440,758	28.505,608
10 (R)		49.026,155	31.631,816
11			37.023,019
12			38.831,532
13			42.547,254
14			44.398,672
15 (R)			46.012,460

Extrapolations for common point R

6, 8 : 42.573,092

8, 10 : 40.654,780

6, 8, 10 : 39.575,730

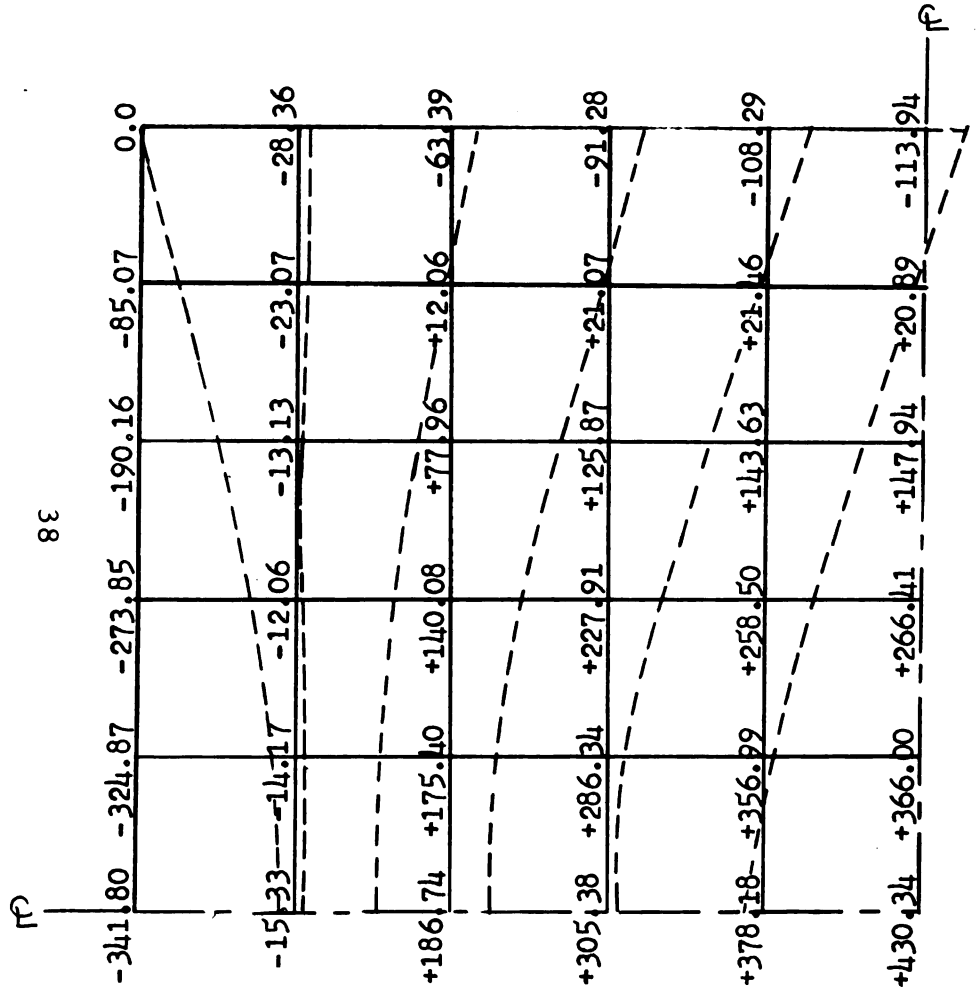

$$\frac{M_x}{qa^2} \cdot 10^4$$

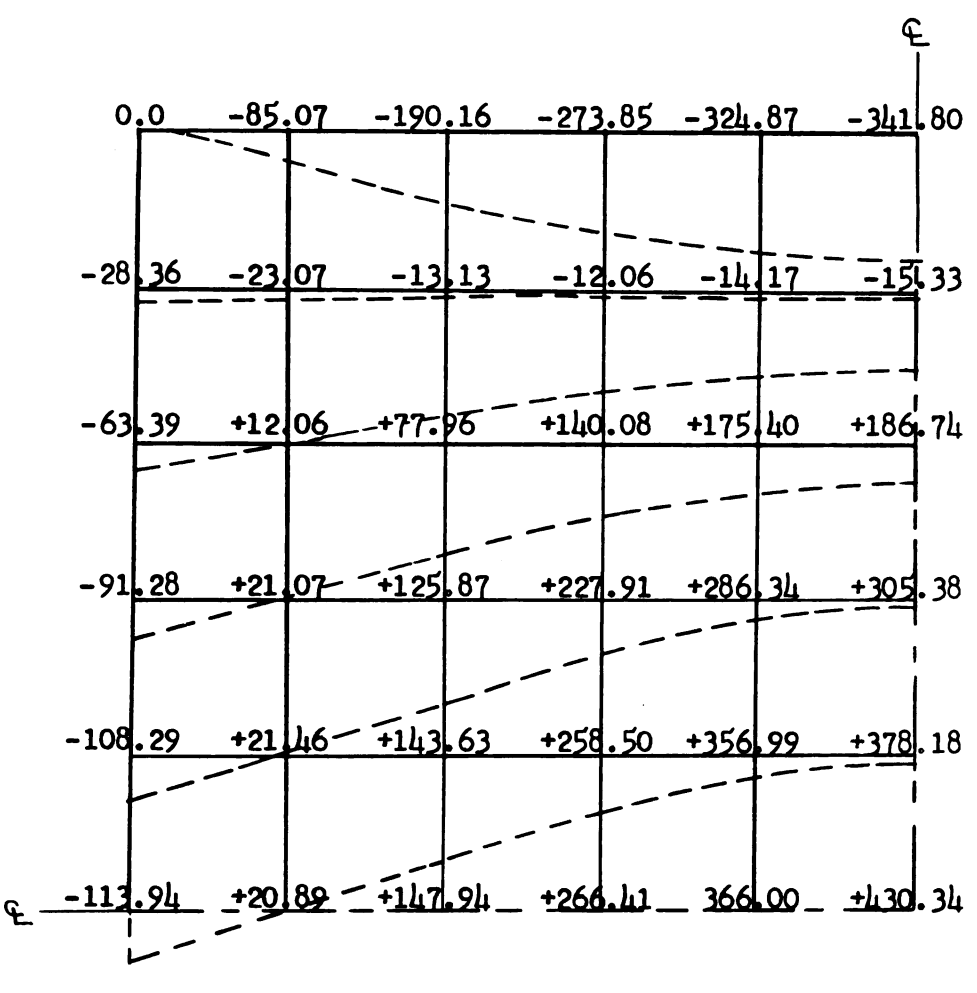

$$\frac{M_y}{qa^2} \cdot 10^4$$

FIGURE 20. Moments for Plate Model B

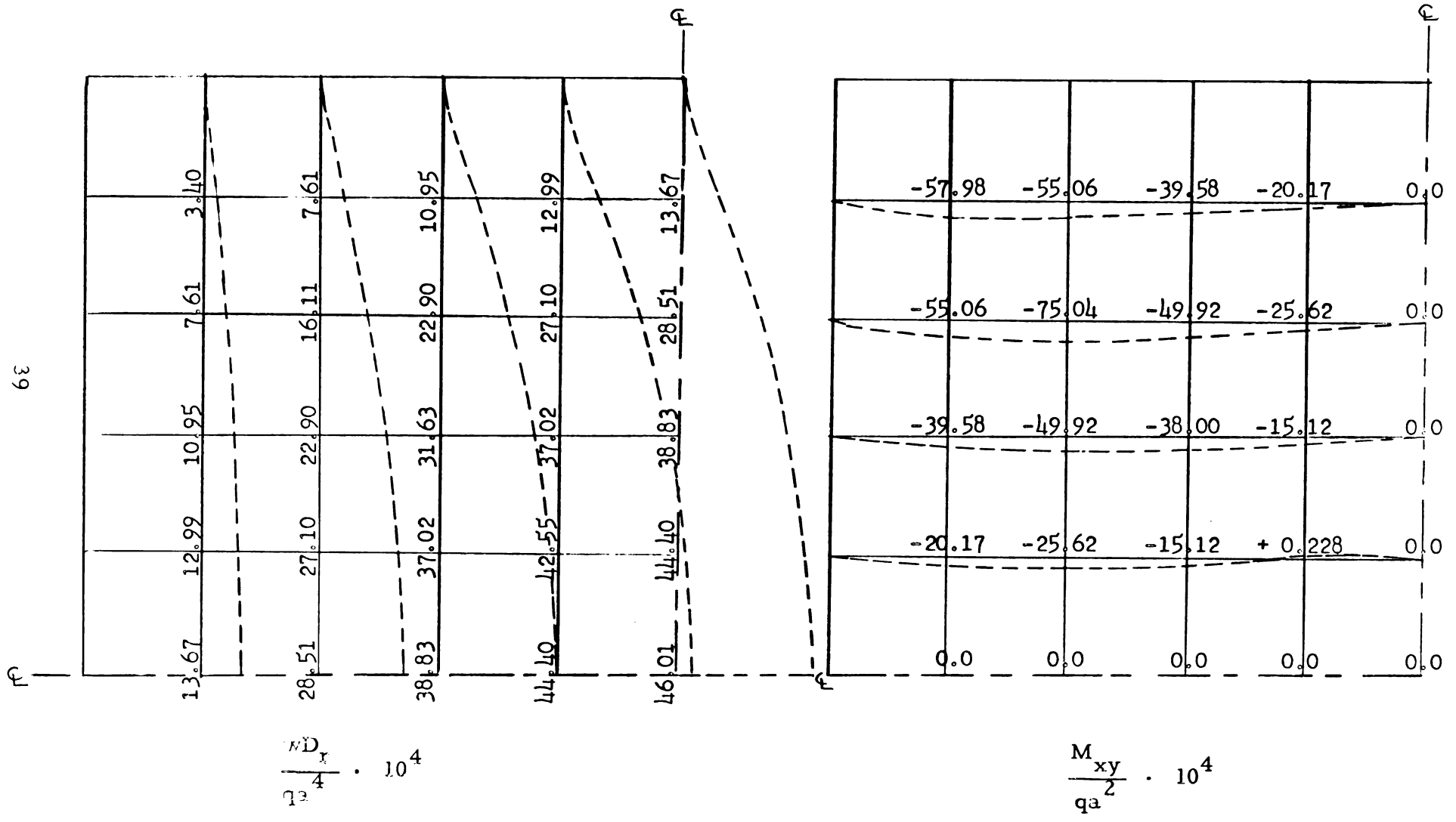

FIGURE 21. Moments and Deflections for Plate Model B

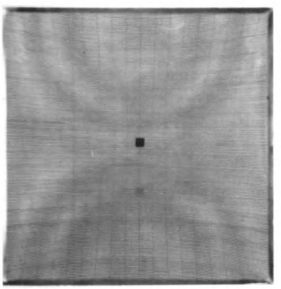

a) $\frac{\partial w}{\partial y}$ Slopes: Load 0.072 psi

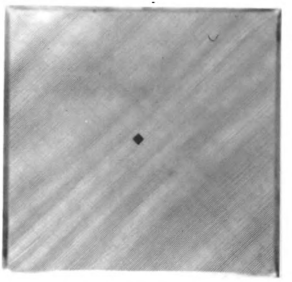

b) $\frac{\partial w}{\partial n}$ ($\theta = 45^{o}$) Slopes: Load 0.108 psi

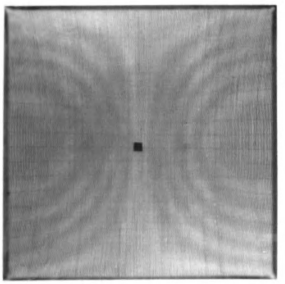

c) $\frac{\partial w}{\partial x}$ Slopes: Load 0.144 psi

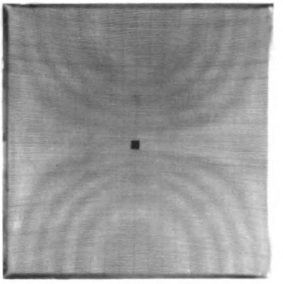

d) $\frac{\partial w}{\partial y}$ Slopes: Load 0.144 psi

FIGURE 22. Fringe Patterns for Uniformly Loaded Simply Supported Plate $t_{edge} = 2\, t_{center}$ (Plate Model D)

TABLE 4. Deflections in Plate Model D

Plate	Deflections $\frac{qa^4}{Dr} \cdot 10^{-4}$		
	Grid Spacing a/6	Grid Spacing a/8	Grid Spacing a/10
1	2.765,189	1.595,511	1.036,898
2	4.688,606	2.871,120	1.920,329
3	5.388,618	3.703,959	2.600,711
4	8.678,977	3.994,683	3.031,666
5	10.191,328	5.453,324	3.179,472
6 (R)	12.833,812	7.171,910	3.694,886
7		7.778,880	5.076,425
8		9.883,184	5.958,423
9		10.867,200	6.262,264
10 (R)		12.369,386	7.195,494
11			8.569,494
12			9.047,210
13			10.505,174
14			11.190,980
15 (R)			12.157,302

Extrapolations for common point R

6, 8 : 11.772,267

8, 10 : 11.780,026

6, 8, 10 : 11.784,763

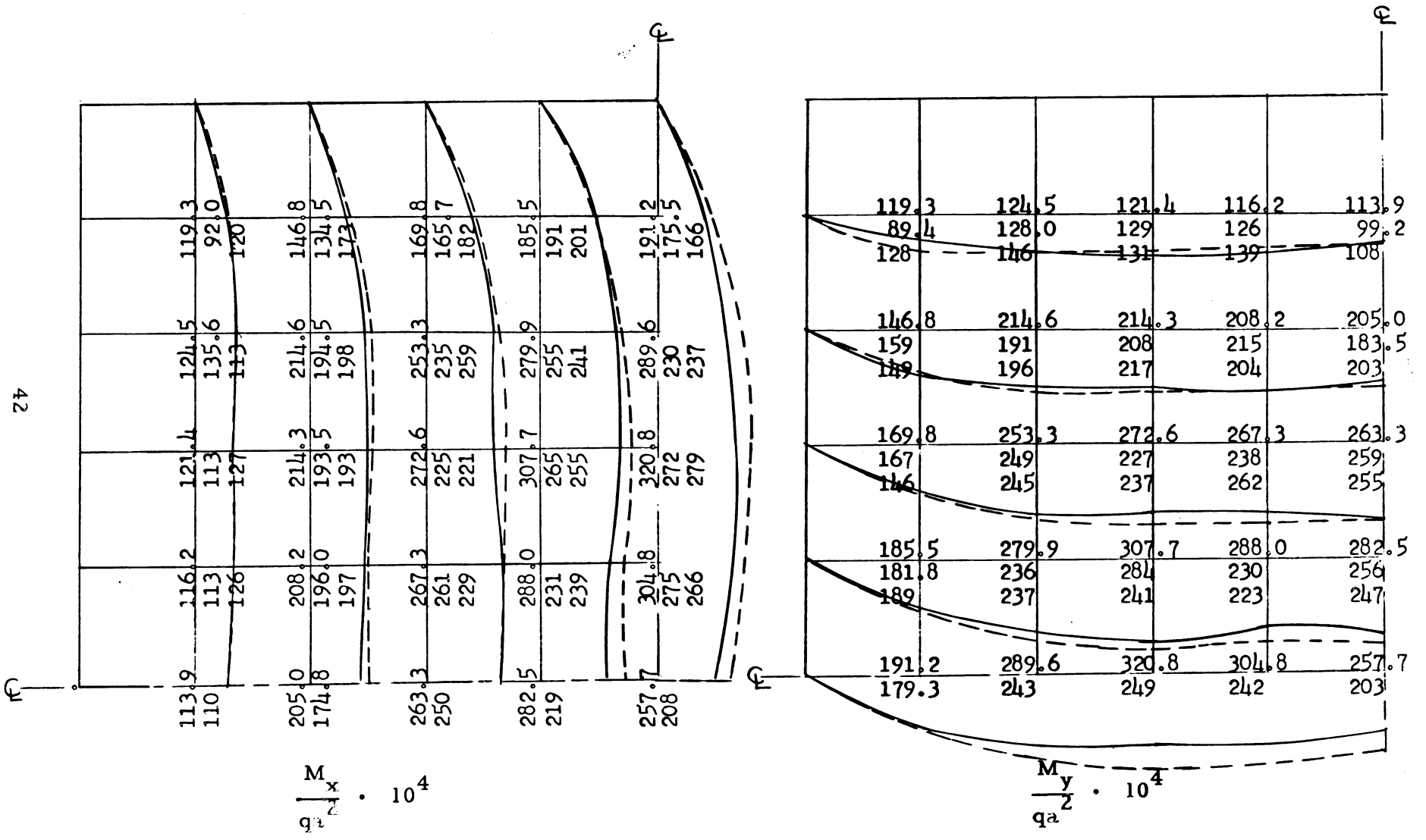

FIGURE 23. Moments for Plate Model D

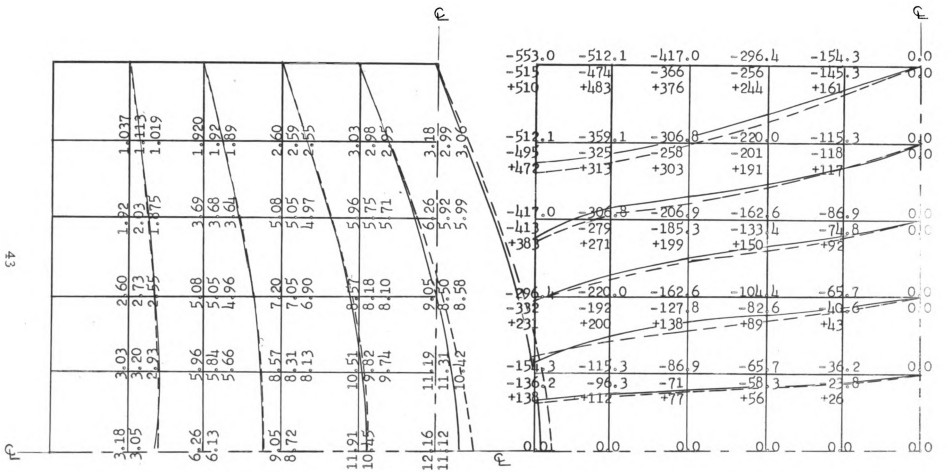

FIGURE 24. Moments and Deflections for Plate Model D

TABLE 5. Deflections in Plate Model E

Point	Deflections $\frac{qa^4}{Dr} \cdot 10^{-4}$		
	Grid Spacing a/6	Grid Spacing a/8	Grid Spacing a/10
1	33.146,245	20,882,548	14.076,655
2	53.688,660	36.682,254	25.832,731
3	60.409,343	46.053,557	34.236,096
4	80.333,430	49.126,448	39.194,855
5	89.058,400	60.709,758	40.827,170
6 (R)	96.275,705	74.988,182	45.223,975
7		79.685,512	59.117,971
8		89.893,656	67.347,465
9		94.799,540	70.062,655
10 (R)		98.929,294	75.328,606
11			84.930,417
12			88.101,545
13			94.314,372
14			97.415,377
15			100.079,462

Extrapolations for common point R

6, 8 : 102.341,052

8, 10 : 102.124,206

6, 8, 10 : 102.002,228

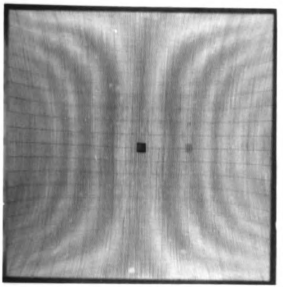

a) $\frac{\partial w}{\partial x}$ Slopes: Load 0.072 psi

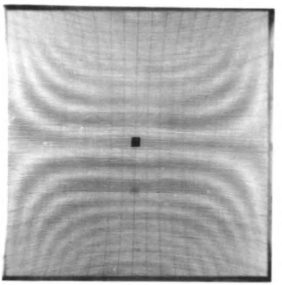

b) $\frac{\partial w}{\partial y}$ Slopes: Load 0.108 psi

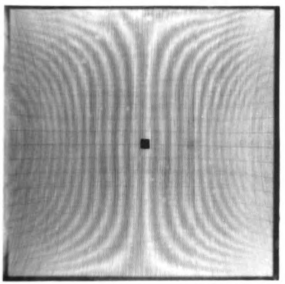

c) $\frac{\partial w}{\partial x}$ Slopes: Load 0.181 psi

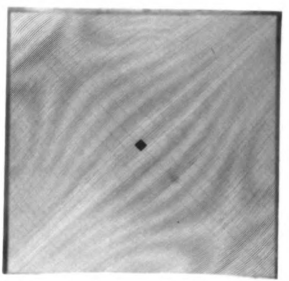

d) $\frac{\partial w}{\partial n}$ ($\theta = 45^{o}$) Slopes: Load 0.108 psi

FIGURE 25. Fringe Patterns for Uniformly Loaded Simply Supported Plate $t_{edge} = 1/2\ t_{center}$ (Plate Model E)

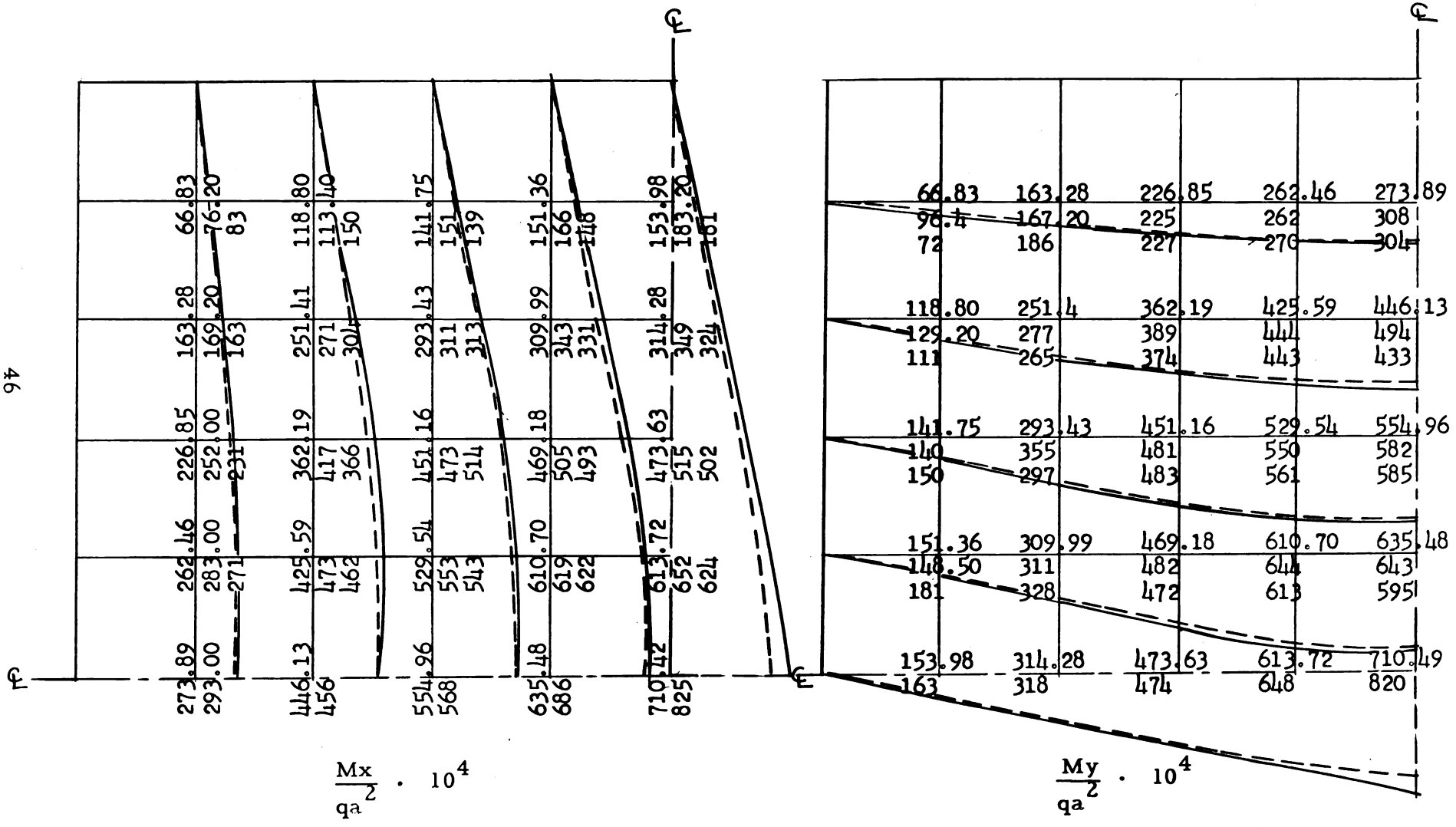

FIGURE 26. Moments for Plate Model E

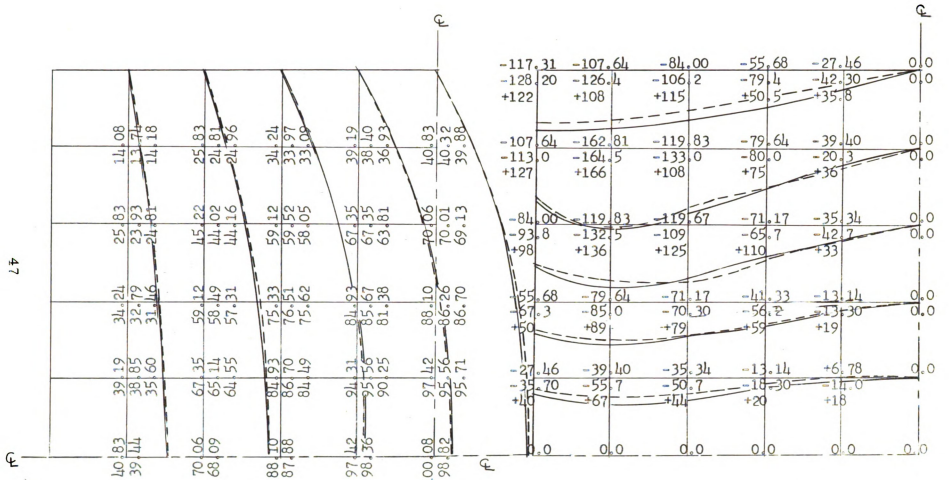

FIGURE 27. Moments and Deflections for Plate Model E

TABLE 6. Extrapolated and Moiré Moments and Deflections

PLATE MODEL	POSITION OF POINT x	POSITION OF POINT y	MOMENT OR DEFLECTION	FINITE DIFFERENCE VALUE λ = a/6	FINITE DIFFERENCE VALUE λ = a/8	FINITE DIFFERENCE VALUE λ = a/10	EXTRAPOLATED VALUE	EXPERIMENTAL VALUE
A CLAMPED $\frac{t_{edge}}{t_{center}} = 2$	0	.5a	Mx	-571.689,898	-587.132,574	-595,178,040	-611.611	623.53
	.5a	0	My					
	.5a	0	Mx	-190.563,300	-195.710,858	-198.392,680	-203.628	208.51
	0	.5a	My					
	.5a	.5a	Mx or My	+110.174,645	+112.671,683	+113.830,567	+115.896	114.80
	.5a	.5a	w	3.860,582,72	3.612,161,00	3.494,591,35	3.281,54	3.2996
B CLAMPED $\frac{t_{edge}}{t_{center}} = \frac{1}{2}$	0	.5a	Mx	-278.873,152	-319.508,770	-341.804,032	-386.888	
	.5a	0	My					
	.5a	0	Mx	- 92.957,717	-106.502,923	-113.934,678	-128.963	
	0	.5a	My					
	.5a	.5a	Mx or My	+460.470,633	+441,241,203	+430.343,366	+407.849	
	.5a	.5a	w	+ 54.045,204	+ 49.026,155	+ 46.012,460	+ 39.575	
SIMPLY SUPPORTED D $\frac{t_{edge}}{t_{center}} = 2$	.5a	.5a	Mx or My	+253.678,448	+256.373,011	+257.685,821	+260.122	+208.00
	.5a	.5a	w	12.833,812,2	12.369,385,9	12.157,302,2	11.784,8	11.12
	0	0	Mxy	-530.916,203	-544.601,050	-553.012,131	-571.210	-553.00
SIMPLY SUPPORTED E $\frac{t_{edge}}{t_{center}} = \frac{1}{2}$	.5a	.5a	Mx or My	+692.861,213	+704.811,375	+710.422,640	+720.523	825.00
	.5a	.5a	w	+ 96.275,705	+ 98.929,294	+100.079,462	+102.002	99.04
	0	0	Mxy	+ 99.438,736	+111.373,590	+117.305,460	+128.488	138.30

Moments are expressed in terms of $qa^2 \cdot 10^{-4}$

Deflections are expressed in terms of $\frac{qa^4}{Dr} \cdot 10^{-4}$

these from different grid spacings and the deflections are shown in Table 3 and 6.

Plate Model D, E

The fringe photos for plate models D and E are shown in Figures 22 and 25, respectively. The moments and deflections determined by both the Moiré method and finite differences are compared in Figures 23, 24, 26, and 27. The deflections and extrapolated values are shown in Table 4, 5, and 6.

Discussion of Bending Results

The possible sources of error arising in the Moiré method have been listed in reference 13 and 17. These are repeated here in order to study their effects with respect to variable thickness plates. These are:

a) Calibration of the material,

b) Plastic behaviour of the material,

c) Lack of precision in loads,

d) Inaccuracies in reduction of data,

e) Variation in plate thickness different from that assumed,

f) Support conditions other than assumed,

g) Changes in dimension of photographic film during developing, and distortion in the enlargements,

h) Membrane action in the plate, and

i) Relative motion of model, grid or camera between exposures.

The curves of Figures 18 and 19 show that the Moiré and difference results are in fair agreement. From Table 6, it is seen that for plate model A, the extrapolated moments are higher than the moments obtained individually for $\lambda = a/6$, $\lambda = a/8$, and $\lambda = a/10$;

it might also be noted that the convergence is fairly rapid. On the otherhand, the extrapolated deflection is smaller than the deflection obtained by three separate grids. The convergence in this case also is quite rapid. The extrapolated moments and deflections differ from the Moiré values by less than one per cent. This, however, may not be the case at other points in the plate. The Moiré moments for these points differ from the finite difference values to a greater per cent although the agreement between Moiré deflections and deflections obtained by finite differences is very close for all points.

These small differences may be due to inaccuracies in the calibration of the model, inaccuracies in reduction of data, or because the actual model differed from the ideal model used for the finite difference calculations. (For plate model A, the actual ratio of edge thickness to center thickness is 1.91 instead of 2.00.) Other sources of error might contribute to the inaccuracy to some extent. Since the maximum deflection was 0.019 inch or about 1/5 of the central plate thickness, the membrane action in the plate is negligible.

From Table 6, it is seen that in the case of plate model B, the negative moments converges monotonically to a higher value, while the positive moment and deflection converges monotonically to a lower value.

In the case of plate model D, (see Figures 23 and 24) the Moiré moments are smaller than the finite difference moments by amounts varying from about 5 per cent to about 20 per cent at the center of the plate and along the valleys. For other points on the plate, the agreement is within about 8 per cent. The Moiré deflections, however, agree very closely with the finite difference deflections.

From Table 6, it is seen that the extrapolations lead to a higher value in moments and lower value in deflection. The maximum deflection and the maximum twisting moment by the Moiré method agree with the extrapolated finite difference values within one per cent. This, however, is not the case with the maximum moment, which differs by 20 per cent. The rapid convergence of the finite differences is also established in Table 6. The great variation of moments at the center of the plate and along the valleys can be attributed to the calibration of the material, the experimental model varying from the ideal finite difference model, inaccuracies in reducing the data and support conditions other than those assumed. The maximum deflection was 0.0239 inch or about 1/4 of the central plate thickness. Hence, the effect of membrane action is negligible.

In the case of plate model E, (see Figures 26 and 27) the Moiré moments are greater than the finite difference moments by amounts varying from about 2 per cent to about 20 per cent at the center of the plate and along the ridges. For other points on the plate the agreement is within 8 per cent. The Moiré deflections agree very closely with the finite difference deflections. From Table 6, it is evident that the extrapolations lead to higher values in moments and deflections. The Moiré deflection is smaller than the extrapolated central deflection by 3 per cent and the Moiré maximum twisting moment is greater than the extrapolated twisting moment by 8 per cent. As in the case of plate model D, the great variation of moments at the center of the plate and along the ridges is attributed to the sources of error as in the case of plate model D. The actual ratio of edge thickness to center thickness is 1/1.94 instead of 1/2. The maximum deflection at the center was 0.1696 inch or about 1/11 of the central plate thickness.

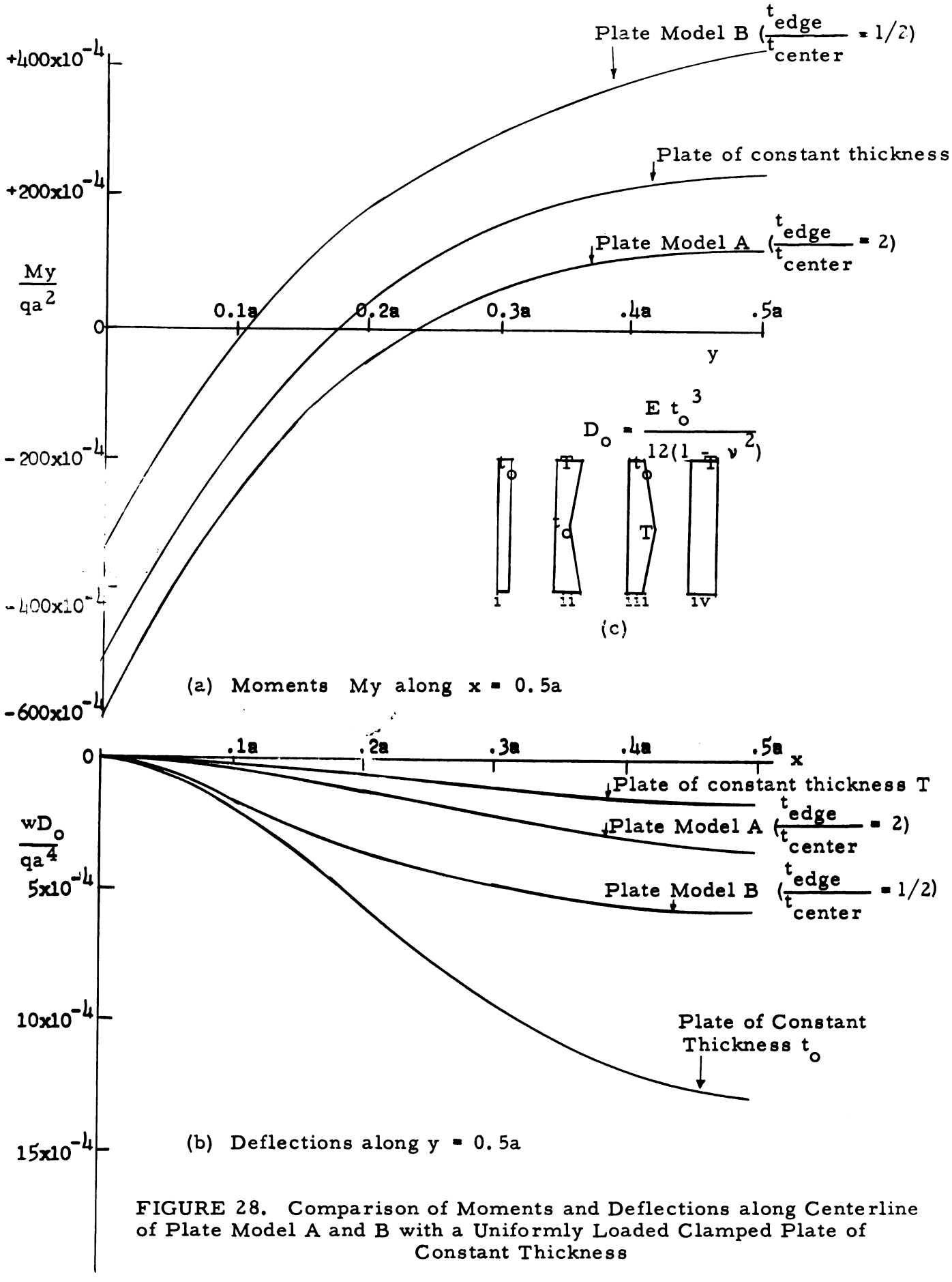

FIGURE 28. Comparison of Moments and Deflections along Centerline of Plate Model A and B with a Uniformly Loaded Clamped Plate of Constant Thickness

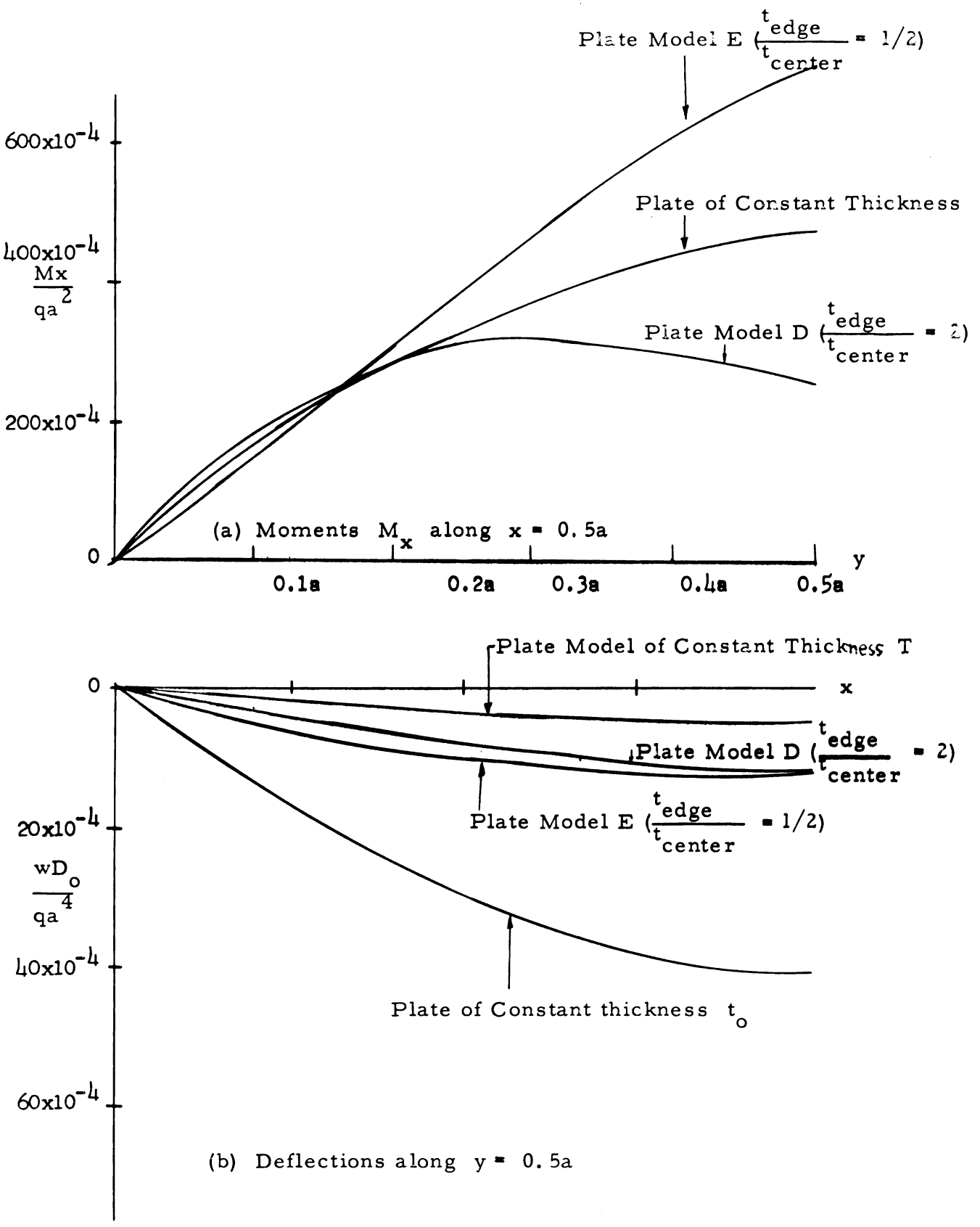

FIGURE 29. Comparison of Moments and Deflections along Centerline of Plate Model D and E with a Uniformly Loaded Simply Supported Plate of Constant Thickness

Hence, the effect of membrance action is negligible.

In Figure 28 (a), My moments are plotted against y at $x = 0.5a$ for clamped plates with thickness ratios shown. For clamped plate with constant thickness, the curve is plotted from values given in reference 17, page 27. The effect of increasing the plate thickness at the edge compared to the thickness at the center is to reduce the center moment and increase the edge moment. The moment curves for $t/t_o > 1$ would lie below the moment curve for constant thickness clamped plate. On the other hand, the effect of decreasing the edge thickness is to increase the center moment and decrease the edge moment; all the moment curves for $t/t_o < 1$ would lie above the moment curve for constant thickness clamped plate. In Figure 28 (b), the deflections along a center line of plate models A and B are compared with the deflections of clamped plates of constant thicknesses of t_o and T (see Figure 28 (c)). The deflection curves for constant thickness plates t_o and T would set up bounding lines within which the deflection curves for plates with thickness ratios of $t/t_o \gtrless 1$ would lie. The effect of increasing the edge thickness is to decrease the deflections, and conversly, decreasing the edge thickness would increase the deflections.

In Figure 29 (a), Mx moments are plotted against y at $x = 0.5a$ for simply supported plate models E and D and also for a simply supported plate of constant thickness. The moment values for simply supported plate of constant thickness are taken from reference 13, page 46. The effect of decreasing or increasing the edge thickness of plate does not seem to appreciably change the moments compared to the moments in plates of constant thickness up to quarter span. Most of the variation occurs in the central region of the plate bounded by quarter span lines.

In the case of plate model E, the center moment increases while in the case of plate model D, the center moment decreases compared to the moment in a plate of constant thickness. In Figure 29 (b), the deflections along the center line of plate models D and E are compared with deflection curves for constant thickness plates t_o and T (see Figure 28 (c)). The behaviour of deflections is the same as in the case of clamped plates.

Vibration Results

The frequencies calculated by finite differences and those determined by experiment have been expressed in terms of a parameter

$$\omega_r = \sqrt{\frac{Dr}{\rho t_r a^4}}$$

where

Dr = flexural rigidity = $\frac{Et_r^3}{12(1 - \nu^2)}$ (lb. in.)

E = Young's modulus of elasticity (lbs/in^2)

ν = Poisson's ratio

a = length of the side of plate (in)

ρ = plate mass density (lb. sec^2/in^4).

The measured frequency and the parameter ω_r are related by

$$\omega = \alpha \omega_r$$

where α is a dimensionless number which is comparable for the different plates despite differences in physical constants and dimensions. The values of α or ω/ω_r are given in Table 7 for clamped plate models A, B, and C. Table 8 shows the values ω/ω_r for simply supported plate models E, D, and F. The node patterns for these different models are

TABLE 7. Natural Frequencies in Clamped Variable Thickness Plates

Model	Mode	Finite Difference Frequency ω/ω_r			Exper. Frequency ω/ω_r
		$\lambda = a/6$	$\lambda = a/8$	Extrapolated Frequency	
Model A	1	59.780	61.534	63.790	63.20
$t_{edge} =$	2	104.583	111.464	120.392	116.70
$2t_{center}$	3	149.239	161.688	178.385	172.20
	4	157.147	171.846	190.745	200.48
	5	150.928	174.234	204.199	201.55
	6	205.307	229.199	259.918	258.57
Model B	1	18.204	19.399	20.936	21.58
$t_{edge} =$	2	36.397	39.541	43.584	46.54
$1/2t_{center}$	3	54.379	60.165	67.604	70.28
	4	60.304	67.936	77.749	87.00
	5	62.752	70.359	80.139	
	6	77.282	85.405	95.848	107.96
Model C	1				179.81
$t_{edge} =$	2				275.57
$5.3t_{center}$	3				384.43
	4				454.25

TABLE 8. Natural Frequencies in Simply Supported Variable Thickness Plates

Model	Mode	Finite Difference Frequenices ω/ω_r			Exper. Frequency ω/ω_r
		$\lambda = a/6$	$\lambda = a/8$	Extrapolated Frequency	
Model D	1	30.836	31.431	32.196	32.84
$t_{edge} =$	2	72.505	75.263	78.809	80.03
$2\ t_{center}$	3	122.643	122.163	121.544	128.63
	4	130.412	134.064	138.759	139.55
	5	124.479	136.759	152.549	145.85
	6	175.524	189.524	207.523	
Model E	1	13.534	13.567	13.568	14.20
$t_{edge} =$	2	31.371	32.169	33.195	34.78
$1/2t_{center}$	3	49.272	50.587	52.279	53.97
	4	56.611	60.771	66.121	68.16
	5	58.782	62.816	68.001	70.93
	6	73.288	77.685	83.339	
Model F	1				99.99
$t_{edge} =$	2				189.98
$5.3t_{center}$	3				304.97
	4				359.83
	5				364.61

TABLE 9. Physical Constants of the Plate Material

Material	Modulus of Elasticity, (E) lb/in^2	Mass Density (ρ) $\frac{lb.\ sec^2}{in^4}$	Poisson's Ratio (ν) (Dimensionless)
Aluminum	10.53×10^6	2.596×10^{-4}	0.263

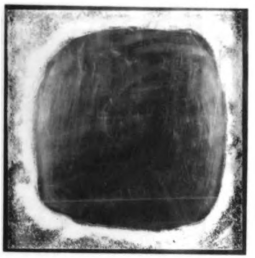

First Mode

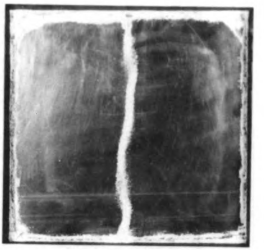

Second Mode

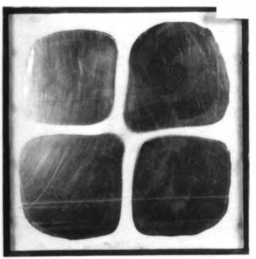

Third Mode

Fourth Mode

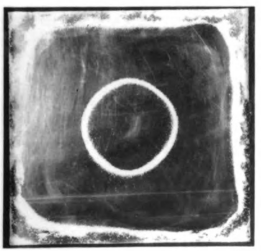

Fifth Mode

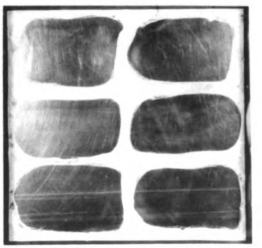

Sixth Mode

FIGURE 30. Node Pattern on Plate Model A

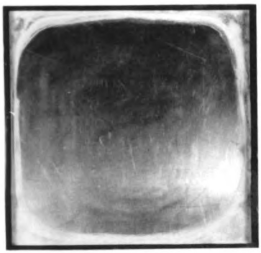

First Mode

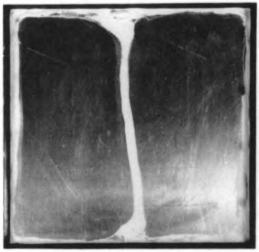

Second Mode

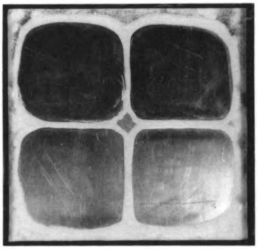

Third Mode

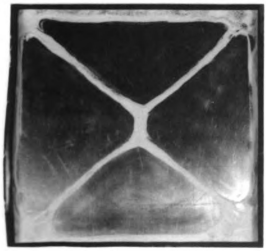

Fourth Mode

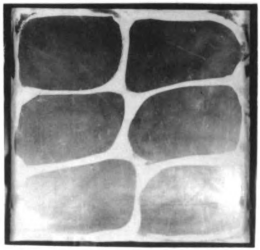

Sixth Mode

FIGURE 31. Node Patterns on Plate Model B

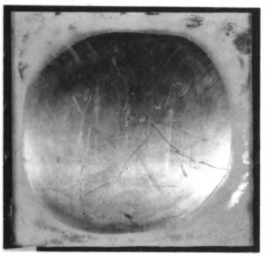

First Mode

Second Mode

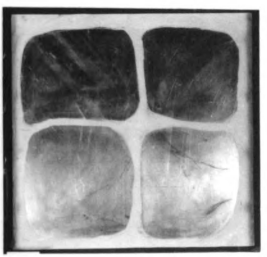

Third Mode

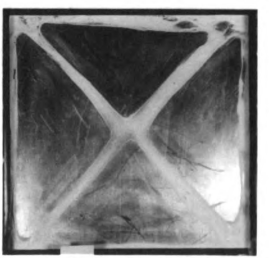

Fourth Mode

FIGURE 32. Node Patterns on Plate Model C

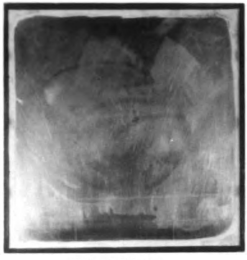

First Mode

Second Mode

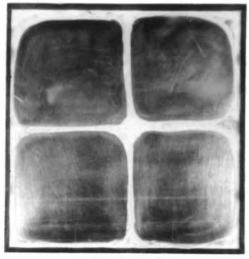

Third Mode

FIGURE 33. Node Patterns on Plate Model D

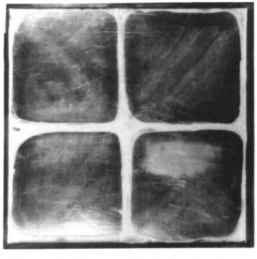

Third Mode

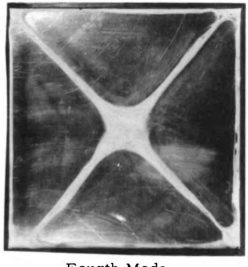

Fourth Mode

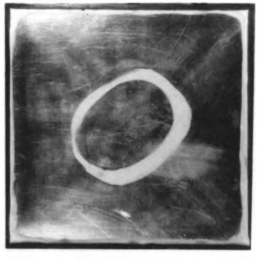

Fifth Mode

FIGURE 34. Node Patterns on Plate Model F

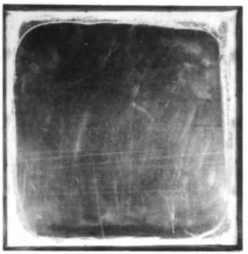

First Mode

Second Mode

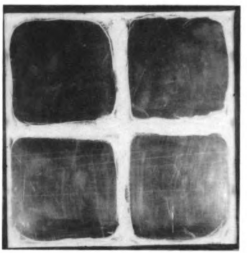

Third Mode

Fourth Mode

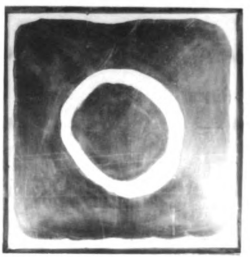

Fifth Mode

FIGURE 35. Node Patterns on Plate Model E

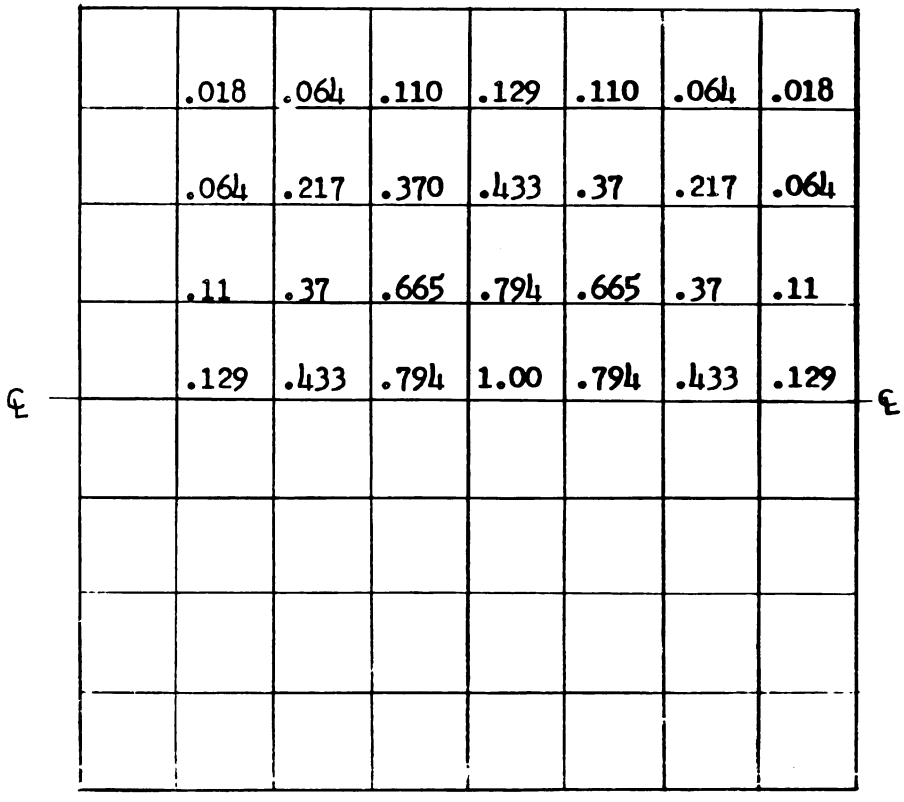

First Mode

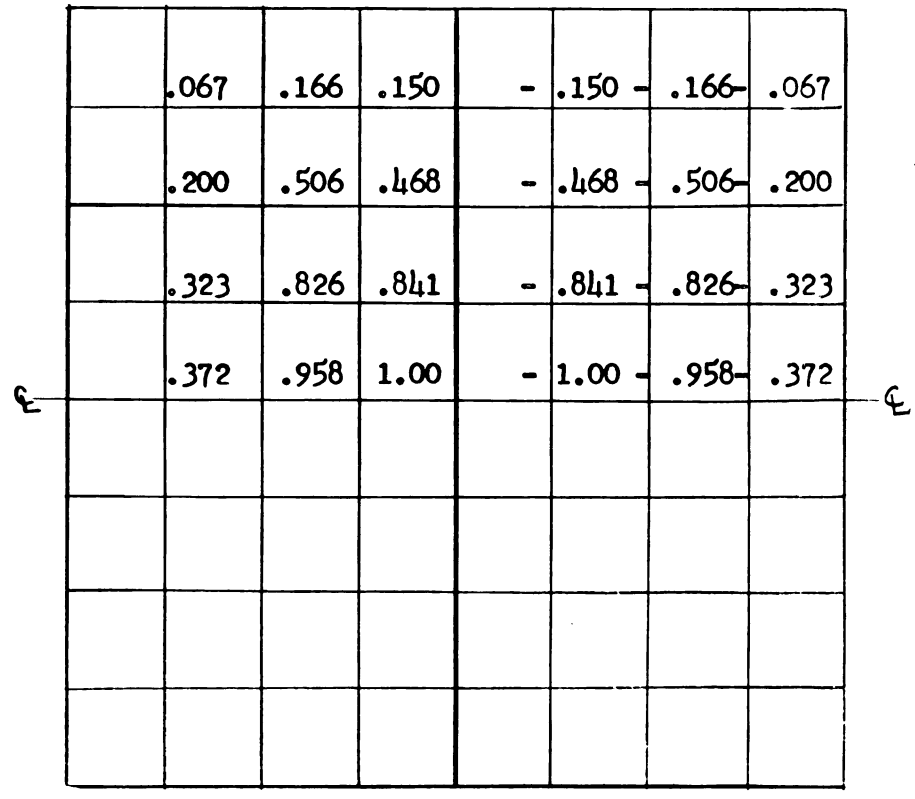

Second Mode

FIGURE 36. Relative Amplitudes in Plate Model A

+	.191+	.421+	.365	-	.365-	.421-	.191
+	.421+	1.00+	.896	-	.896-	1.00-	.421
+	.365+	.896+	.929	-	.929-	.896-	.365
-	.365-	.896-	.929	+	.929+	.896+	.365
-	.421-	1.00-	.896	+	.896+	1.00+	.421
-	.191-	.421-	.365	+	.365+	.421+	.191

Third Mode

	+	.099+	.356+	.497+	.356+	.099	
-	.099	+	.626+	1.00+	.626	-	.099
-	.356-	.626	+	.589	-	.626-	.356
-	.497-	1.0 -	.589	-	.589-	1.00-	.497
-	.356-	.626	+	.589	-	.626-	.356
-	.099	+	.626+	1.0 +	.626	-	.099
	+	.099+	.356+	.497+	.356+	.099	

Fourth Mode

FIGURE 37. Relative Amplitudes in Plate Model A

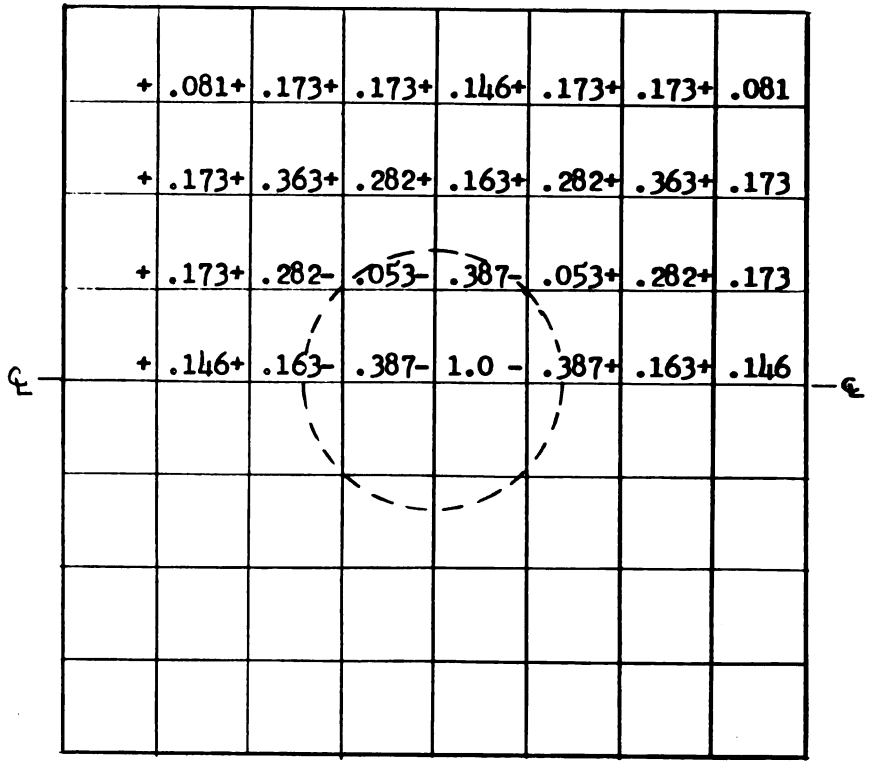

Fifth Mode

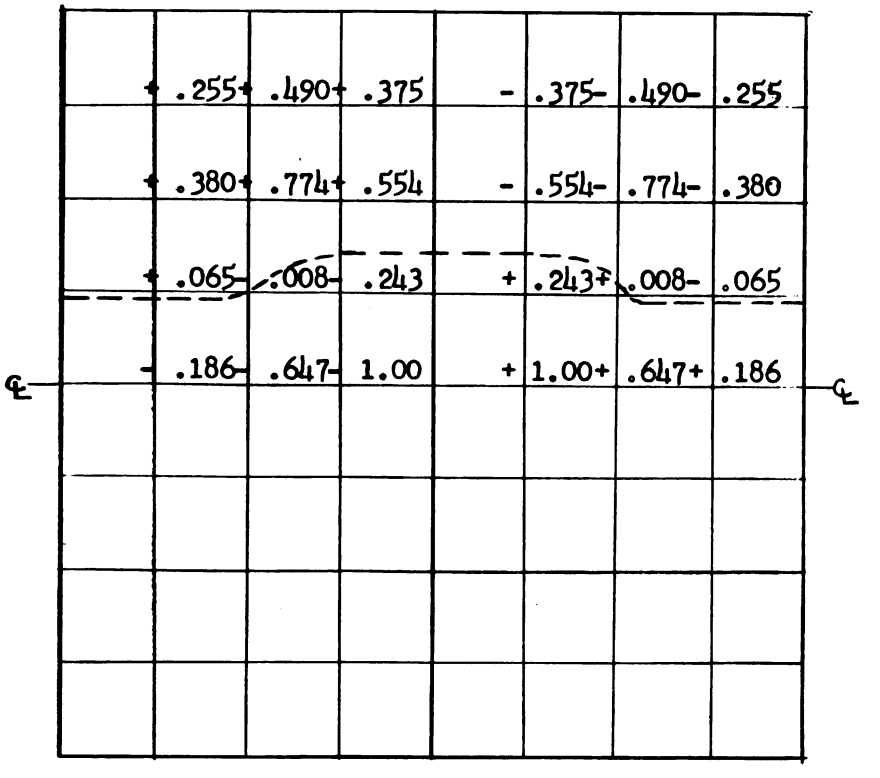

Sixth Mode

FIGURE 38. Relative Amplitudes in Plate Model A

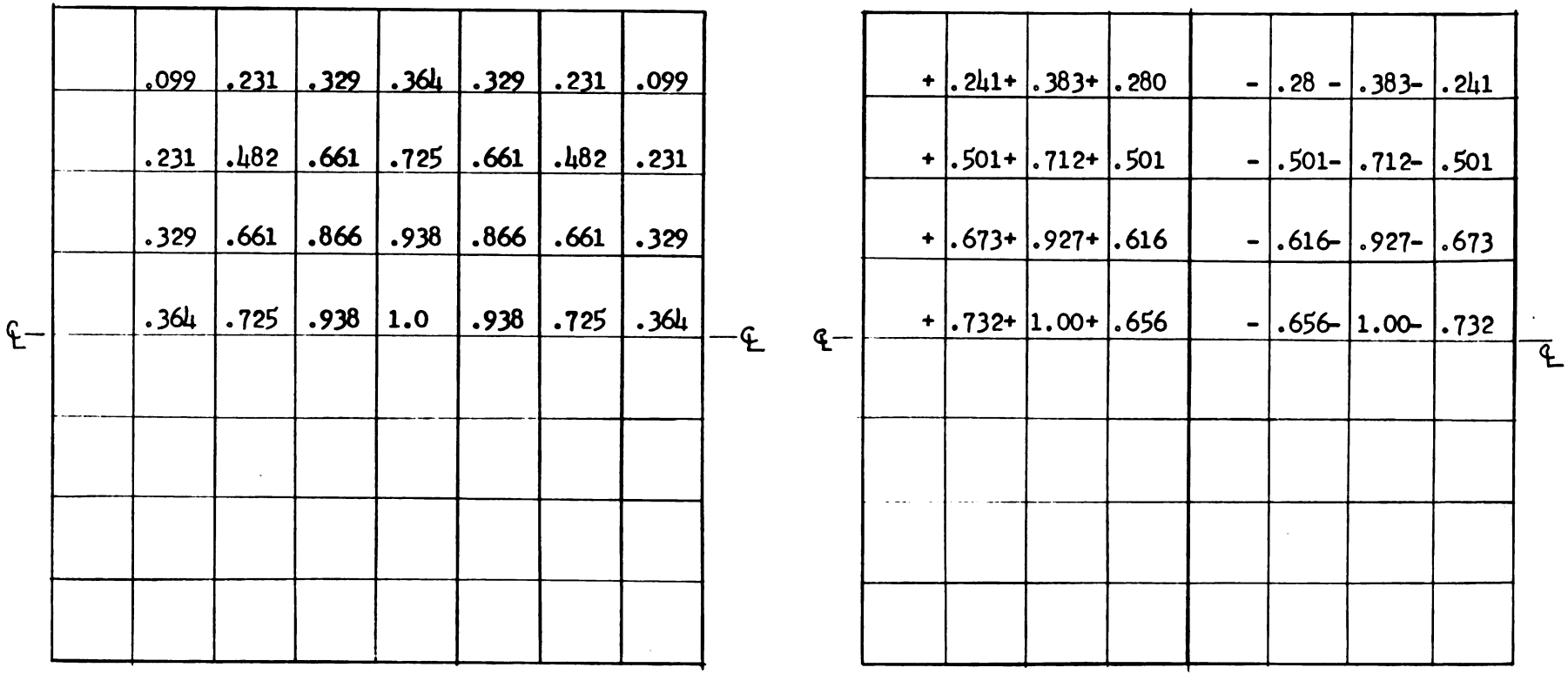

First Mode

Second Mode

FIGURE 39. Relative Amplitudes in Plate Model B

+	.508+	.777+	.56	-	.56 -	.777-	.508
+	.73 +	1.0 +	.696	-	.696-	1.0 -	.73
+	.462+	.657+	.425	-	.425-	.657-	.462
-	.462-	.657-	.425	+	.425+	.657+	.462
-	.73 -	1.0 -	.696	+	.696+	1.0 +	.73
-	.508-	.777-	.56	+	.56 +	.777+	.508

Third Mode

	+	.303+	.772+	1.0 +	.772+	.303	
-	.303	+	.613+	.921+	.613	-	.303
-	.772-	.613	+	.30	-	.613-	.772
-	1.0 -	.921-	.30	-	.30 -	.921-	1.0
-	.772-	.613	+	.30	-	.613-	.772
-	.303	+	.613+	.921+	.613	-	.303
	+	.303+	.772+	1.0 +	.772+	.303	

Fourth Mode

FIGURE 40. Relative Amplitudes in Plate Model B

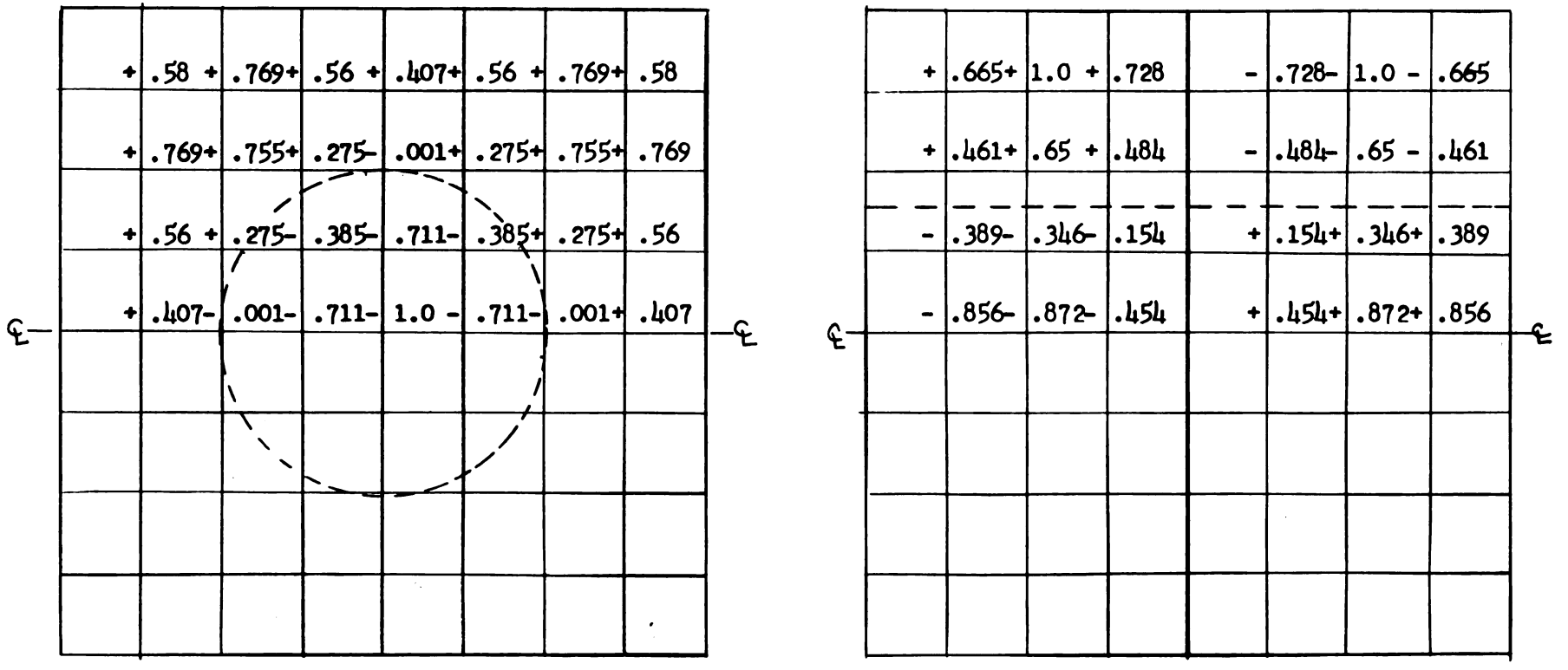

Fifth Mode

Sixth Mode

FIGURE 41. Relative Amplitudesin Plate Model B

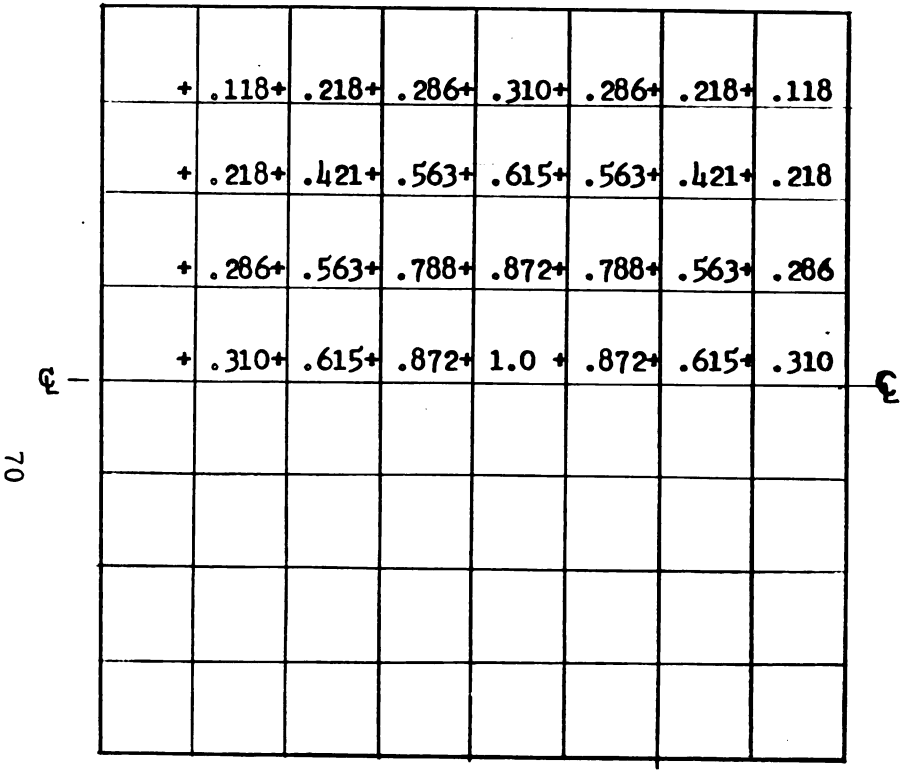

First Mode

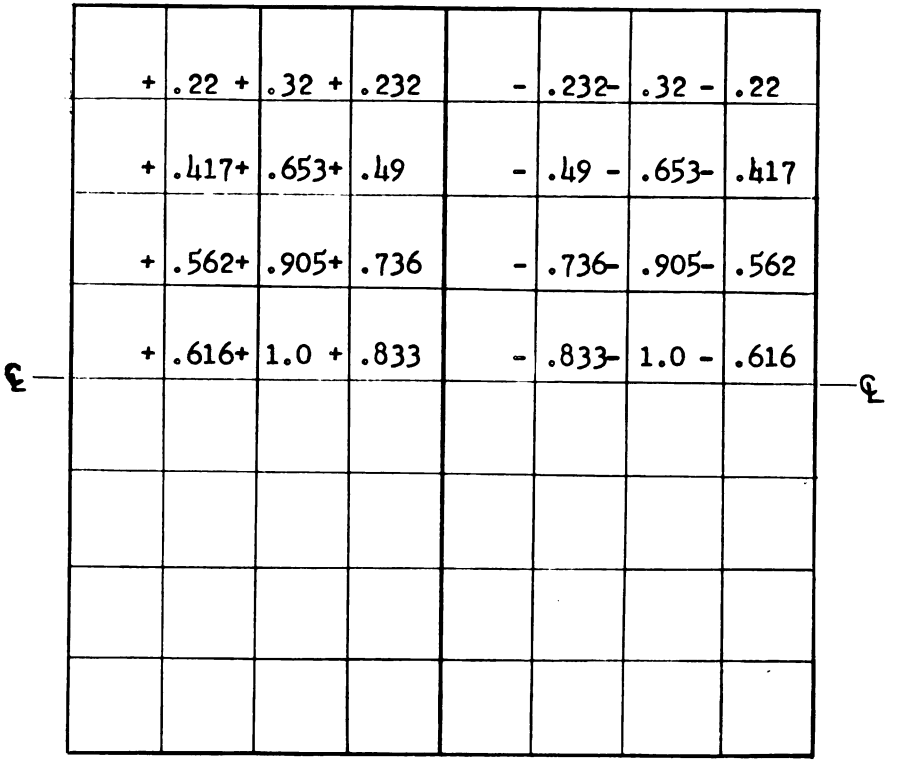

Second Mode

FIGURE 42. Relative Amplitudes in Plate Model D

+	.412+	.611+	.45	-	.45 -	.611-	.412
+	.611+	1.0 +	.765	-	.765-	1.0 -	.611
+	.45 +	.765+	.667	-	.667-	.765-	.45
-	.45 -	.765-	.667	+	.667+	.765+	.45
-	.611-	1.0 -	.765	+	.765+	1.0 +	.611
-	.412-	.611-	.45	+	.45 +	.611+	.412

Third Mode

	+	.195+	.551+	.724+	.551+	.195	
-	.195	+	.661+	1.0 +	.661	-	.195
-	.551-	.661	+	.485	-	.661-	.551
-	.724-	1.0 -	.485	-	.485-	1.0 -	.724
-	.551-	.661	+	.485	-	.661-	.551
-	.195	+	.661+	1.0 +	.661	-	.195
	+	.195+	.551+	.724+	.551+	.195	

Fourth Mode

FIGURE 43. Relative Amplitudes in Plate Model D

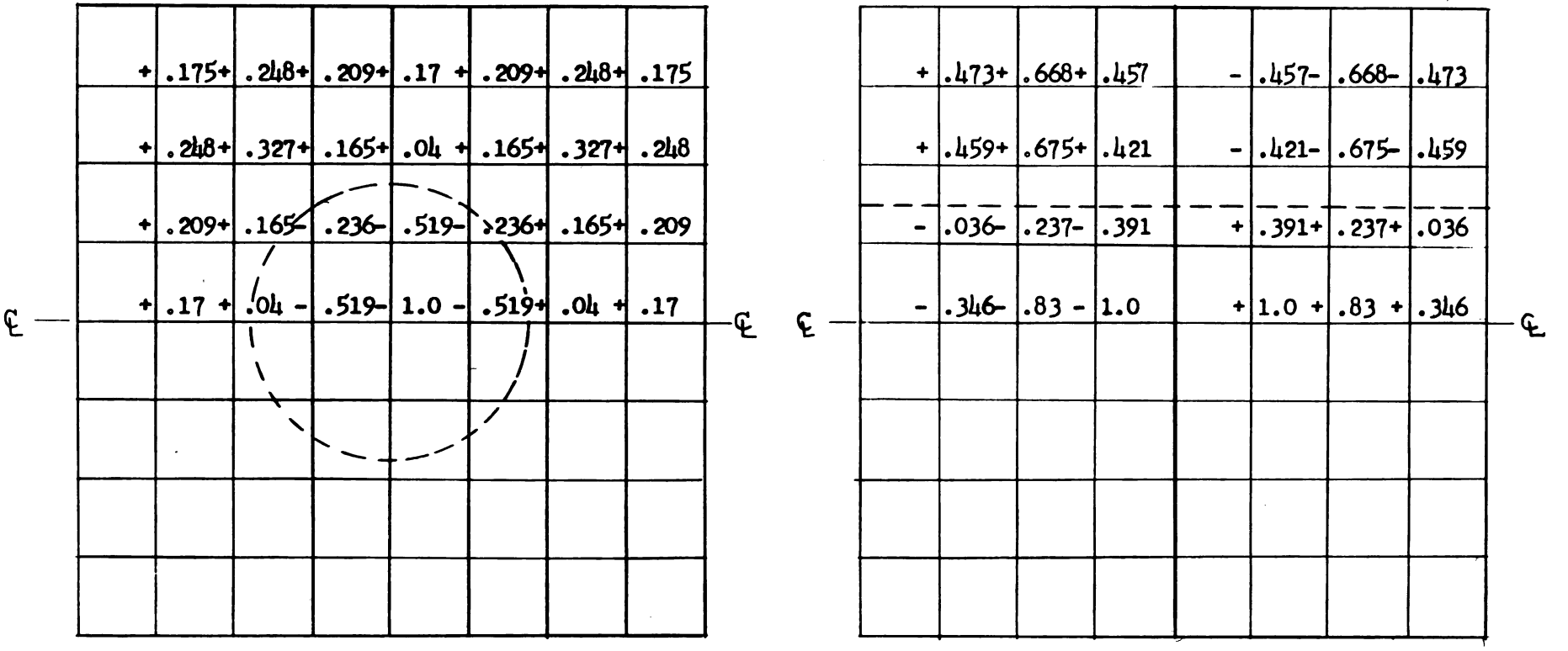

Fifth Mode

Sixth Mode

FIGURE 44. Relative Amplitudes in Plate Model D

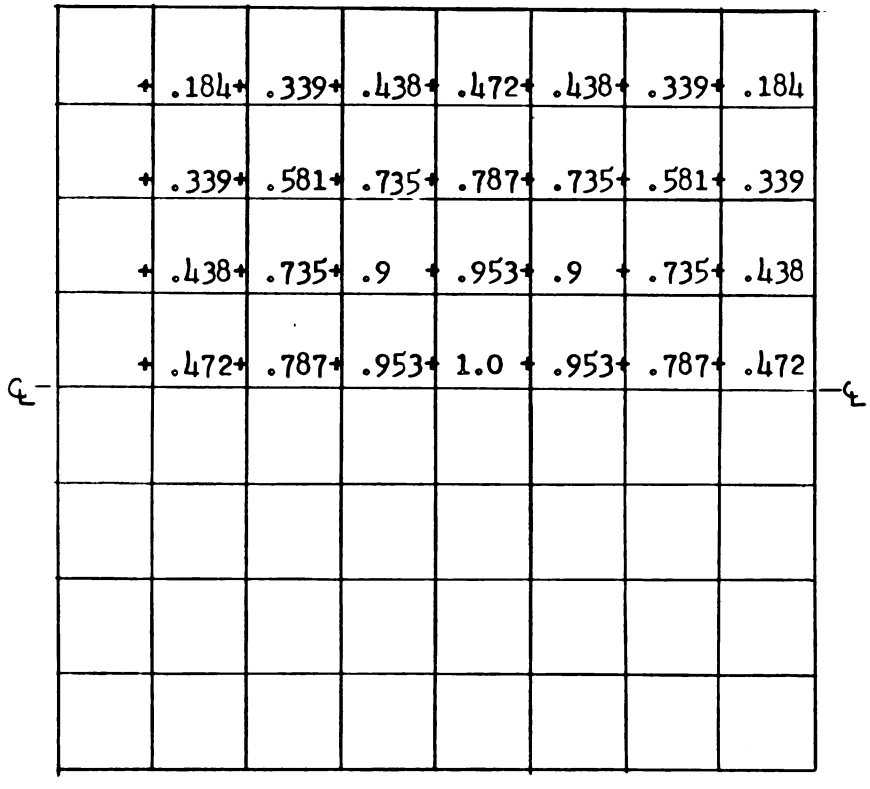

First Mode

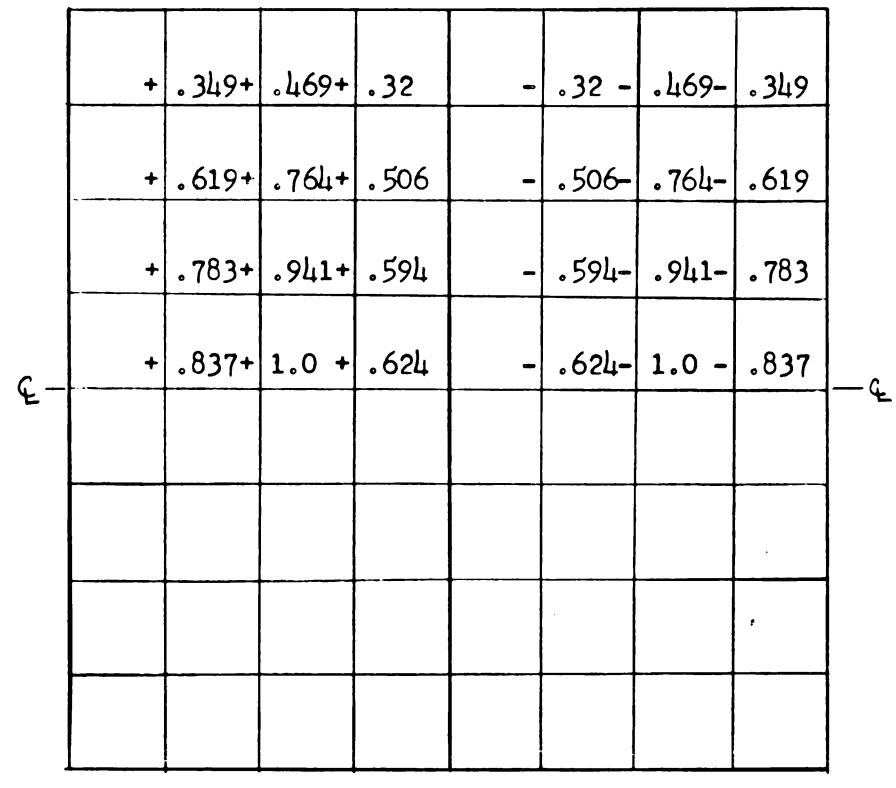

Second Mode

FIGURE 45. Relative Amplitude in Plate Model E

+	.64	+ .846	+ .572	−	.572	− .846	− .64
+	.846	+ 1.00	+ .651	−	.651	− 1.0	− .846
+	.572	+ .651	+ .391	−	.391	− .651	− .572
−	.572	− .651	− .391	+	.391	+ .651	+ .572
−	.846	− 1.0	− .651	+	.651	+ 1.0	+ .846
−	.64	− .846	− .572	+	.572	+ .846	+ .64

Third Mode

	+	.321	+ .782	+ 1.0	+ .782	+ .321	
−	.321	+	+ .564	+ .838	+ .564	−	− .321
−	.782	− .564	+	+ .264	−	− .564	− .782
−	1.0	− .838	− .264	−	− .264	− .838	− 1.0
−	.782	− .564	+	+ .264	−	− .564	− .782
−	.321	+	+ .564	+ .838	+ .564	−	− .321
	+	.321	+ .782	+ 1.0	+ .782	+ .321	

Fourth Mode

FIGURE 46. Relative Amplitudes in Plate Model E

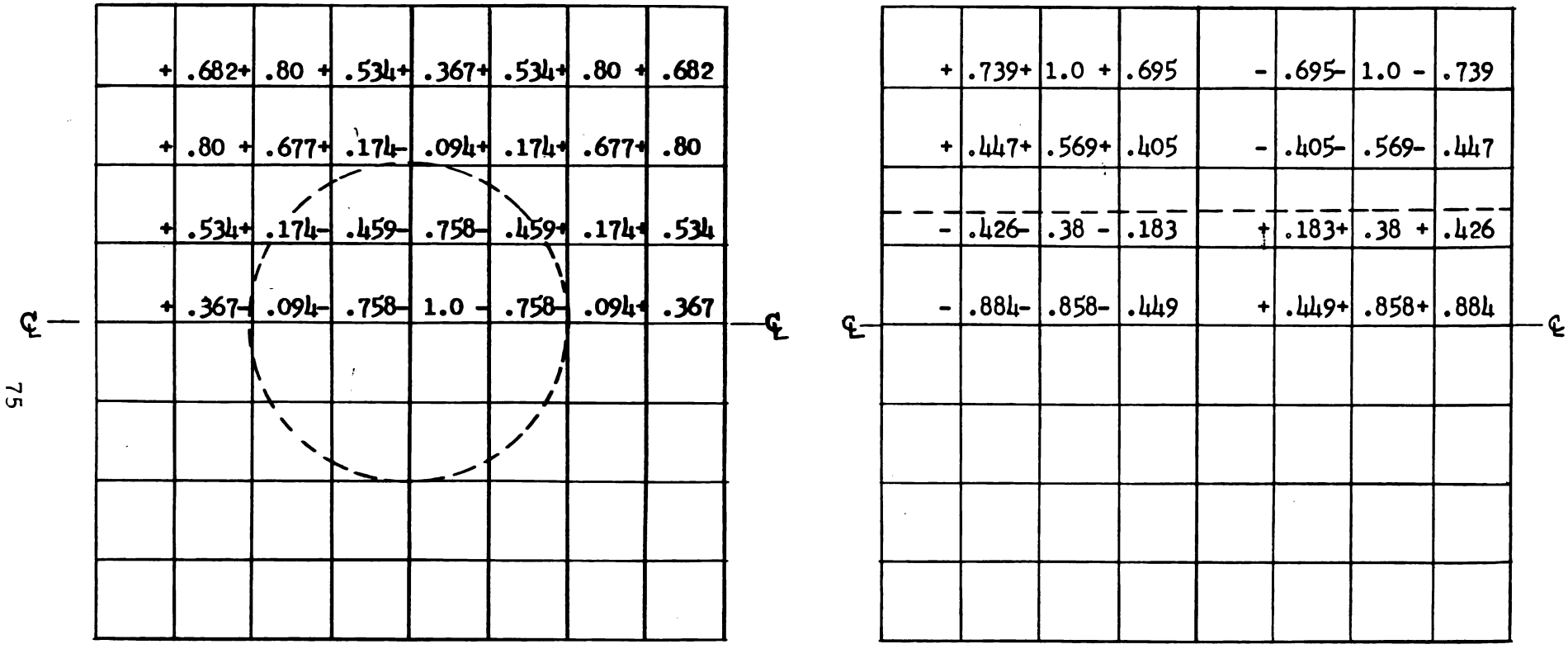

Fifth Mode

Sixth Mode

FIGURE 47. Relative Amplitudes in Plate Model E

shown in Figures 30 - 35. The relative amplitudes determined by finite differences in plate models A, B, D, and E are shown in Figures 36 - 47.

Discussion of the Results

From Table 7 and 8, it can be inferred that the finite difference method converges fairly rapidly except for some higher modes, as in the case of fourth mode frequencies of plate models A and D. It seems desirable to use finer grids than $\lambda = a/6$ in these cases. This is accountable since the fourth mode imposes additional constraints along the diagonals of the plate (the nodal lines) and this would be equivalent to using a coarser grid than $\lambda = a/6$. The extrapolated values are higher than the values obtained for individual grid spacings. In the case of plate model A, the fundamental frequency obtained by experiment agrees very closely (within one per cent) with the extrapolated frequency. For higher modes, the disagreement between the experimental and extrapolated finite differences is from 1 to 4 per cent. In plate model B, the disagreement in the fundamental mode frequency is within 3 per cent and the higher mode frequencies disagree from amounts 3 to 13 per cent. The difference between the experimental and finite difference frequencies is 2 per cent for the first mode and 1 to 6 per cent for higher modes in plate model D, while in the plate model E, the difference is 9 per cent for the first mode and from 3 to 5 per cent for higher modes. Except in the case of plate model A, the experimental frequencies are higher than the extrapolated finite difference frequenices.

The following are the possible sources of error in the determination of frequencies:

a) Determination of exact resonance

b) Errors in the reading instruments

c) The actual plate model different from the ideal finite difference model

d) Inaccuracies in the determination of physical constants

e) Support conditions other than assumed

f) Vibration of support

g) Large amplitudes

h) Effect of rotatory inertia and shear

i) Damping in the material

j) The effect of air mass.

(a) Determination of exact resonance: The presence of extremely sharp resonance peaks for free vibration of plates eliminates the possibility of any large error due to this cause. The maximum error attributable to this source is within one per cent.

(b) Errors in the reading instruments: In the frequency range measured in this study, the electronic counter gives the frequencies to the accuracy of ±1 count. Hence, the error due to this source is negligible.

(c) The actual plate model different from the ideal finite difference model: In plate model A, the actual ratio of edge thickness to center thickness is 1.987 instead of 2.00 while in the plate model B, the ratio is 0.522 instead of 0.500. A lower actual ratio would give smaller frequencies while a higher ratio would yield higher frequencies. This is evident from the frequencies of plate model A and B shown in Table 7. The magnitude of the error depends on how much the actual ratio differs from the ideal ratio. For the models used in this study the error due to this source is estimated to be from 1

to 6 per cent.

(d) Inaccuracies in the determination of physical constants: The physical constants appear in the dimensionless parameter ω_r in terms of which all the frequencies are expressed. The effect on ω_r of errors in these physical quantities is discussed in reference [16]. From Table 9, it is evident that the Poisson's ratio is the least precise of all the measured quantities but it has the least effect on ω_r. Young's modulus of Elasticity (E) and the mass density of the material (ρ) have been found with good accuracy. The quantities such as the side dimensions of the plate and the thickness, which have a great effect on ω_r, have been measured to the accuracy of 1 in 1000 of an inch. Because of these reasons, the error introduced from this source is less than one per cent.

(e) Support conditions other than assumed: The error introduced due to this source is negligible in clamped supports. But, in simple supports errors up to a maximum of 4 per cent could be introduced, as a slight increase in tightness of support nuts could introduce small moments at the edge, thus increasing the frequency.

(f) Vibration of support: Because the clamped and simple supports were mounted tightly on a sturdy steel base, the error due to this source is negligible.

(g) Large amplitudes: Large amplitudes of vibration introduce non-linearity in which frequency of vibration is dependent on the amplitudes of vibration as contrasted with the linear theory where frequency is independent of amplitudes. Influence of large amplitudes on free vibrations of rectangular elastic plates has been discussed theoretically by H. N. Chu and G. Herrmann in reference [18]. The effect of large amplitudes on the fundamental frequency in plate model B was studied

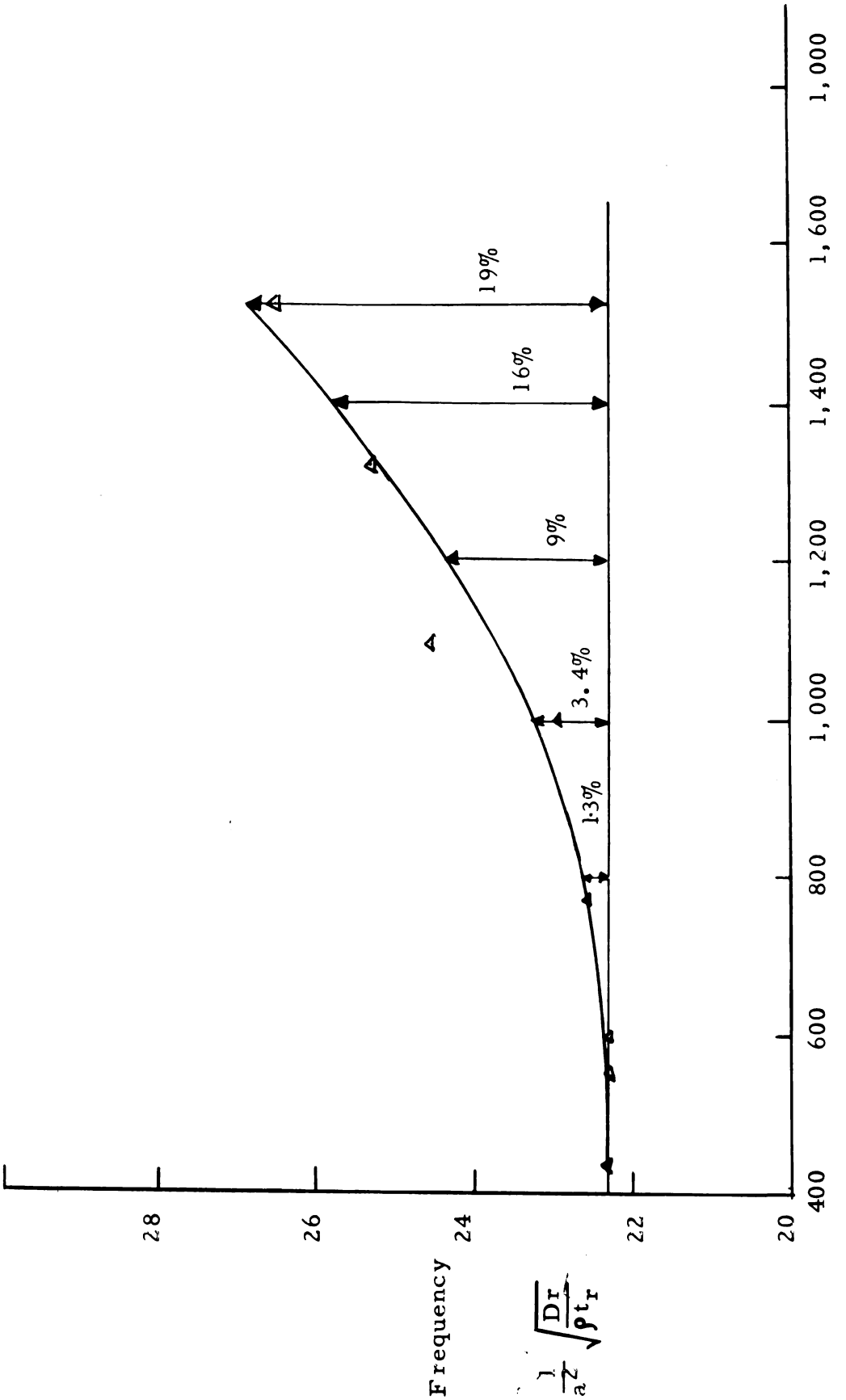

FIGURE 48. Effect of Large Amplitudes in Plate Model B

experimentally and the results are plotted in Figure 48. Instead of amplitudes, the dynamic strain is measured at a strain gauge station situated close to the center. The frequency in terms of ω_r is plotted against the dynamic strain. The frequency remained constant up to a dynamic strain of 600 microinch per inch; beyond this point, the percentage increase in frequency for different dynamic strains are indicated in Figure 48. Since the amplitudes in all plate models were controlled to a level for which the dynamic strain is below 800 microinch per inch, the error due to this source is within one per cent.

(h) Effect of rotatory inertia and shear: This correction becomes more important at higher modes. If the wave length (the length of half waves in which the plate is subdivided) becomes less than 10 times the plate thickness, the classical plate theory which neglects rotatory inertia and shear is very inaccurate. The effect of rotatory inertia and shear in vibration of plates has been discussed by R. D. Mindlin [19]. The highest mode found in this study is the sixth mode for which the wave length is about 18 times the maximum thickness of the plate and hence no correction is made for rotatory inertia and shear.

(i) Damping in the material: The effect of viscous damping of the material on the natural frequency is to decrease the frequency with an increase in the value of damping coefficient. For a material like aluminum the effect of damping could be negligible although for plastic models damping effects should be taken into account.

(j) The effect of air mass: In the vibration test, the plate model is vibrating in an air medium while theoretical frequencies are referred to plates vibrating in vacuo. The vibrating plate induces a

mass of air around it to vibrate and hence a correction for air mass is justified. M. V. Barton [20] makes a crude approximation to correct the test results for air mass by finding an 'equivalent' air mass which moves with the plate on the basis of the theory of aerodynamic forces on an oscillating airfoil. Due to this effect, the frequencies determined by experiment are estimated by Barton to increase in small amounts and in some cases to an extent of about 1.5 per cent.

The node lines obtained experimentally are in fair agreement with those calculated by finite differences (Figures 30 - 35, Figures 36 - 47). Because of slight imperfections in the models the actual node lines deviate to some extent from the ideal node lines. The node patterns do not seem to change from model to model although the boundary conditions and thickness variations were different for each model. However, the position of point of maximum amplitude varies for different models for some higher modes. For the fundamental mode and the fifth mode, the maximum amplitude occurs always at the center of the plate, while for the third mode the point of maximum amplitude (maximum stress also) is always at the quarter point of the plate for all models. For the second mode the maximum amplitude changes along the horizontal centerline while for the fourth mode it changes along the vertical centerline.

A phenomenon was observed in the vibration of plates. This is the presence of 'ultraharmonic or multiple harmonic resonance' in which the plate vibrates with a frequency which is an integral multiple of the driving frequency. This type of resonance occurs whenever an 'impure' applied force of frequency f is in resonance with a system whose frequency is an integral multiple of f. The applied force in the present case is a pressure pulsation whose wave-form is triangular,

becoming sawtooth as the distance from the source is increased [15]. The actual motion of the plate at resonance is essentially sinusoidal. The sawtooth or triangular wave-form can be obtained by a superposition of several sine harmonic functions. Among these higher harmonics, if there exists a harmonic whose frequency is the natural frequency of the plate, then, this type of resonance will occur.

The ultraharmonic resonance helps in finding the higher mode frequencies of the plate from a strain gauge signal although the forcing frequency is limited to only a submultiple of the plate frequency. Most of the modes found in this work showed this type of resonance; and in particular the case in which the plate frequency is twice that of the frequency of pressure pulse is quite common. In some cases the plate vibrates at a frequency which is 3 times the driving frequency.

CHAPTER IV

SUMMARY AND CONCLUSIONS

Summary:

The Moirē method is used to find the moments and deflections in laterally loaded clamped and simply supported square plates of linearly variable thickness. Moirē fringe patterns for different plate models are shown and they are analysed to find the deflection and moments in the plates. The differential equation of a variable thickness plate is approximated by difference equation and the plate problem is solved for different boundary conditions and for different grid spacings by the use of Digital Computer. Experimental results are presented and the comparison with the finite difference results are discussed.

The natural frequencies and the node patterns for clamped and simply supported square plates of linearly variable thickness have been found experimentally using a pulsed-air vibrator. Finite difference approximation is used to solve the vibrating plate problem and the resulting eigen value problem is solved by the use of digital computer. Eigen values are the frequencies and the eigen vectors represent the relative plate amplitudes. Experimental results are compared with finite difference results and disagreements between the two, if any, are discussed in detail.

Conclusions:

The Moirē method is equally easy to apply to plates of variable thickness with different boundary conditions and different types of loading. This method seems to be better suited to find deflections than moments. The principal reasons for inaccuracies in the determination of moments seem to be:

a) the actual models different from the ideal models used for mathematical analysis, b) support conditions other than assumed, c) the errors in calibration of the material and the reduction of data. With the set-up and the models used and the general procedure followed in reducing data, the inaccuracies in moments amounted to from a very small value to about 10 per cent,although for some regions such as valleys and ridges the inaccuracies were quite high. The experimental and theoretical deflections agreed within 3 per cent. With improved models (both material and workmanship) and the improved support conditions (especially simple supported) the inaccuracies in moments could be kept well below 10 per cent.

The convergence of the finite difference method is very good both for deflections and moments. This method seems to be quite general because it could be applied to plates with any boundary conditions, acted upon by any conceivable type of loading and with thickness variation being quite arbitrary. Further, the loading and thickness functions can be either continuous or discontinuous.

Comparing the plates of variable thickness with plates of constant thickness, it is concluded that the effect of increasing the plate thickness at the edge compared to the thickness at the center is to reduce the center moment and increase the edge moment,while decreasing the edgethickness has the opposite effect. But in simply supported plates the only moments which are changed considerably are those near the center region bounded by quarter span lines. A plate thick at the edge would have smaller center moment than the one thin at the edge.

The finite difference method should be applied with care to vibration problems. For lower modes, grid sizes of a/6 and a/8 give good convergence, but for higher modes, still finer grids should

be used in order to give reasonable convergence. For still higher modes (beyond sixth mode) the rotatory inertia and shear should be included in the difference equation of variable thickness plate to give good accuracy. In particular, this would add terms in the B matrix of the plate eigen value problem

$$[A - \chi B]_w = 0.$$

In general it is concluded that the finite difference approximation used in this study gives sufficient accuracy in the case of variable thickness plate problems.

The experimental results are in fair agreement with the finite difference results. The inaccuracies are due to the actual model deviating from the ideal model, support conditions other than assumed.

In this work the inaccuracies range from very small amounts to about 6 per cent, although in a few cases, the inaccuracy was up to 13 per cent. With better models and improved support conditions, an accuracy of one per cent can be achieved with the pulsed-air vibrator.

The nodal lines are in fair agreement with the calculated positions of node lines. Ultraharmonic resonance was observed for nearly all modes studied.

Further investigations are suggested along several lines:

(1) Thickness variation and loads being discontinuous.

(2) Study of viscoelastic plates of variable thickness.

(3) Effect of large thickness variation in plates.

(4) Development of a technique to measure the amplitudes in the vibrating plate.

(5) Study of higher modes of variable thickness plate. Inclusion of rotatory inertia and shear in the difference

equation of variable thickness vibrating plate.

(6) Study of large amplitudes in vibrating plate.

(7) Application of Ritz and Galerkin methods to the study of variable thickness plates.

BIBLIOGRAPHY

1. Olsson, R. Gran, "Biegung der Rechteckplatte bei Linear Veränderlicher Biegungs-Steifigkeit," Ingenieur Archiv, v Band, 1934, pp. 363-373.

2. Olsson, R. Gran, "Biegung der Rechteckplatte von Exponentiell Veränderlicher Dicke," Der Bauingenieur, 1940, pp. 230-235.

3. Favre, Henry and Gilg, Bernhard, "La Plaque Rectangulaire Fléchie d' Épaisseur Linéairement Variable," Zeitschrift für Angewandte Mathematik und Physik, Vol. 3, 1952, pp. 354-370.

4. Favre, H. and Schumann, W., "Study of Bending of Rectangular Plates with Linear Varying Thickness and Different Edge Conditions: Application to Case of Hydrostatic Load," Bull. Tech. Suisse. Rom 81, 11, May, 1955, pp. 161-174. Also see Applied Mechanics Review, Vol. 9, 1956, Review No. 699.

5. Contri, L. "Study of Plates of Linearly Variable Thickness," Atti. Ist. Veneto. Sci. Lelt. Arti. Cl. Sci. Mat. Nat. 111, 1953, pp. 183-195. Also see A. M. Review, Vol. 8, 1955, Review No. 1631.

6. Contri, L., "Retangular Plate with Linearly Variable Thickness," (in Italian), G. Gen, Civ., 93, 2, Feb., 1955, pp. 136-142. Also see A. M. Review, Vol. 9, 1956, Review No. 1048.

7. MacNeal, R. H., "The Solutions of Elastic Plate Problems by Electrical Analogies," J. of Applied Mechanics, Vol. 18, 1951, pp. 59-67.

8. Fung, Y. C., "Bending of Thin Elastic Plates of Variable Thickness," J. of the Aeronautical Sciences, Vol. 20, 1953, pp. 455-468.

9. Gumenyuk, V. S., "Free Oscillations of Plates of Variable Thickness," (in Ukranian), Dopovidi. Akad. Nauk. URSR No. 2, 1956, pp. 130-133. Also see A. M. Review, Vol. 11, 1958, Review No. 4856.

10. Kogaev, V. P., "Determination of the Frequency and Forms of the Natural Oscillations of Plates of Variable Thickness," (Blade type), (in Russian), Trudi. Mosk. Aviats. Tekhnol in-ta. No. 25, 1954, pp. 75-91.

11. Hulsbos, C. L. and Ti-ta Lee, "Moment Analysis for Bridge Abutment Wingwalls of Variable Thickness," The Iowa State Bulletin 184, 1959.

12. Bradley, W. A., "The Determination of Moments and Deflections in Plates by the Moire Method and by Finite Differences with Application to the Square Clamped Plate with Square Cutouts," A Doctoral Thesis submitted to the University of Michigan, 1956.

13. Raju, Basava, B., "A Study of Simply Supported Square Plates by the Moire Method and by Finite Differences," A Master Thesis submitted to the Michigan State University, 1958.

14. Palmer, P. J., "The Bending Stresses in Cantilever Plates by Moire Fringes," Aircraft Engineering, 29, 346, Dec. 1957, pp. 377-380.

15. Truman, J. C., Martin, J. R., Klint, R. V., "A Pulsed-Air Vibration Technique for Testing High Performance Turbomachinery Blading," No. 584, The Society for Experimental Stress Analysis, May, 1960.

16. Dalley, J. W., and Ripperger, E. A., "Experimental Values of Natural Frequencies for Skew and Rectangular Cantilever Plates," Proceedings of the Society for Experimental Stress Analysis, Vol. IX, No. 2, 1952, pp. 51-66.

17. Bradley, W. A., "Theoretical and Experimental Investigations of Laterally Loaded Thin Flat Plates," A Report to the Division of Engineering Research, Michigan State University.

18. Chu, Hu-Nan and George Herrmann, "Influence of Large Amplitudes on Free Vibrations of Rectangular Elastic Plates," Journal of Applied Mechanics, 1956, pp. 532-540.

19. Mindlin, R. D., "Influence of Rotatory Inertia and Shear on Flexural Motions of Isotropic, Elastic Plates," Journal of Applied Mechanics, 1951-52, pp. 31-38.

20. Barton, M. V., "Vibration of Rectangular and Skew Cantilever Plates," Journal of Applied Mechanics, 18, June, 1951, pp. 129-134.

21. Nielsen, N. J., "Bestemmelse af Spaendinger I Plader," Copenhagen, 1920.

22. Ludeke, C. A., "Resonance," Journal of Applied Physics, Vol. 13, 1942, pp. 418-423.

23. Grinter, L. E., "Numerical Methods of Analysis in Engineering," The Macmillan Co., New York, 1959, pp. 138-168.

APPENDIX A

Finite Difference Equation of Variable Thickness Plate Derived by Plate Analogy

In the plate analogy [23], the plate is replaced by an analogous structure which is made up of a series of rigid bars and blocks joined by springs. The ends of rigid bars are connected to the blocks by means of springs which transfer only moments and shear between the bars and the joint block, while the mid-points of the bars are connected by torsional springs which transmit only twisting moment. The loads are applied only at the joints. The bending moments are expressed in terms of the displacements of the joints from the unloaded position and the plate rigidity at the joint. The twisting moments are expressed in terms of the plate rigidity at the center of the grid and the twist of the surface, which can be expressed in terms of the displacements of the joints. By considering the equilibrium of the joints and the bar, the difference equation of variable thickness plate and the edge and corner reactions are derived in the following. Nielsen [21] obtains the difference equation of variable thickness plate by considering the equilibrium in the plate element and his equation agrees with the equation obtained by plate analogy. Considering the bar 'on' and taking moments about n (Figure 49),

$$Q_{on} \cdot \lambda^2 = \lambda \cdot M_{on} - \lambda \cdot M_{no} + \lambda \cdot M_{on-w} - \lambda M_{on-e} \cdot$$

$$M_{on} = -\frac{D_o}{\lambda^2}\left[(W_n - 2W_o + W_s) + \nu\,(W_e - 2W_o + W_w)\right]$$

$$M_{no} = -\frac{D_n}{\lambda^2}\left[(W_{nn} - 2W_n + W_o) + \nu\,(W_{ne} - 2W_n + W_{nw})\right]$$

$$M_{on-e} = \frac{(1-\nu)D_a}{\lambda^2} \cdot (W_e + W_n - W_o - W_{ne})$$

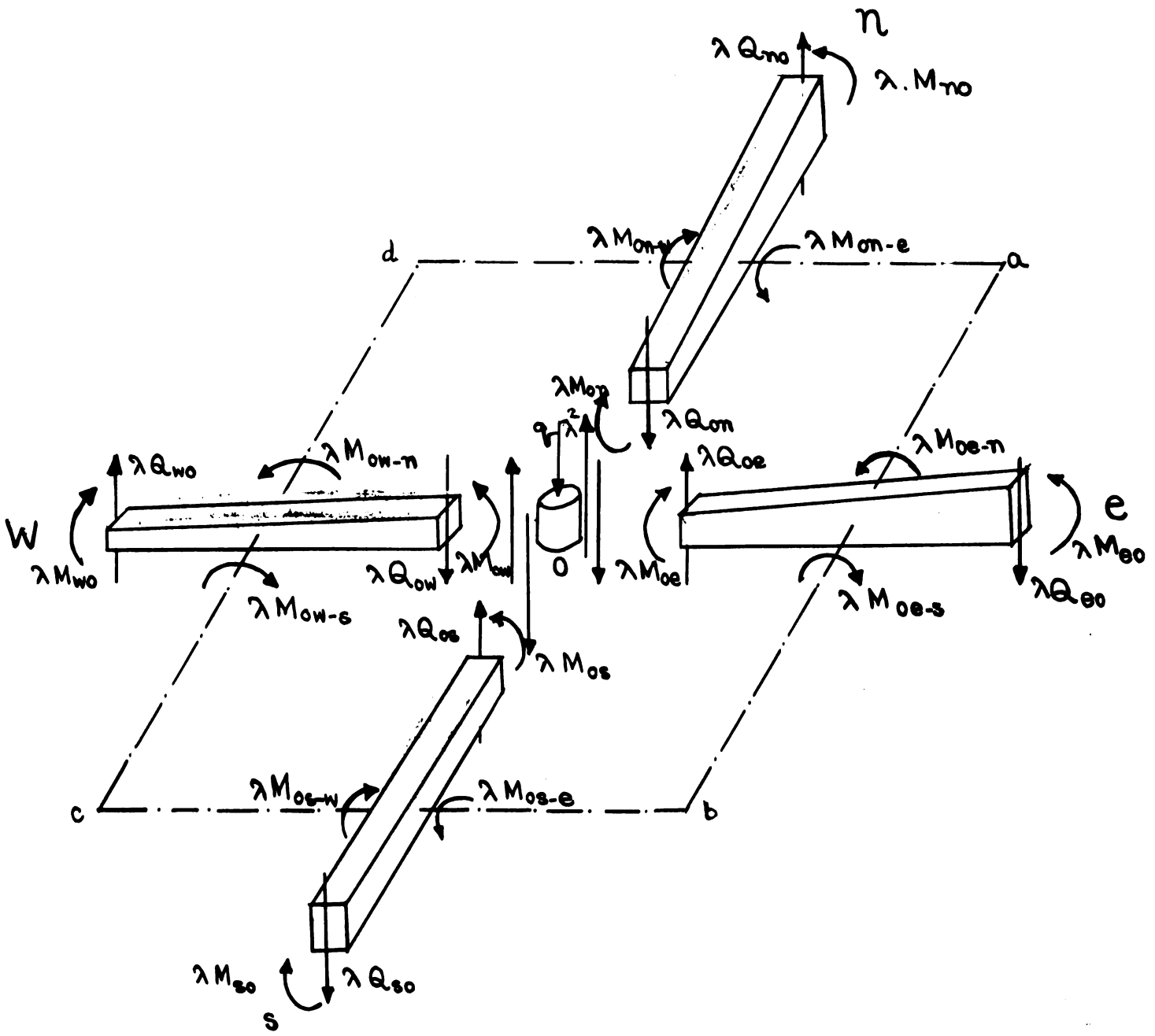

FIGURE 49. Forces Acting on Elements of Analogous Plate Structure at a General Point of a Variable Thickness Plate

$$M_{on-w} = \frac{(1-\nu)\,D_d}{\lambda^2} \cdot (W_o + W_{nw} - W_w - W_n)$$

Now

$$D_n = \delta_n D_o \quad , \quad D_a = \delta_a D_o \quad , \quad D_d = \delta_d D_o$$

$$\begin{aligned} Q_{on} \cdot \lambda = \frac{D_o}{\lambda^2} [& - (W_n - 2W_o + W_s) - \nu\,(W_e - 2W_o + W_w) \\ & + \delta_n\,(W_{nn} - 2W_n + W_o) + \nu\delta_n\,(W_{ne} - 2W_n + W_{nw}) \\ & + (1-\nu)\,\delta_d\,(W_o + W_{nw} - W_w - W_n) \\ & - (1-\nu)\,\delta_a\,(W_e + W_n - W_o - W_{ne})] \end{aligned}$$

Similarly considering the equilibrium of oe:

$$Q_{oe} \cdot \lambda^2 = \lambda M_{eo} - \lambda M_{oe} + \lambda M_{oe-n} - \lambda M_{oe-s} \cdot$$

$$\begin{aligned} Q_{oe} \cdot \lambda = \frac{D_o}{\lambda^2} [& - \delta_e (W_{ee} - 2W_e + W_o) - \nu\delta_e\,(W_{se} - 2W_e + W_{ne}) \\ & + (W_e - 2W_o + W_w) + \nu\,(W_s - 2W_o + W_n) \\ & + (1-\nu)\,\delta_a\,(W_e + W_n - W_o - W_{ne}) \\ & - (1-\nu)\,\delta_b\,(W_{se} + W_o - W_e - W_s)] \end{aligned}$$

Considering the equilibrium of os:

$$Q_{os} \cdot \lambda^2 = \lambda M_{so} - \lambda M_{os} + \lambda M_{os-w} - \lambda M_{os-e} \cdot$$

$$\begin{aligned} Q_{os} \cdot \lambda = \frac{D_o}{\lambda^2} [& - \delta_s\,(W_{ss} - 2W_s + W_o) - \nu\delta_s\,(W_{se} - 2W_s + W_{sw}) \\ & + (W_s - 2W_o + W_n) + \nu\,(W_e - 2W_o + W_w) \end{aligned}$$

$$+ (1 - \nu)\,\delta_c\,(W_s + W_w - W_o - W_{sw})$$

$$- (1 - \nu)\,\delta_b\,(W_{se} + W_o - W_s - W_e)]$$

Considering the equilibrium of 'ow':

$$Q_{ow} \cdot \lambda^2 = \lambda M_{ow} - \lambda M_{wo} + \lambda M_{ow-n} - \lambda M_{ow-s}$$

$$Q_{ow} \cdot \lambda = \frac{D_o}{\lambda^2}[-(W_e - 2W_o + W_w) - \nu\,(W_s - 2W_o + W_n)$$

$$+ \delta_w\,(W_o - 2W_w + W_{ww}) + \nu\delta_w\,(W_{sw} - 2W_w + W_{nw})$$

$$+ (1 - \nu)\,\delta_d\,(W_o + W_{nw} - W_w - W_n)$$

$$- (1 - \nu)\,\delta_c\,(W_s + W_w - W_o - W_{sw})]$$

Summing the vertical forces on the joint at O:

$$(Q_{ow} - Q_{oe})\,\lambda + (Q_{on} - Q_{os})\,\lambda = q\lambda^2$$

Substituting the values of Q's and rearranging the terms the plate equation takes the pattern shown in Figure 2.

Finite Difference Equation for Edge Reaction in Simply Supported Plate of Variable Thickness

Considering the bar 'ow' and taking moments about w (Figure 50),

$$Q_{ow} \cdot \frac{\lambda^2}{2} = \lambda \cdot M_{ow-n}$$

$$Q_{ow} \cdot \frac{\lambda}{2} = \frac{D_o}{\lambda^2}\,\delta_d\,(1 - \nu)(W_{nw} + W_o - W_n - W_w)$$

Boundary condition: $W_o = W_w = 0$

$$Q_{ow} \cdot \frac{\lambda}{2} = + \frac{D_o}{\lambda^2}\,\delta_d\,(1 - \nu)(W_{nw} - W_n)$$

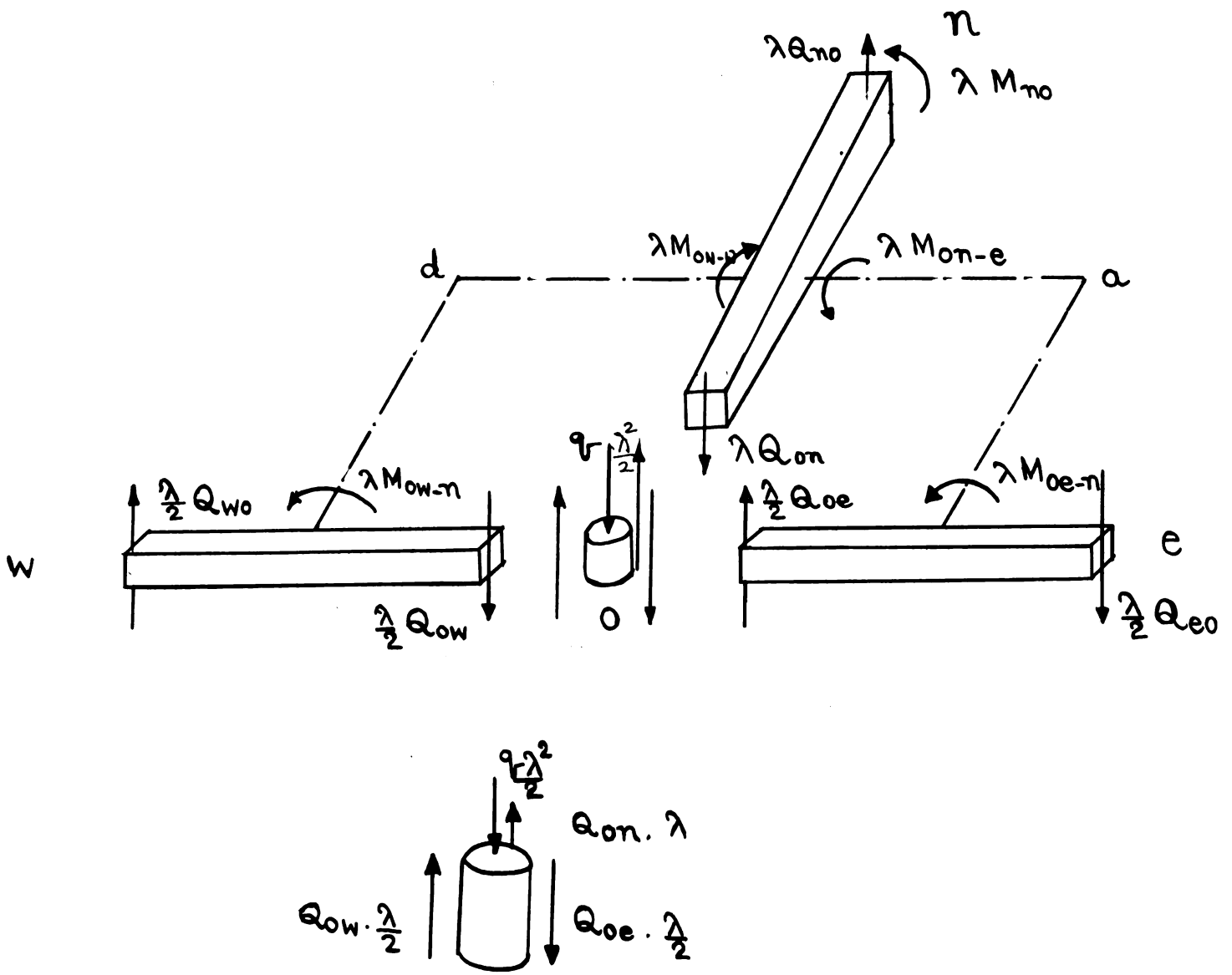

FIGURE 50. Forces Acting on Elements of Analogous Plate Structure at a Point on the Simply Supported Edge of a Variable Thickness Plate

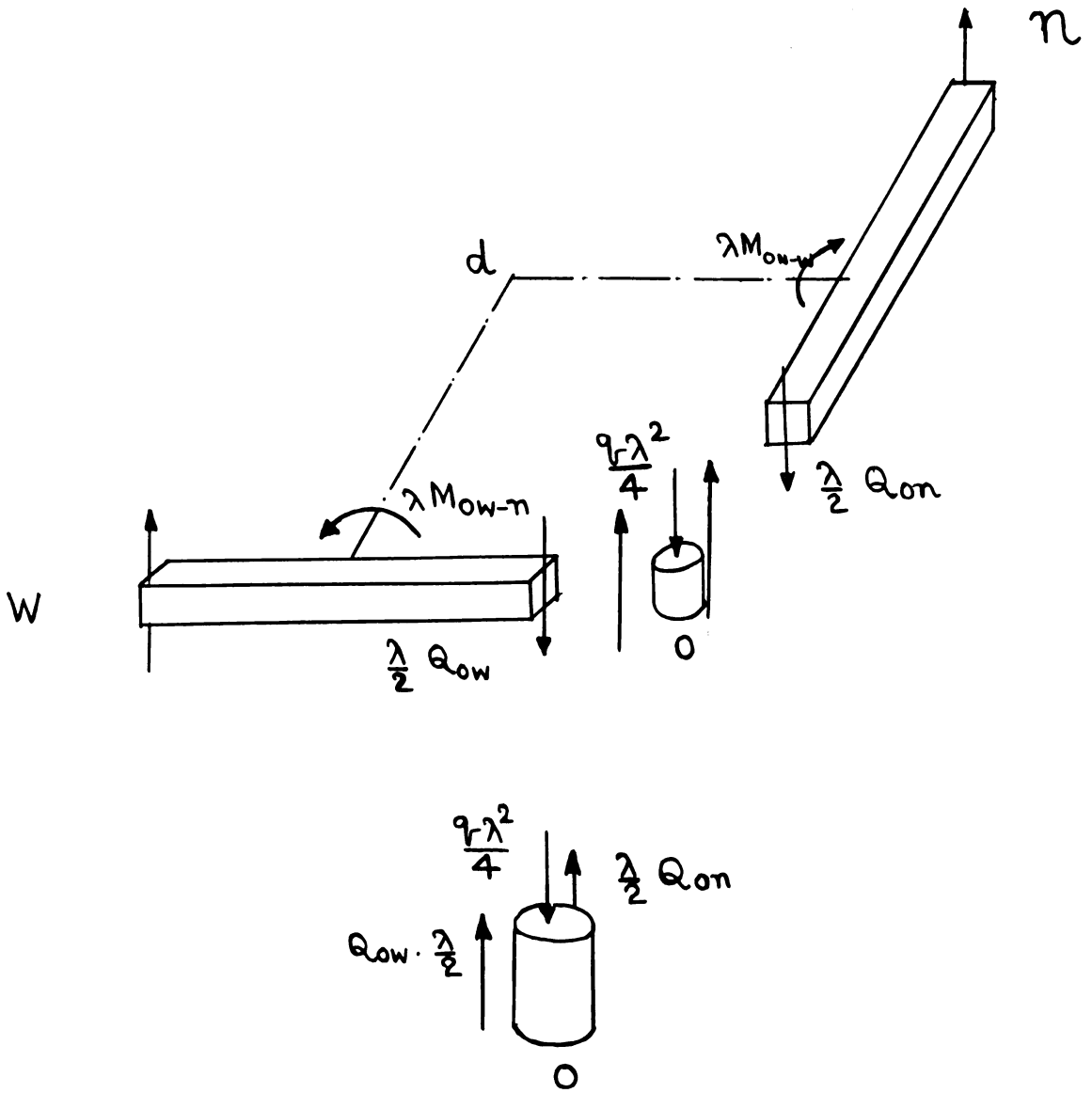

FIGURE 51. Forces Acting on Elements of Analogous Plate Structure at the Corner of a Simply Supported Plate of Variable Thickness

Similarly

$$Q_{oe} \cdot \frac{\lambda}{2} = \frac{D_o}{\lambda^2} \delta_2 (1 - \nu)(W_n - W_{ne})$$

$$Q_{on} \cdot \lambda = \frac{D_o}{\lambda^2} [- \delta_a (1 - \nu)(W_n - W_{ne}) + \delta_d (1 - \nu)(W_{nw} - W_n)$$

$$+ \delta_n (W_{nn} - 2W_n) + \nu\delta_n (W_{ne} - 2W_n + W_{nw})]$$

Summing the vertical forces on the joint 0,

$$Q_{on} \cdot \lambda + Q_{ow} \cdot \frac{\lambda}{2} - Q_{oe} \cdot \frac{\lambda}{2} = \frac{q\lambda^2}{2} + V \cdot \lambda$$

Substituting the values of Q's and rearranging the terms,

$$V = - \frac{q\lambda}{2} + \frac{D_o}{\lambda^3} [W_{nn} \cdot \delta_n + W_{nw}\{\nu\delta_n + 2(1 - \nu)\delta_d\}$$

$$+ W_{ne}\{\nu\delta_n + 2(1 - \nu)\delta_a\} - 2W_n\{(1 + \nu)\delta_n + (1 - \nu)(\delta_a + \delta_d)\}]$$

Finite Difference Equation for Corner Reaction in Simply Supported Plate of Variable Thickness

Considering the bar 'ow' and taking moments about w (Figure 51)

$$Q_{ow} \cdot \frac{\lambda^2}{2} = \lambda \cdot M_{ow} - n$$

$$Q_{ow} \cdot \frac{\lambda}{2} = \frac{D_o}{\lambda^2} \cdot \delta_d (1 - \nu)(W_{nw} + W_o - W_n - W_w)$$

Boundary condition: $W_n = W_o = W_w = 0$

$$Q_{ow} \cdot \frac{\lambda}{2} = \frac{D_o}{\lambda^2} \cdot \delta_d (1 - \nu) W_{nw}$$

Similarly

$$Q_{on} \cdot \frac{\lambda}{2} = \frac{D_o}{\lambda^2} \delta_d (1 - \nu) W_{nw} \cdot$$

Summing the vertical forces at the joint 0.

$$Q_{on} \cdot \frac{\lambda}{2} + Q_{ow} \cdot \frac{\lambda}{2} = \frac{q\lambda^2}{4} + R \quad .$$

$$R = -\frac{q\lambda^2}{4} + \frac{D_o}{\lambda^2} \cdot \delta_d \, (1 - \nu) \, W_{nw} \quad .$$

APPENDIX B

Finite Difference Approximation of the Differential Equation of Variable Thickness Plate

Summing all the forces in the direction of z - axis: Fig. 45

$$\frac{\partial Q_x}{\partial x} + \frac{\partial Q_y}{\partial y} + q = 0$$

Taking moments of all the forces acting on the element with respect to x - axis:

$$\frac{\partial M_{xy}}{\partial x} + \frac{\partial M_y}{\partial y} - Q_y = 0 \ .$$

In the same manner, by taking moments with respect to y - axis, we obtain

$$\frac{\partial M_{xy}}{\partial y} + \frac{\partial M_x}{\partial x} - Q_x = 0 \ .$$

Eliminating shearing forces Q_x and Q_y from these equations we obtain

$$\frac{\partial^2 M_x}{\partial x^2} + 2\frac{\partial^2 M_{xy}}{\partial x \partial y} + \frac{\partial^2 M_y}{\partial y^2} = -q\,(x, y)$$

The moment curvature relations are given by

$$M_x = -D\,(x, y)\left[\frac{\partial^2 w}{\partial x^2} + \nu \frac{\partial^2 w}{\partial y^2}\right]$$

$$M_y = -D\,(x, y)\left[\frac{\partial^2 w}{\partial y^2} + \nu \frac{\partial^2 w}{\partial x^2}\right]$$

$$M_{xy} = -(1 - \nu)\,D\,(x, y)\frac{\partial^2 w}{\partial x \partial y}$$

Substituting the expressions for moments in the plate equilibrium equation

$$\frac{\partial^2 M_x}{\partial x^2} = -D\frac{\partial^2}{\partial x^2}\left(\frac{\partial^2 w}{\partial x^2} + \nu \frac{\partial^2 w}{\partial x^2}\right) - 2\frac{\partial D}{\partial x}\frac{\partial}{\partial x}\left(\frac{\partial^3 w}{\partial x^3} + \nu \frac{\partial^3 w}{\partial x \partial y^2}\right)$$

$$- \frac{\partial^2 D}{\partial x^2}\left(\frac{\partial^2 w}{\partial x^2} + \nu \frac{\partial^2 w}{\partial y^2}\right)$$

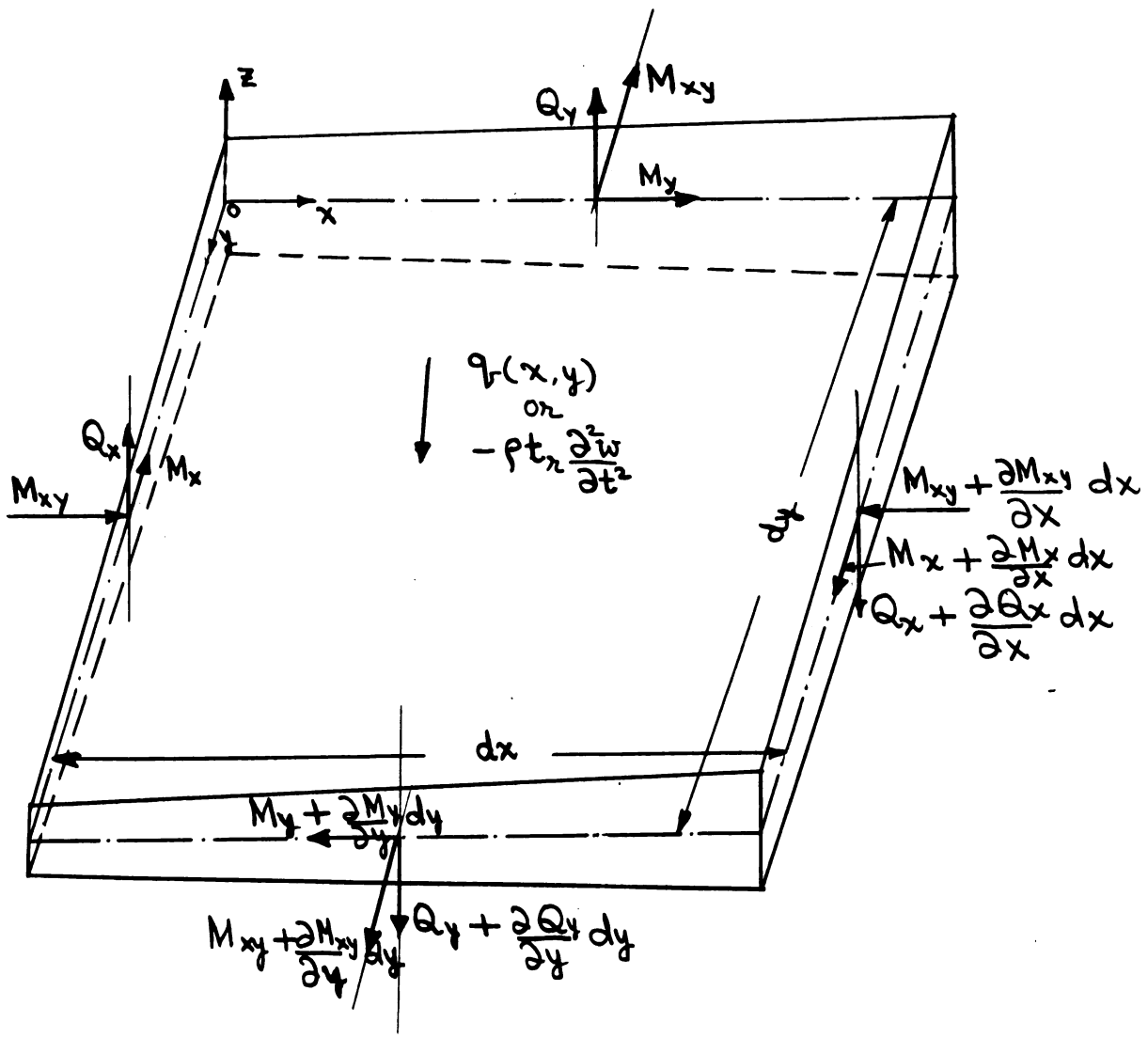

FIGURE 52. Moments and Forces Acting on a Plate Element of Variable Thickness

Directions are Positive as Shown

$$\frac{\partial^2 M_{xy}}{\partial x \partial y} = -(1-\nu)\left(\frac{\partial^2 D}{\partial x \partial y} \cdot \frac{\partial^2 w}{\partial x \partial y} + \frac{\partial D}{\partial x} \cdot \frac{\partial^3 w}{\partial x \partial y^2} + \frac{\partial D}{\partial y} \cdot \frac{\partial^3 w}{\partial x^2 \partial y} + D \cdot \frac{\partial^4 w}{\partial x^2 \partial y^2}\right),$$

$$\frac{\partial^2 M_y}{\partial y^2} = -D\frac{\partial^2}{\partial y^2}\left(\frac{\partial^2 w}{\partial y^2} + \nu\frac{\partial^2 w}{\partial x^2}\right) - 2\frac{\partial D}{\partial y}\frac{\partial}{\partial y} \cdot \left(\frac{\partial^3 w}{\partial y^3} + \nu\frac{\partial^3 w}{\partial x^2 \partial y}\right) - \frac{\partial^2 D}{\partial y^2}\left(\frac{\partial^2 w}{\partial y^2} + \nu\frac{\partial^2 w}{\partial x^2}\right)$$

If

$$\nabla = \frac{\partial^2}{\partial x^2} + \frac{\partial^2}{\partial y^2}$$

we get

$$D\nabla\nabla w + 2\frac{\partial D}{\partial x} \cdot \frac{\partial}{\partial x}\nabla w + 2\frac{\partial D}{\partial y} \cdot \frac{\partial}{\partial y}\nabla w + \nabla D \nabla w - (1-\nu)\left(\frac{\partial^2 D}{\partial x^2} \cdot \frac{\partial^2 w}{\partial y^2} - 2\frac{\partial^2 D}{\partial x \partial y} \cdot \frac{\partial^2 w}{\partial x \partial y} + \frac{\partial^2 D}{\partial y^2} \cdot \frac{\partial^2 w}{\partial x^2}\right) = q(x, y)$$

or

$$-\rho t \frac{\partial^2 w}{\partial t^2} .$$

Each term of the above expression is replaced by its finite difference equivalent. Thus

$$\lambda^4 \nabla\nabla w = 20 w_o - 8(w_n + w_w + w_e + w_s) + 2(w_{nw} + w_{ne} + w_{se} + w_{sw}) + (w_{nn} + w_{ee} + w_{ss} + w_{ww})$$

$$2\lambda^3 \cdot \frac{\partial}{\partial x}\nabla w = (w_{ne} + w_{se} - w_{nw} - w_{sw}) + 4(w_w - w_e) + w_{ee} - w_{ww}$$

$$2\lambda^3 \cdot \frac{\partial}{\partial y}\nabla w = (w_{se} + w_{sw} - w_{ne} - w_{nw}) + 4(w_n - w_s) + w_{ss} - w_{nn}$$

$$\lambda^2 \nabla D = D_o (\delta_n + \delta_s + \delta_e + \delta_w - 4)$$

$$\lambda^2 \nabla W = (W_n + W_s + W_e + W_w - 4W_o)$$

$$\lambda^2 \frac{\partial^2 D}{\partial x^2} = D_o (\delta_e - 2 + \delta_w)$$

$$\lambda^2 \frac{\partial^2 D}{\partial y^2} = D_o (\delta_n - 2 + \delta_s)$$

$$4\lambda^2 \frac{\partial^2 D}{\partial x \partial y} = D_o (\delta_{nw} + \delta_{se} - \delta_{ne} - \delta_{sw})$$

$$\lambda^2 \cdot \frac{\partial^2 w}{\partial x^2} = (W_e - 2W_o + W_w)$$

$$\lambda^2 \cdot \frac{\partial^2 w}{\partial y^2} = (W_n - 2W_o + W_s)$$

$$4\lambda^2 \frac{\partial^2 w}{\partial x \partial y} = (W_{nw} + W_{se} - W_{ne} - W_{sw})$$

Substituting the above and rearranging the terms the difference equation of variable thickness plate as shown in Figure 53 results.

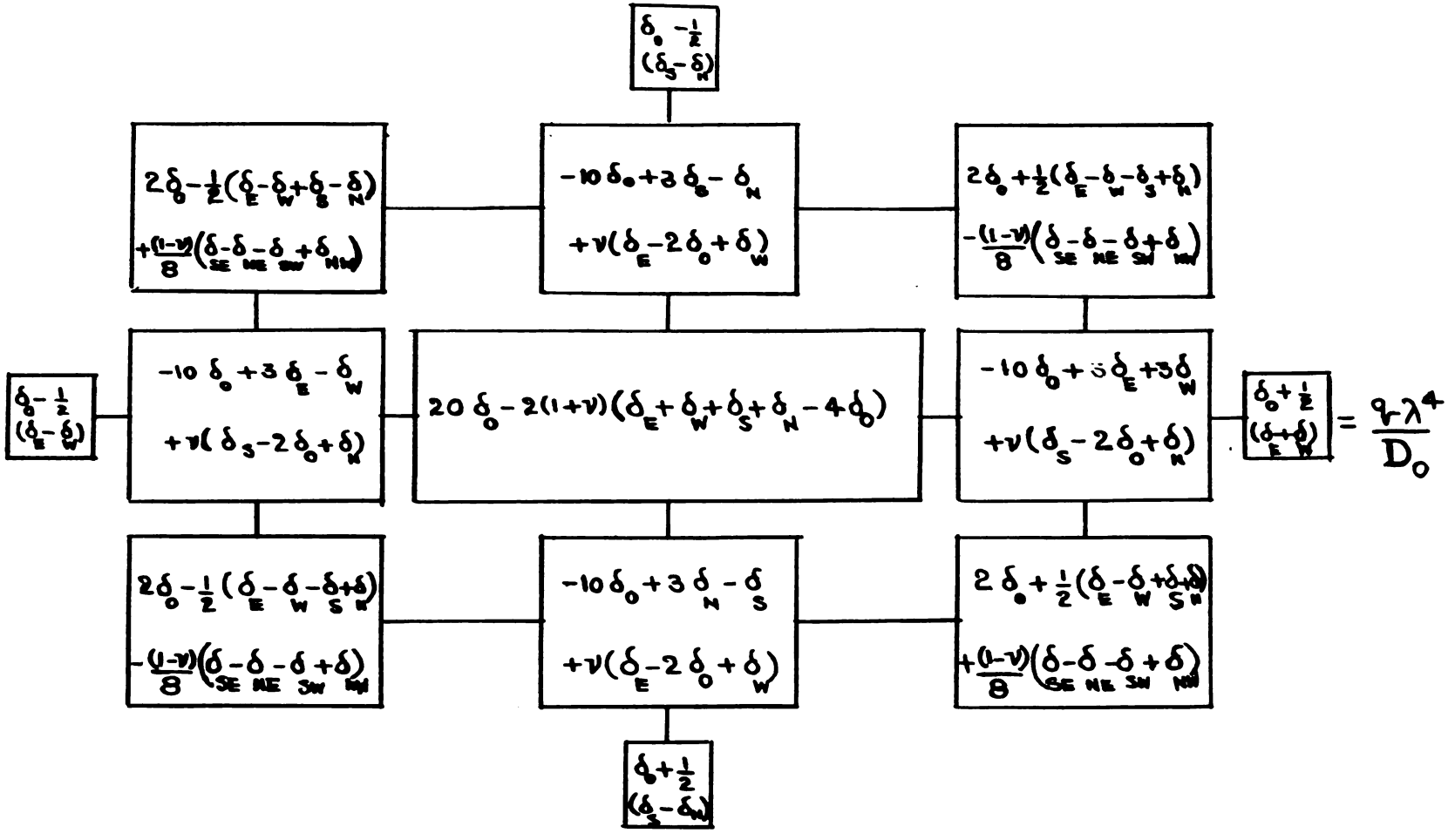

FIGURE 53. Finite Difference Approximation for Plate Equation of Variable Thickness

ROOM USE ONLY

MICHIGAN STATE UNIVERSITY LIBRARIES
3 1293 03175 7523